

Structural Analysis of Dibenzofurans and Dibenzothiophenes as Promising Matrix Metalloproteinase-12 Inhibitors: Ligand and Structure-Based Molecular Modelling Approaches to Pinpoint Crucial Structural Attributes

Submitted by

Jigme Sangay Dorjay Tamang

EXAM ROLL NO.: M4PHC23014

CLASS ROLL NO.: 002111402023

REG. NO.: 160252 of 2021-2022

Department of Pharmaceutical Technology
Jadavpur University
Session- *2021-2023*

Under The Guidance Of

Prof. Tarun Jha

Natural Science Laboratory
Department of Pharmaceutical Technology
Jadavpur University, Kolkata-700032

*Thesis submitted in partial fulfilment of the requirements for the
Degree of Master of Pharmacy
Department of Pharmaceutical Technology
Faculty of Engineering and Technology
Jadavpur University, Kolkata*

2023

Jadavpur University

Jadavpur, Kolkata-700032

CERTIFICATE OF APPROVAL

This is to certify that ***Jigme Sangay Dorjay Tamang*** (Exam Roll No. M4PHC23014 - , Reg. No.160252 – of 2021-2022) has sincerely carried out the research work on the subject entitled “**Structural Analysis of Dibenzofurans and Dibenzothiophenes as Promising Matrix Metalloproteinase-12 Inhibitors: Ligand and Structure-Based Molecular Modelling Approaches to Pinpoint Crucial Structural Attributes**” under the supervision of **Prof. Tarun Jha**, Professor, Natural Science Laboratory, Department of Pharmaceutical Technology of Jadavpur University. He has incorporated his findings in this thesis submitted by him in partial fulfillment of the requirements for the degree of **master’s in pharmacy** (Pharmaceutical Technology) of Jadavpur University. He has carried out the research work independently and sincerely with proper care and attention to our entire satisfaction.

Head of the Department

Department of Pharmaceutical
Technology
Jadavpur University
Kolkata-700032

Prof. Tarun Jha

Natural Science Laboratory
Department of Pharmaceutical
Technology
Jadavpur University
Kolkata-700032

Dean

Faculty of Engineering and Technology
Jadavpur University
Kolkata-700032

Acknowledgent

The final outcome of this thesis required a lot of guidance and assistance from many people. I am extremely fortunate to have these all along the completion of my work. Whatever I have done is only due to such guidance and assistance and I would not forget to thank them.

I am highly obliged and like to express my deep gratitude and profoundness to my reverend mentor **Prof. Tarun Jha** of Department of Pharmaceutical Technology, Jadavpur University, Kolkata for his excellent and constant guidance and help, endless encouragement, thoughtful and freedom and stupendous cooperation throughout the term paper till its successful completion. I am greatly indebted to his motivation, fruitful suggestions and inspirations.

I owe my deep respect to **Prof. Amalesh Shamanta**, Head of the Department and **Prof. Sanmoy Karmakar** former Head of the Department, Department of Pharmaceutical Technology, Jadavpur University, Kolkata for all the necessary help and encouragement. I would like to convey my sincere gratitude to AICTE and Jadavpur University for their financial and equipmental support for my M. Pharm course.

I am both extremely honoured and grateful to **Dr. Nilanjan Adhikari, Mr. Sandip Kr. Baidya, and Mr. Suvankar Banerjee** for their priceless guidance and support which assisted me to gather knowledge about the different aspects of this work. I would express my sincere thanks to my laboratory colleague **Mr. Rahul Jana, Mr. Chayenta Sen, Mr. Vishal saha,** and my juniors **Mr. Sandeep Jana Mr. Tuhin Baran Samoi** Natural Science Laboratory Department of Pharmaceutical Technology, Jadavpur University, Kolkata-700032

I would like to thank **Dr. Balaram Gosh**, BITS-Pilani, Hyderabad, India for the continuous encouragement, necessary help and support to perform my work.

Finally, I would like to express my deep respect to my father **Mr. Birbahadur Tamang**, mother **Mrs. Nimasang Tamang**, my friends and relatives for their continuous help, love, encouragement and moral support throughout the period of my work.

[Jigme Sangay Dorjay Tamang]

Date:

Place: Department of Pharmacy, Jadavpur University,
Kolkata.

Declaration of Originality and Compliance Of Academic Ethics

I hereby declare that this thesis contains literature survey and original research work performed by me (Jigme Sangay Dorjay Tamang) as a part of my Master of Pharmacy studies. All the information in this document have been obtained and presented in accordance with academic rules and ethical conduct.

I also declare that, as required by these rules and conduct, I have cited and referenced the materials and results that are not original to this work.

Name: Jigme Sangay Dorjay Tamang

Exam Roll Number: M4PHC23014

Class Roll Number: 002111402023

Registration Number: 160252 of 2021-2022

Thesis Title: “Structural Analysis of Dibenzofurans and Dibenzothiophenes as Promising Matrix Metalloproteinase-12 Inhibitors: Ligand and Structure-Based Molecular Modelling Approaches to Pinpoint Crucial Structural Attributes”.

Signature with Date

(Jigme Sangay Dorjay Tamang)

Dedicated to
My Parents, Teachers, Seniors
and
Friends

Contents

Chapters	Page Numbers
Preface	7-8
1. Introduction	9-29
2. Literature Review	30-45
3. Rationale Behind the Study	46-48
4. Materials and Methods	49-56
5. Results & Discussion	57-86
6. Conclusion & Future Perspective	87-89
References	90-108
Appendix	109-125

Preface

Cancer is a pervasive disease that has affected millions of people worldwide, as it is one of the leading causes of death. It is characterised by the body's cells growing abnormally, which can result in tumours or invade other tissues. Cancer is a complex and difficult disease to comprehend and cure since it can manifest in any place of the body and take many different forms. Furthermore, cancer patients need expensive and difficult therapies, endangering our economy and society.

There are several factors like genetics and environmental factors that may work together for the development and spread of cancer. These risk factors include tobacco or alcohol, being exposed to toxic substances or radiation, having chronic inflammation, having inherited gene mutations, having certain infections, having hormonal abnormalities, and leading an unhealthy lifestyle. It's crucial to remember that not everyone with risk factors will get cancer, and some people may have cancer without having any observable risk factors.

Matrix metalloproteinase-12 (MMP-12), referred to as macrophage elastase, is an enzyme that plays a significant role in various physiological and pathological conditions, like chronic obstructive pulmonary disease (COPD), emphysema, asthma, skin diseases, arthritis, vascular diseases such as atherosclerosis and aneurysms, and neurological diseases such as spinal cord injury (SCI), multiple sclerosis (MS), intracerebral hemorrhage (ICH), and ischemic stroke and cancer. While MMP-12 is primarily associated with tissue remodelling and repair, its deregulation has been implicated in cancer progression and metastasis. Here, we'll look at how selective MMP-12 inhibitors can be used to treat various malignancies and disorders that are related to them.

The majority of the MMP-12 inhibitors have three important pharmacophoric properties in common, which includes a zinc binding group, a hydrophobic moiety and a hydrogen bond doner and acceptor group. Among these three properties the zinc-binding group is crucial for anchoring the inhibitor to the active site and blocking the enzymatic activity of MMP-12

The use of quantitative structure-activity relationship (QSAR) and quantitative structure-property relationship (QSPR) studies are one of the most used statistical techniques to the biological properties of a molecule from the known chemical structure. The utilization of

QSAR/QSPR is often employed in the early drug development processes such as lead discovering and lead optimization. Additionally, they have been employed in screening and enrichment processes to find compounds that are hazardous or non-druglike substances. Specific MMP-12 inhibitors with dibenzofuran and dibenzothiophene moiety have been investigated in order to shed insight on these and maybe contribute to the development of a therapeutic treatment. In this study, a series of potential MMP-12 inhibitors were subjected to a combined inter-validatory ligand-based QSAR and structure-based molecular modelling study to determine the key structural components and how they affect these compounds' ability to inhibit MMP-12.

(Jigme Sangay Dorjay Tamang)

Chapter 1: Introduction

According to the World Health Organization (WHO) cancer is one of the fastest growing diseases. Every tissue in the body has the possibility to grow into some form of cancer. Cancer affects one out of every five men and six women [1-2]. Among all these cases, Lung cancer is the 2nd most common cancer around 2.2 million new cases worldwide and around 1 million deaths as represented in **Figure 1** [3]. Globally lung cancer death by smoking is around 80% whereas the other factors include exposure to air pollution and person having a lung cancer history [4]. Small cell lung cancer (SCLC) and non-small cell lung cancer (NSCLC) are the two main kinds of lung cancer, out of which 86% of the lung cancer comprises of NSCLC. They can be divided into subgroups type's squamous cell carcinoma 30%, large scale carcinoma 10%, and adenocarcinoma 50% [3]. The treatment of lung cancer mainly consists of a combination of different methods like chemotherapy, immunotherapy, radiotherapy, target therapy and surgical resection [5].

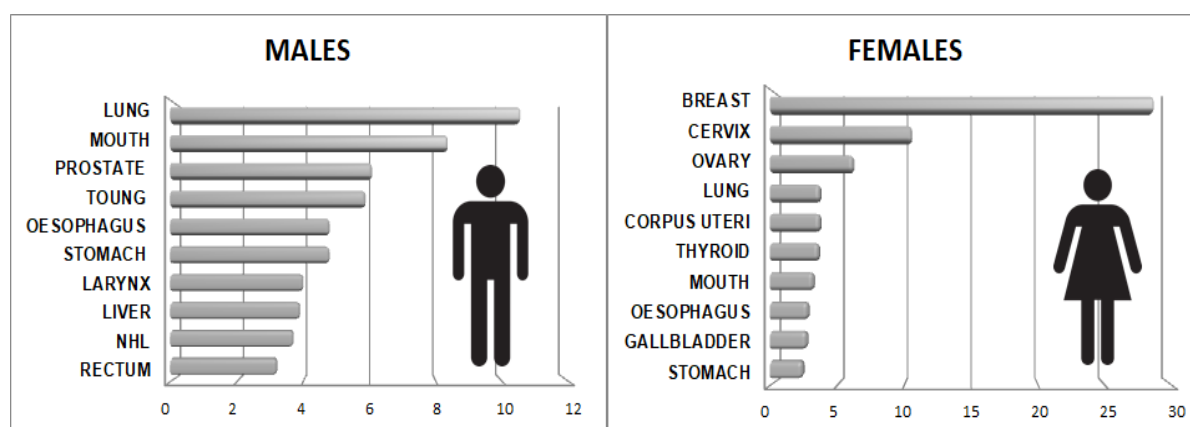


Figure 1: Cancer related death in male and female.

The Matrix metalloproteinase (MMPs) are calcium and Zn^{2+} dependent proteolytic enzymes involved in physiological and pathological processes in humans [6]. Although earlier studies revealed that these MMPs had little activity against extracellular matrix (ECM), it was later found that these enzymes were involved in processes other than ECM breakdown [6]. Pro-peptide sequences, catalytic metalloproteinase domains with catalytic Zn^{2+} ions, hinge portions or linker peptides, and hemopexin domains are among the typical structural components of MMPs.[7]. These MMPs are implicated in a wide range of pathophysiological conditions, including arthritis, cancer, neurological disorders, cardiovascular disease, etc. This protease family consists of 26 members and is further split into six subclasses based on structural and functional characteristics. These subclasses include membrane-type MMPs, collagenases, gelatinases, stromelysin, matrilysin, and other types of MMPs [8]. Matrix

metalloproteinase-12 (MMP-12) is a peptidase from the M10 subfamily of the matrix metalloproteinase (MMP) family that is found on chromosome 11q22 [9]. MMP-12, also known as macrophage metalloelastase, was initially identified as a kind of metalloproteinase produced as a result of an inflammatory response in 1975.[10]. The human MMP-12 that is in its inactive form consists of 54kDa protein and then after the loss N-terminal residue it generates around 45kDa form and then only 22kDa is obtained as the active form due to loss C- terminal residues [11]. MMP-12, however has a controversial role in the development of cancer even though MMPs are known to promote tumor formation.[12]. Additionally, lung tumor growth acts by cleaving with elastin, which is produced by activated macrophages that are typically present in lung illnesses like chronic obstructive pulmonary disease (COPD) and emphysema [13]. There is relatively little information available on how the immune response may affect someone with COPD since it might lead to lung cancer [14]. MMP-12 is associated with lungs as the pro-inflammation allergen in chronic airway remodelling, ECM degradation that involves emphysema, asthma, and lung cancer [12]. Only few people who smoke heavily acquire cancer despite the enormous mutational load that accumulates in their lung tissue.[14]. The expression of MMP-12 has been observed in other types of cancer such as adamantinomatous craniopharyngioma (ACP), colorectal cancer, gastric cancer and liver cancer [10]. Due to its numerous associations with cancer and pathophysiological diseases, MMP-12 has gained attention as a possible target for therapeutic improvements.

To predict a molecule's biological qualities from its known chemical structure, statistical techniques like quantitative structure-activity relationship (QSAR) and quantitative structure-property relationship (QSPR) studies have been utilised [15-16]. Drug discovery procedures like lead discovery and lead development optimization frequently make use of QSAR/QSPR. Additionally, they have been employed as screening and enrichment methods to find toxic substances and non-drug-like substances.[17]. These may be clarified by specific MMP-12 inhibitors, which may also help in the development of a novel treatment [18]. As a result, a series of compounds having MMP-12 inhibitory activity were put through combined inter-validatory ligand-based and structure-based QSAR molecular modelling studies to determine the key structural attributes and their impact on the MMP-12 inhibitory activity.

1.1 Classification of MMPs

Based on the substrate specificity of MMPs, six major classes have been identified.. These are collagenase, gelatinase, stromelysin, matrilysin, membrane type and other type MMP [19]. The detailed classification of the MMPs has been given in Table 1.

Table 1: Classification of MMPs

Sub-types	MMP No	Chromosome	MW kDa pro/active	Domain
Collagenase				
Interstitial collagenase	MMP-1	11q22.3	55/45	Signal peptide, pro domain, catalytic, Hemopexin-like
Neutrophil-collagenase	MMP-8	11q22.3	75/55	Signal peptide, pro domain, catalytic, hemopexin-like
Collagenase-3	MMP-13	11q22.3	60/48	Signal peptide, pro domain, catalytic, hemopexin-like
Collagenase-4	MMP-18	12q14	70/53	Signal peptide, pro domain, catalytic, hemopexin-like
Gelatinases				
Gelatinase-A	MMP-2	16q13-21	72/63	Signal peptide, pro domain, catalytic, hemopexin-like, fibronectin
Gelatinase-B	MMP-9	20q11.2-q13.1	92/86	Signal peptide, pro domain, catalytic, hemopexin-like, fibronectin
Matrilysins				
Matrilysin-1	MMP-7	11q-q22	29/20	Signal peptide, pro domain, catalytic
Matrilysin -2/Endometase	MMP-26	11p15	28/19	Signal peptide, pro domain, catalytic
Stromelysins				
Stromelysin-1	MMP-3	11q22.3	57/45	Signal peptide, pro domain, catalytic, hemopexin-like
Stromelysin-2	MMP-10	11q22.3	57/44	Signal peptide, pro domain, catalytic, hemopexin-like

Stromelysin-3	MMP-11	22q11.23	51/44	Signal peptide, pro domain, catalytic, hemopexin-like
Membrane type				
MT1-MMP	MMP-14	14q11-q12	66/56	Signal peptide, pro domain, catalytic, hemopexin-like, type 1 transmembrane, cytoplasmic
MT2-MMP	MMP-15	16q13-q21	72/50	Signal peptide, pro domain, catalytic, hemopexin-like, type 1 transmembrane, cytoplasmic
MT3-MMP	MMP-16	8q21	64/52	Signal peptide, pro domain, catalytic, hemopexin-like, type 1 transmembrane, cytoplasmic
MT4-MMP	MMP-17	12q24.3	57/53	Signal peptide, pro domain, catalytic, hemopexin-like, GPI anchor
MT5-MMP	MMP-24	20q11.2	57/53	Signal peptide, pro domain, catalytic, hemopexin-like, type 1 transmembrane, cytoplasmic
MT6-MMP	MMP-25	16p13.3	25-34/28	Signal peptide, pro domain, catalytic, hemopexin-like, GPI anchor
Others				
Macrophage metallo elastase	MMP-12	11q22.2-q22.3	54/45-22	Signal peptide, pro domain, catalytic, hemopexin-like
RASI-1	MMP-19	12q14	54/45	Signal peptide, pro domain, catalytic, hemopexin-like
Enamelysin	MMP-20	11q22.3	54/22	Signal peptide, pro domain, catalytic, hemopexin-like
XMMP from Xenopus	MMP-21	11q24	62/49	Signal peptide, pro domain, catalytic, hemopexin-like
CMMP from chicken	MMP-23	1p36.3	28/19	Signal peptide, pro domain, catalytic, cysteine array region, IgG-like domain

➤ Collagenases

Collagenases consist of four subgroups that are Interstitial collagenases (MMP-1), Nutrophil-collagenases (MMP-8), Collagenases-3 (MMP-13) and Collagenases-4 (MMP-18). These have an ability to cleave with the triple helix into characteristics 3/4 and 1/4 fragments. The other

function of the collagenases is to proteolytically process the ECM proteins and number of bioactive molecules such as interleukin-8 (IL-8), protumor necrosis factor (TNF α), protease-activated receptor-1, and several insulin-like growth factor binding proteins (IGFBPs) [19-20]

➤ Gelatinases

The gelatinases have been subdivided into gelatinase-A (MMP-2) and gelatinase-B (MMP-9). The fibronectin domain located inside the catalytic domain present in the MMPs allows binding and denaturation of the collagen and gelatin. The key role of these enzymes is the remodelling of collagenous ECM, due to which they degrade most of the molecules such as collagens type I, IV, V, VII, X, IX, fibronectin, aggrecan, vitronectin, laminin, which also includes nonECM molecules and pro-TNF α [20].

➤ Stromelysins

Stromelysins are subdivided into two groups stromelysin-1 (MMP-3) and stromelysin-2 (MMP-10). It was observed that they have similar structural design as collagenases that can degrade many ECM components but cannot cleave with the native collagens. Stromelysins can remove the propeptide domain of the three procollagenases by the activation pro MMP. The other subtype of stromelysins known as stromelysin-3 (MMP-11) has similar structural features as stromelysin 1 and 2 but has been divided into different subtype due to some additional features [20-22].

➤ Matrilysins

Matrilysins are also subdivided into two categories that are matrilysin-1 (MMP-7) and matrilysin-2 (MMP-26). They are expressed in different pathological conditions under normal circumstances and have been involved in the progression of different types of cancer. They are known to degrade ECM molecules like laminin, type IV collagen, entactin and non-ECM molecules and promote embryo implantation and remodelling of postpartum uterus [20].

➤ Membrane type MMPs (MT-MMPs)

There are around six subtypes of membrane-type metalloproteinases (MT-MMPs) in the MMP family. They are usually designated as MT1-MMP (MMP-14), MT2-MMP (MMP-15), MT3-MMP (MMP-16), MT4-MMP (MMP-17), MT5-MMP (MMP-24) and MT6-MMP (MMP-26) [23]. All MT-MMP have a transmembrane domain, but they are mainly differed by two major features: MT1-, MT2-, MT3-, and MT5-MMP have a short cytoplasmic tail, while MT4- and MT6-MMP have a glycosylphosphatidyl inositol anchor. [24]. However, several in-vivo and in-vitro studies illustrated the role of MT-MMPs in promoting cell migration, invasion, experimental metastasis, angiogenesis for the development of various forms of cancer [25].

➤ Other MMPs

In the case of other MMPs, which includes MMP-9, MMP-12, MMP-19, MMP-20, MMP-21 and MMP-23, only MMP-12 is the most widely studied MMP [19]. MMP-12 is known to be expressed by lung stromal cells. MMP-12 expression rises when macrophages are activated traditionally with LPS and considerably more so when they are activated alternatively by IL-4, whereas in the case of MMP-19, they are expressed by monocytes, macrophages, fibroblasts and endothelial cells which depends on the ERK1/2 and p38 signalling pathways [26]. Out of all these MMPs, MMP-20 was initially cloned from porcine enamel organ and from human odontoblasts which belongs to the gene family. Their overexpression may also lead to different types of cancer like pancreatic ductal carcinoma laryngeal squamous cell carcinoma [27]. In the case of MMP-21 and MMP-23 both are cloned, where MMP-21 has been cloned from placenta DNA and MMP-23 has been cloned from an ovary cDNA library. There are very few studies that have been associated with these MMPs specifically [28-29].

Structure of MMP-12 enzyme

MMPs consists of a zinc-binding sequence like HExxHxxGxxH/D due to which they have been categorized within the metzincin superfamily, they also called as Met-turn due to an invariant methionine-containing 1,4-b-turn [30]. All the MMPs including MMP-12 consist of three domains that are the N-terminal propeptide domain, the protease or the catalytic domain and the C-terminal, hemopexin-like domain that has a molecular mass of 54 kDa. Whereas, in the case of MMP-12, stromelysin-1 (MMP-13) and interstitial collagenase (MMP-1) they are the most closely related to MMP-12 as it has 49% similarity. The domain 1 consists of an N-terminal proenzyme having a mass of 9 kDa including a short signalling peptide and highly conserved cysteine residue with a proenzyme that coordinates the zinc. The domain II consists of the catalytic domain with a molecular mass of 22 kDa that consist of the zinc-binding HExxHxxGxxH sequence motif. Domain III consists of a C-terminal (hemopexin-like) that has a molecular mass of 23 kDa which exhibits sequence homology to vitronectin and hemopexin represented in **Figure 2** [31-32].

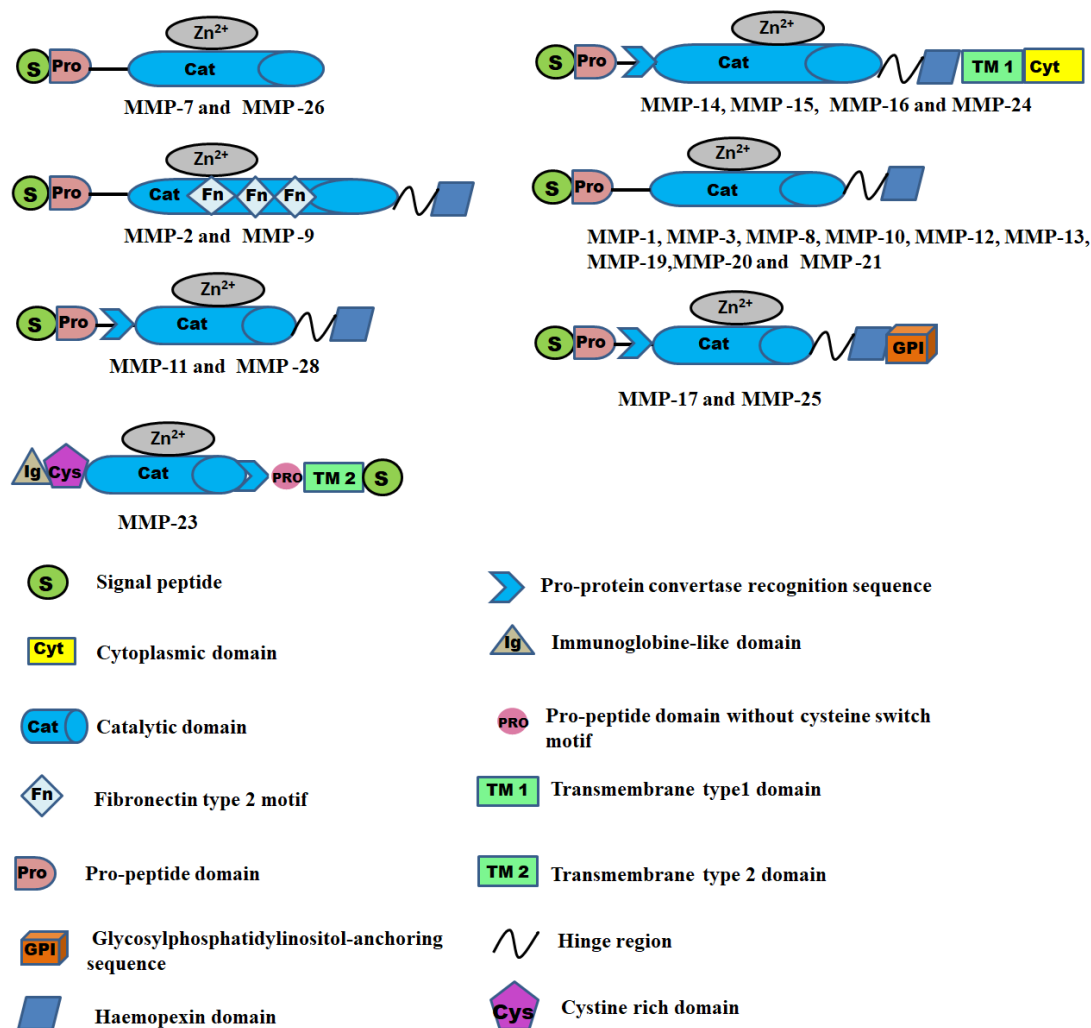


Figure 2: Classification of MMPs based on structural domain.

Structural Similarity of MMP-12 in comparison with other MMPs

When compared to the structure of MMP-12 with other MMPs, they have similar 3D structures, but the main difference occurs in the size of the S1-pocket mainly due to the sequence variability and the length S1-loop and the position of the amino acids. For MMP-1 and MMP-7 they have large residues like arginine and tyrosine due to which their pocket size is small and closed. In the case of MMP-3, MMP-8 and MMP-13 the pocket size is much larger as it has only leucine residue [33]. MMP-12 S1-loop is similar to that of MMP-8 as both of them have similar one helical turn at residues D244-F248, but whereas, in respect to 3D shape and S1-pocket pocket they are very similar to MMP-3 and MMP-13 [34].

Activation of MMP-12

It has been well established that MMPs play a vital role in many levels of in-vivo regulation. Initially, MMPs are secreted in the extracellular environment as a proenzyme which is inactive or in a dormant state and later it is activated subsequently by proteolytic removal of the propeptide [31]. The mechanism by which the activation of the proMMPs by in vivo method is still not clear [35]. However, the activation of the proMMP-12 can be done by various factors such as organomercurials, serine proteinases, acid exposure and hypochlorous acid. Several studies have demonstrated the activation of active MMPs intermolecular from proMMPs [36]. There are several physiological activators, including plasmain, plasma kallikrein, neutrophil elastase, and cathepsin G [37]. According to the research on the biochemistry of the activation process, pro-MMPs have the ability to change its conformation that may result in the self-cleavage of the roughly 80 N-terminal amino acids [35]. Prior to the ultimate cleavage of the remaining propeptide, which necessitates a major rearrangement of the enzyme's structural elements, it was found that initial proteolysis of the residues between the α -helx and destabilisation of the Cys-Zn connection had an influence on the activation of MMPs [38]. In the case of MMP-12 proenzyme that has a molecular weight of 54 kDa which consists of three domains the N-terminal propeptide domain, the catalytic domain and the C-terminal, hemopexin like domain is activated, after activation it loses its N-terminal domain and forms a 45 kDa enzyme. In the end, it loses the C-terminal domain that has a molecular mass of 23 kDa and forms the 22 kDa active MMP-12 the activation process has been represented in Figure 3 [35-39].

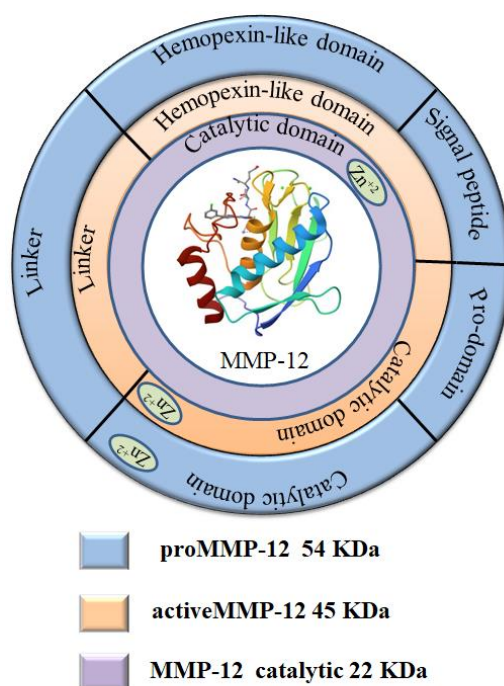


Figure 3. Activation of MMP-12

Crystal structure of MMP-12 inhibitors

The crystal structure of MMPs has been divided into a different class of MMP inhibitors that includes hydroxamic acids, phosphinic acids and thiols. There are around 85 MMP-12 crystal structures that have been derived from humans and bacteria. These crystal structures were mainly identified by using two methods: X-ray crystallography and NMR-solution. The crystals that have been discovered to date have been represented in Table 2. The crystal structure is very important as it helps in the designing of disease-specific selective MMP-12 inhibitors by identifying the active site in the protein structure.

Table 2: Crystal structure of MMP-12 inhibitors.

PDB ID	Method	Sequence length	Organism	Ligand	Binding affinity	Reference
1OS2/1OS9	X-RAY Diffraction	165	Homo sapiens	Acetohydroxamic acid	--	[40]
1JIZ	X-RAY Diffraction	166	Homo sapiens	N-Hydroxy-2(R)-[[[(4-Methoxyphenyl)Sulfonyl](3-Picolyl)Amino]-3-Methylbutanamidehydrochloride	IC ₅₀ =2 nM	[35]

1JK3	X-RAY Diffraction	158	Homo sapiens	4-(N-Hydroxy Amino)-2R-Isobutyl- 2S-(2-Thienylthiomethyl)Succinyl- L-Phenylalanine-N-Methylamide	--	[41]
1RMZ	X-RAY Diffraction	159	Homo sapiens	N-isobutyl-N-[4- Methoxyphenylsulfonyl]Glycyl Hydroxamic Acid	Ki=4.3 nM	[42]
1ROS	X-RAY Diffraction	163	Homo sapiens	[2-(1,3-Dioxo-1,3-Dihydro-2H- Isoindol-2-yl)Ethyl]-4-(4'-Ethoxy- 1,1'-Biphenyl-4-YL)-4-Oxobutanoic Acid	IC ₅₀ =1.7 nM	[43]
1YCM	X-RAY Diffraction	159	Homo sapiens	N-Isobutyl-N-[4- methoxyphenylsulfonyl]glycyl hydroxamic acid	Ki=4.3 nM	[42]
1UTT	X-RAY Diffraction	159	Homo sapiens	2-(1,3-Dioxo-1,3-Dihydro-2H- Isoindol-2-yl) Ethyl-4-(4'-Ethoxy [1,1'-Biphenyl]-4-YL)-4- Oxobutanoic Acid	IC ₅₀ =2400 0 nM	[42]
1UTZ	X-RAY Diffraction	159	Homo sapiens	(2R)-3-({[4-[(Pyridin-4-yl)Phenyl]- Thien-2- yl]Carboxamido)(Phenyl)Propanoic acid	IC ₅₀ =14 nM	[42']
1Y93	X-RAY Diffraction	159	Homo sapiens		Kd=80000 00 nM	[42]
1Z3J	X-RAY Diffraction	159	Homo sapiens	N-isobutyl-N-4- Methoxyphenylsulfonyl]Glycyl Hydroxamic Acid	Ki=4.3 nM	[42]
2HU6	X-RAY Diffraction	159	Homo sapiens	(1S,5S,7R)-N-7-(Biphenyl-4-yl Methyl)-N-3-Hydroxy-6,8-Dioxa-3- Azabicyclo[3.2.1]Octane-3,7- Dicarboxamide	IC ₅₀ =1490 00 nM	[44]
2JXY	NMR solution	194	Homo sapiens		--	[45]
2KRJ	NMR solid-state	152	Homo sapiens		--	[46]
2K9C	NMR solution	152	Homo sapiens		--	[47]
2K2G	NMR solution	165	Homo sapiens	N-(Dibenzo[b,d]Thiophen-3-yl Sulfonyl)-L-Valine	Kd=7.4 nM	[48]

2MLR	NMR solution	164	Homo sapiens	1,2-DimyristoyL-sn-Glycero-3-Phosphocholine	--	[49]
2MLS	NMR solution	164	Homo sapiens	1,2-Dimyristoyl-sn-Glycero-3-Phosphocholine	--	[49]
2N8R	NMR solution	164	Homo sapiens	--	--	[50]
2OXU	X-RAY Diffraction	159	Homo sapiens	--	--	[51]
2OXW	X-RAY Diffraction	159	Homo sapiens	--	--	[51]
2OXZ	X-RAY Diffraction	159	Homo sapiens	--	--	[51]
2POJ	NMR solution	164	Homo sapiens	--	--	[52]
2WO8	X-RAY Diffraction	164	Homo sapiens	Beta Hydroxy Carboxylic Acid	IC ₅₀ =520 nM	[53]
2WO9	X-RAY Diffraction	164	Homo sapiens	Beta Hydroxy Carboxylic Acid	IC ₅₀ =62 nM	[53]
2WOA	X-RAY Diffraction	164	Homo sapiens	Beta Hydroxy Carboxylic Acid	IC ₅₀ =1150 nM	[53]
2W0D	X-RAY Diffraction	164	Homo sapiens	N-Hydroxy-2(R)-[[4-Methoxyphenyl)Sulfonyl](3-Picolyl)Amino]-3-Methylbutanamide Hydrochloride	IC ₅₀ =2 nM	[54]
3BA0	X-RAY Diffraction	365	Homo sapiens	Acetohydroxamic acid	--	[45]
3EHX	X-RAY Diffraction	158	Homo sapiens	I-2-(Biphenyl-4-yl Sulfonamido)-4-Methylpentanoic Acid	Ki=25 nM	[55]
3EHY	X-RAY Diffraction	158	Homo sapiens	I-2-(4-MethoxyphenylSulfonamido)Propanoic Acid	Ki= 1400 nM	[55]
3F15	X-RAY Diffraction	158	Homo sapiens	2-[[4(2S)-2,3-Dihydroxypropyl)-(4-Methoxyphenyl)Sulfonyl-Amino]-N-oxo-Ethanamide	Kd=7.88 nM	[56]
3F16	X-RAY Diffraction	158	Homo sapiens	(2R)-3-Hydroxy-2-[(4-Methoxyphenyl)Sulfonylamino]-N-oxo-Propanamide	Kd=5.91 nM	[56]

3F17	X-RAY Diffraction	158	Homo sapiens	N-(2-Nitroso-2-Oxoethyl)Biphenyl- 4-Sulfonamide	Ki=2 nM	[56]
3F18	X-RAY Diffraction	158	Homo sapiens	4-Fluoro-N-(2-Hydroxyethyl)-N-(2- Nitroso-2-oxo Ethyl)Benzenesulfonamide	Kd=39.5 nM	[56]
3F19	X-RAY Diffraction	158	Homo sapiens	4-Fluoro-N-(2-Nitroso-2- Oxoethyl)Benzenesulfonamide	Kd=65.1 nM	[56]
3F1A	X-RAY Diffraction	158	Homo sapiens	N-(2-Nitroso-2- Oxoethyl)Benzenesulfonamide	Kd=61.1 nM	[56]
3LIK	X-RAY Diffraction	159	Homo sapiens	Non-Zinc Chelating Inhibitor	Ki=1.92 nM	[57]
3LIL	X-RAY Diffraction	159	Homo sapiens	Non-Zinc Chelating Inhibitor	Ki=8.3 nM	[57]
3LIR	X-RAY Diffraction	159	Homo sapiens	Non-Zinc Chelating Inhibitor	Ki=119 nM	[57]
3LJG	X-RAY Diffraction	159	Homo sapiens	Non-Zinc Chelating Inhibitor	Ki=18.6 nM	[57]
3LKA	X-RAY Diffraction	158	Homo sapiens	Hydroxamic Acid and Paramethoxy- Sulfonyl Amide	Ki= 1500000 nM	[58]
3LK8	X-RAY Diffraction	158	Homo sapiens	N-hydroxy-N-2-[(4- Methoxyphenyl)Sulfonyl]Glycinami de	Ki=20 nM	[56]
3N2U	X-RAY Diffraction	158	Homo sapiens	N-Hydroxy-2-{[(4- Methoxyphenyl)Sulfonyl](2- {[(2R,3R,4S,5S,6R)-3,4,5- Trihydroxy-6- (Hydroxymethyl)Tetrahydro-2H- Pyranyl]oxy}Ethyl)Amino}Acetamide	Ki=14.3 nM	[59]
3N2V	X-RAY Diffraction	158	Homo sapiens	N-hydroxy-2-(N- Hydroxyethyl)Biphenyl-4- ylSulfonamido)Acetamide	Ki= 31 nM	[59]
3NX7	X-RAY Diffraction	158	Homo sapiens	N-Hydroxy-2-(N-(2- Hydroxyethyl)4- Methoxyphenylsulfonamido)Acetam ide	Ki=7.6 nM	[56]

3RTS	X-RAY Diffraction	158	Homo sapiens	N-Hydroxy-N-2-[(2-Phenylethyl) Sulfonyl]Glycinamide	Ki=23 nM	[60]
3RTT	X-RAY Diffraction	158	Homo sapiens	N-hydroxy-1-[(2- Phenylethyl)Sulfonyl]-D- Prolinamide	Ki=16 nM	[60]
3TS4	X-RAY Diffraction	159	Homo sapiens	L-Glutamate Motif Inhibitor	Ki=1.9 nM	[61]
3TSK	X-RAY Diffraction	159	Homo sapiens	L-Glutamate Motif Inhibitor	Ki=317 nM	[61]
4ESF	X-RAY Diffraction	159	Homo sapiens	L-Glutamate Motif Inhibitor	Ki = 2.5 nM	[61]
4GQL	X-RAY Diffraction	159	Homo sapiens	RXP470.1	Ki=0.26 nM	[61]
4GR0	X-RAY Diffraction	159	Homo sapiens	RXP470B	Ki=0.28	[62]
4GR3	X-RAY Diffraction	159	Homo sapiens	RXP470A	Ki=15.5 nM	[62]
4GR8	X-RAY Diffraction	152	Homo sapiens	RXP470C	Ki=14.7 nM	[62]
4H30	X-RAY Diffraction	159	Homo sapiens	--	--	[63]
4H49	X-RAY Diffraction	159	Homo sapiens	--	--	[63]
4H76	X-RAY Diffraction	159	Homo sapiens	Hydroxamate Inhibitors	--	[63]
4H84	X-RAY Diffraction	159	Homo sapiens	Carboxylate Based Inhibitors	--	[63]
4IJO	X-RAY Diffraction	158	Homo sapiens	--	--	[64]
4I03	X-RAY Diffraction	159	Homo sapiens	PEG-linked Bifunctional L- Glutamate Motif	--	[63]
4EFS	X-RAY Diffraction	159	Homo sapiens	L-Glutamate Motif Inhibitor	IC ₅₀ =2.5 nM	[60]
5CXA	X-RAY Diffraction	159	Homo sapiens	RXP470	--	[65]
5CZM	X-RAY Diffraction	159	Homo sapiens	N-[(2s)-3-[(s)-(4- Bromophenyl)(Hydroxy)Phosphoryl	Ki=0.19- 0.26 nM	[65]

]-2- {[3-(3'-Chlorobiphenyl-4-yl)-1,2-Oxazol-5-yl]Methyl}Propanoyl]-1-Alpha-Glutamyl-1-Alpha-Glutamine		
5D2B	X-RAY Diffraction	159	Homo sapiens	RXP470	--	[65]
5D3C	X-RAY Diffraction	159	Homo sapiens	N-[(2R)-2- {[3-(3'-Chlorobiphenyl-4-yl)-1,2-Oxazol-5-yl]Methyl}-4-(Hydroxyamino)-4-Oxobutanoyl]-L-Alpha-Glutamyl-L-Alpha-Glutamine	--	[65]
5I0L	X-RAY Diffraction	159	Homo sapiens	Sugar-Conjugated Arylsulfonamide Carboxylate Water-Soluble Inhibitor (DC27)	IC ₅₀ =18 nM	[66]
5I4O	X-RAY Diffraction	159	Homo sapiens	N-({1-[2-(Acetylamino)-2-Deoxy-Beta-D-Glucopyranosyl]-1H-1,2,3-Triazol-4-yl}Methyl)-N-([1,1'-Biphenyl]-4-yl)sulfonyl]-D-Valine	--	[66]
5I2Z	X-RAY Diffraction	159	Homo sapiens	Sugar-conjugated Triazole-linked Carboxylate Chelating Water-Soluble Inhibitor (DC24).	--	[66]
5I3M	X-RAY Diffraction	159	Homo sapiens	Sugar-conjugated thiourea-linked Carboxylate Zinc-Chelator Water-Soluble Inhibitor (DC31)	--	[66]
5I43	X-RAY Diffraction	159	Homo sapiens	sugar-conjugated triazole-linked carboxylate chelator water-soluble inhibitor (DC32)	--	[66]
5LAB	X-RAY Diffraction	159	Homo sapiens	N-Isobutyl-N-[4-Methoxyphenylsulfonyl]Glycyl Hydroxamic Acid	Ki=4.3 nM	[67]
5L79	X-RAY Diffraction	159	Homo sapiens	RXP470.1 Conjugated with Fluorophore Cy5,5 in space group P21212.	Ki=0.26 nM	[68]
5L7F	X-RAY Diffraction	159	Homo sapiens	K421A I complex RXP470.1 conjugated with Fluorophore Cy5,5 in space group P21	Ki=0.19-0.26 nM	[68]

5N5J	X-RAY Diffraction	158	Homo sapiens	3-(5-(1,2-Dithiolan-3-yl)Pentanamido)Propane-1-Sulfonate	--	[69]
5N5K	X-RAY Diffraction	156	Homo sapiens	5-(1,2-Dithiolan-3-yl)-N-(3-Hydroxypropyl)Pentanamide	--	[69]
6RD0	X-RAY Diffraction	159	Homo sapiens	AP280	Ki= 1.7700 nM	[70]
6ENM	X-RAY Diffraction	159	Homo sapiens	LP168	IC ₅₀ =4.8 nM	[71]
6EOX	X-RAY Diffraction	159	Homo sapiens	LP165	IC ₅₀ = 140-170 nM	[71]
6EKN	X-RAY Diffraction	159	Homo sapiens	BE7	IC ₅₀ =510 nM	[71]
6ELA	X-RAY Diffraction	159	Homo sapiens	BE4	IC ₅₀ =26 nM	[71]
6RLY	X-RAY Diffraction	159	Homo sapiens	AP316	Ki= 17500 nM	[70]
7OVY	X-RAY Diffraction	159	Homo sapiens	JG34	--	[69]
8B2N	X-RAY Diffraction	158	Homo sapiens, Tannerella forsythia	--	--	[72]

1.2 Role of MMP-12 in cancer

It is established that most of the MMPs are degrading the extracellular matrix as it is the root cause for the acceleration of the cancer progression [73]. Numerous studies have shown that MMPs are essential for the growth of various forms of tumor invasion and metastasis.. Matrix metalloproteinase-12 also known as matrix metalloelastase has the ability to degrade plasminogen into angiostatin, as it can stop tumor angiogenesis [74-75]. Among the different types of MMPs, MMP-2 has high significant as it has a direct relation to cancer pathogenesis. Other MMPs such as MMP-8, -9, -12, and -14 act as anti-targets of cancer means their inactivation by exogenous compounds causes cancer [29]. All the MMPs have come under the consideration of gelatinase enzyme possess a Zn²⁺ ion as metallic atom MMP degrade the extracellular matrix which is composed of two types of sugar says glycosaminoglycan and proteoglycan as well as three types of proteins fibronectin, collagenase, and elastase by

degradation of the extracellular matrix of vascular endothelial cells of blood vessel [30]. MMP-12 has been proven to be one of the most efficient angiostatin-producing MMPs [76]. The expression of MMP-12 has also been associated with different types of cancer like hepatocellular carcinoma (HCC), colorectal carcinoma, pancreatic cancer, non-small cell lung cancer (NSCLC), renal cell carcinoma, skin cancer and vulva carcinoma [77]. There has been numerous experiments that have been conducted on animal models mainly mice to point out how the expression of MMP-12 is linked with cancer.

MMP-12 in hepatocellular carcinoma (HCC)

Hepatocellular carcinoma (HCC) has one of the highest cancer-related deaths in the world and is the 6th most commonly diagnosed cancer. In vitro experiments have been conducted to find out the role of MMP-12 in HCC. Man et al., [78] reported an in-vitro experiment that had been conducted on rat liver transplantation model on the whole and small- for- size (50%) graft, to find out the molecular mechanism of tumour invasiveness. Using cDNA microarray analysis and quantitative RT-PCR study, gene signatures of acute phase graft damage (days 1 and 3) and late-phase tumour recurrence (days 14 and 21) were evaluated. The result indicated the overexpression of numerous inflammatory markers like CXCL10, IL-6 were present in the small-size graft. The RTPCR studies also confirmed that the CXCL10 was expressed not only in the early phases but also in the later phase. It was found that increased expression of these markers in tumor tissue of the small-for-size grafts in the late phase will not only increase macrophage infiltration, which has a direct impact on the tumor microenvironment but will also induce liver cancer cells to express invasion-related characteristics. Rivas et al., [77] studied the expression of human macrophage metalloelastase (HME) mRNA expression and angiotensin generation in HCC. The tissue of 40 patients with HCC who went under partial hepatectomy having tumorous and non-tumorous tissue was obtained. It was found that 25 out of 40 samples detected the presence of HME mRNA using the Northern blot hybridization, whereas western blot was used to find out the angiostatin expression and they were significantly linked with HME mRNA. The tumor tissue of the patient which did not show any signs of HME mRNA and angiostatin had a very low survival rate. Thus, MMP-12 may act as a predictive indicator and help in the survival of people suffering from HCC and may be targeted for designing inhibitors in the future.

MMP-12 in non-small cell lung cancer (NSCLC)

Non-small cell lung cancer (NSCLC) is one of the most common types of cancer. There have been numerous cases where a number of MMPs like the MMP-1, MMP-9, and MMP-12 have been related to NSCLC. Hofmann et al., [79] reported the expression of MMP-12 in NSCLC in human tissue, as they have performed numerous techniques like the DNA microarray techniques to find out the expression of MMPs in surgically treated NSCLC patients and then validated using RT-PCR and immunohistology. The test results revealed that, compared to non-tumor cells, the expression of MMP-12 was very high in tumor cells, followed by the expression of other MMPs. Ellila et al., [80] performed a test for the indication of MMP-12 in human lung cancer using methods like tissue array and published non-small cell lung cancer gene expression database. The report indicated that the presence of a high level of MMP-12 mRNA in NSCLC was the reason for the poor patient survival rate.

MMP-12 in gastric cancer

MMP-12 is known to enhance tumour invasion and metastasis in different types of cancer, so different types of in-vitro experiments have been conducted. In the case of squamous cell carcinoma in humans, it was detected that the expression of the MMP-12 both in-vivo and in-vitro and the amount of MMP-12 expression level as well as the tumor progression was very high, but in the case of gastric cancer, the role of MMP-12 is still unknown [81]. Other methods like gene therapy, where there is the transfer of the MMP-12 gene has been observed for the treatment of different types of cancer in animal models may be used for the treatment of gastric cancer [75-77]. Zheng et al., [82] reported the investigation for the association of MMP-12 in gastric cancer. Two types of tissue were used normal and gastric cancer tissue and the expression of MMP-12 was obtained by histological staining. It was found that the MMP-12 was one of the mediators associated with the progression of gastric cancer. It may also act as a diagnostic marker for patients suffering from gastric cancer.

MMP-12 in colorectal carcinoma (CRC)

Colorectal carcinoma (CRC) or colorectal cancer is the third and the fourth most common cancer in both males and females. With more than 1.9 million cases and 9,30,000 cancer-related

deaths recorded globally in 2020, it is one of the most prevalent human malignant neoplasms [84]. As of now, the most standard therapy for colorectal cancer is surgery, or in combination with chemotherapy is the only means for treatment, but this eventually led to recurrence and metastasis. Thus, it is very crucial to develop a new therapeutic target for CRC by exploring the molecular mechanism [84]. Nguyen et al., [85] detected a functional single nucleotide polymorphism (SNP) and they are -82A→G (rs2276109) and -77A→G (rs2252070) for MMP-12 and MMP-13. They conducted a study on DNA extraction and genotype determination using the TaqMan system on 385 CRC patients as well as 619 control subjects. It was found out patients with MMP-12 (rs2276109) and MMP-13 (rs2252070) genotypes had a higher risk of having CRC.

MMP-12 in other diseases

In many cases, it was observed that MMP-12 was expressed in mRNA and protein levels which depend on the state of cellular differentiation due to the absence of the monocytes. The diseases like (COPD), emphysema, asthma, skin diseases, arthritis, vascular diseases (atherosclerosis, aneurysms) and neurological diseases (spinal cord injury (SCI), multiple sclerosis (MS), Theiler murine encephalomyelitis, intracerebral hemorrhage (ICH), ischemic stroke) and many other diseases have shown the presence of MMP-12 during the clinical and experimental studies [86].

MMP-12 in chronic obstructive pulmonary diseases (COPD)

In the case of chronic obstructive pulmonary disease (COPD), MMP-12 has been observed to play an important role in in-vitro studies that were conducted on alveolar macrophages represented in **Figure 4**. These studies indicated the positive sign of MMP-12 macrophage in both COPD and control samples [83]. The mechanism by which COPD releases MMP-12 is still unknown, but based on animal experiments, it may be caused due to lack of transforming growth factor 1 (TGF-1), an increase in interleukin-13 (IL-13), or a decrease in interferon- γ (IFN- γ) that has caused MMP-12 to be produced [87]. Demedts et al., [87] performed studies where induced sputum samples were collected from patients suffering from COPD (n = 28), healthy smokers (n = 14), never-smokers (n = 20), and former smokers (n = 14). The identification of the induced sputum was done using enzyme-linked immuno sorbent assay (ELISA), whereas fluorescence quenched substrate that is cleaved by casein zymography has been used for the evaluation of the enzymatic activity in induced sputum. It was found that the

level of MMP-12 was very high in patients suffering from COPD as compared to healthy smokers, non-smokers and former smokers. Therefore, this indicates that MMP-12 is released only during COPD but not in the case of smoking.

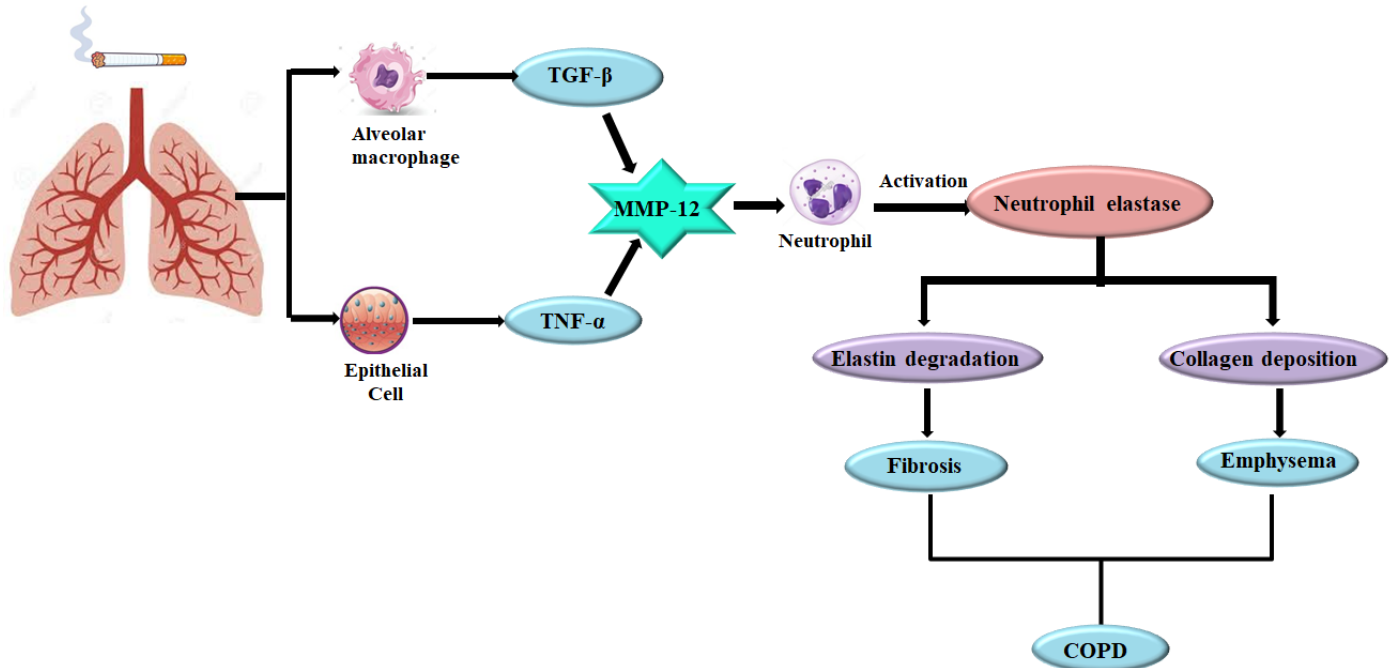


Figure 4: Mechanism by which COPD is induced.

MMP-12 in spinal cord injury (SCI)

In the case of spinal cord injury, the determination of the MMP-12 was done in the rat model. It was observed that from the 3 days of post SCI there was an increase in MMP-12 mRNA. In the 5th day, it was observed that the release of MMP-12 after injury was mainly from the cells of the mononuclear phagocyte lineage. In the other experiment which was conducted using mice with deleted MMP-12 gene and wild-type mice, it was found that the mice without MMP-12 genes had significantly recovered faster than the other type of mice. However, till now the molecular mechanism of MMP-12 that contributes to the cause of SCI is still unknown [88].

MMP-12 in aortic dissection (AD) and coronary artery diseases (CAD)

Serious heart conditions like aortic dissection (AD) and diseases like coronary artery disease (COD) are caused by elastin degradation. About 2 to 5% of deaths worldwide account for AD and CAD. Song et al., [89] performed tests to find out the expression of MMP-12 in AD and CAD. The serum samples of 15 patients who had Aortic dissection at the time of aortic

replacement were taken. The samples from 10 healthy people who acted as the control group were also taken. Methods like reverse transcriptase polymerized chain reaction (RT-PCR), Western blotting, immuno-histochemistry, fluorescence resonance energy transfer (FRET) activity assay and enzyme-linked immuno sorbent assay (ELISA) were used to find out the expression of MMP-12. The level of MMP-12 in AD and CAD was much higher as compared to healthy patients.

MMP-12 in cardiovascular diseases (CVD)

There are some experiments that have been conducted to show the effects of MMP-12 on cardiovascular diseases (CVD). The conditions like atherosclerosis have been the steppingstones for the development of CVD. The experiment that was conducted using human MMP-12 in transgenic rabbits has shown elevated levels of atheroma when they were given a diet of fatty steak [90-91]. However, more experiments have been conducted; Johnson et al., [92] used apolipoprotein-E (Aop-E) and MMP-12 knock-out mice for the comparative study of atherosclerosis plague. It was observed that there was a decrease in the level of atherosclerosis plague in MMP-12 knock-out mice as compared to only Aop-E knock-out mice. This indicates the level of MMP-12 is directly related to atherosclerosis, which also indicates that the higher the release of MMP-12, the more will be the risk for CVD.

Chapter 2: Literature Review

Tumor metastasis accounts for a major amount of the morbidity and death associated with malignant illness. Metastasis formation is a complicated process that requires the execution of a series of discrete steps in a timely and successful manner to create a tumor in a distant place. Several of these biological mechanisms such as primary tumor vascular invasion malignant cell extravasation into the target organ, and suitable angiogenesis assumed to occur at the new site of tumor development require the presence of matrix metalloproteinase. The MMP family consists of 26 members and has the ability to destroy extracellular matrix proteins. All MMPs have a common NH₂-terminal a zinc-containing pro-enzyme domain [93]. Retrospective analysis suggests that the inclusion of strong zinc-binding groups, such as hydroxamate functionalities, potentiates MMP inhibition, but regrettably in an indiscriminate manner, impacting most members of the MMP family as well as other unrelated zinc-proteinases. The addition of a less avid zinc-binding group, such as the phosphoryl group found in phosphinic peptide transition state analogs, has resulted in a second generation of more selective MMP inhibitors, such as MMP-12 (macrophage-metalloelastase) selective inhibitors [94]. Recent discoveries indicating MMP-12 overexpression in numerous human illnesses, such as emphysema, support the push for the creation of highly selective MMP-12 inhibitors. A harmful role for MMP-12 overexpression was recently attributed to a large clinical investigation searching for a relationship between both asthma and chronic obstructive lung disease and single-nucleotide polymorphisms in the gene encoding MMP-12 [94]. In some cases, MMP-12 overexpression may lead to tumor invasion and metastasis in different types of cancer like hepatocellular cancer, gynecological cancer, prostate cancer, colorectal cancer, and endometrial cancer. In addition, MMP-12 has also been reported to regulate tumor angiogenesis and may be required to activate the angiogenic switch that occurs during tumor neovascularization [95].

2.1 An overview of the reported MMP-12 inhibitors

Over the years several studies have indicated that the expression of MMP-12 may lead to various types of pathological disorders such as COPD, emphysema, inflammatory diseases, and different types of cancer like lung cancer, liver cancer, prostate cancer, breast cancer and skin cancer. Due to the involvement of MMP-12 in different diseases and conditions, there has always been a desire to develop selective MMP-12 inhibitors that can act on different pathological conditions [96]. Therefore, apart from the potential MMP-12 inhibitors as well as the binding mode of interactions analysis have been studied in detail to gain an idea of the designing of potent selective MMP-12 inhibitors. Several companies have been trying to

develop MMP-12 inhibitors but have failed mainly due to toxicity and adverse problems during their development. AstraZeneca is one of these companies that claimed their compounds to be specific MMP-12 inhibitors. Apart from that, other companies also claimed to have compounds with MMP-12 inhibitory activity like Ranbaxy produced MMP-9/MMP-12 dual inhibitors, Serono disclosed MMP-2/MMP-9/MMP-12 triad inhibitors, Medivir disclosed MMP-12 inhibitors, Novartis on the other hand produced MMP-9/MMP-12/MMP-13 triad inhibitors and Pfizer disclosed MMP-12/MMP-13 dual inhibitors namely CP-271485 and PF-0035623 [97].

Li et al., [98] reported a selective MMP-12 inhibitor known as MMP408, used for the treatment of COPD. Out of the dibenzofuran-based derivative (MMP408), compound **1** and **2** (**Figure. 5**) was selected based on higher MMP-12 inhibitory activity of (MMP-12 IC_{50} = 2 and 0.9 nM) when compared between these two compounds in the series. Compound **2** was had better exposure and bioavailability than the other compounds. Compound has been tested in the mouse model for lung inflammation, it was found that compound **2** showed better in-vivo results and was advanced for further pre-clinical evaluation. The compound **2** also had lower potency in rodents as compared to other human MMPs but had very good metabolic stability when the studies were carried out in rats, dogs, monkeys and humans.

Li et al., [99] reported a continuation of the above research, where MMP-12 inhibitors having a dibenzofuran and dibenzothiophene moiety was used for the treatment of airway inflammation and remodelling. The compound **3** in (**Figure. 5**) was obtained from potent MMP-12 and MMP-13 inhibitors through lead optimization. The compound **3** is the extension of compound **2**. It was selected based on its good physicochemical properties and had the highest MMP-12 inhibitory activity (MMP-12 IC_{50} = 1.4 nM). The pharmacological studies were performed which implicated that the compound had good oral efficacy in MMP-12 induced ear swelling.

Wu et al., [100] reported an extension of the above two research, selective MMP-12 inhibitors having a dibenzofuran and dibenzothiophene scaffold as a potential treatment of asthma. A series of synthesis and structural activity relationships (SAR) had been done to find out the compounds having a potent MMP-12 inhibitory property. Compound **3** also known as (MMP118) in (**Figure. 5**), was selected based on the physical properties and had good MMP-12 inhibitory activity (MMP-12 IC_{50} = 1.4 nM). The crystal structure of compound **2** had good solubility and had shown negative results for Ames and hERG tests. The in vitro profiling and

pharmacokinetic experiments revealed good oral effectiveness in MMP12-induced ear-swelling inflammation and pulmonary inflammation in animal models.

Various syntheses have been performed using different types of analog to design potent selective MMP-12 inhibitors. Ando et al., [101] designed and synthesized potent MMP-12 inhibitors. They have explored the effect of pyrrole ring in an ageladine A analogous having MMP-12 inhibitory activity. Compound **4** (**Figure. 5**) was found to be the potent and had an inhibitory activity (MMP-12 IC_{50} = 1,240 nM). The SAR studies were performed, and this indicated the introduction of the halogen group at the 2nd and 4th positions of the pyrrole ring of the ageladine A analog highly increased the MMP-12 inhibitory activity.

Ando and Tarshima [102] continued their study on ageladine A analog and synthesised 37 ageladine A derivatives by employing the natural synthetic rules of ageladine A. Out of the 37 compounds, only one was selected based on its inhibitory activity, which is a dibromoimidazole analog represented as compound **5** (**Figure. 5**) (MMP-12 IC_{50} = 860 nM). The SAR studies indicated that the presence of the halogen group at the 3rd and 4th positions was very important for potency, whereas the proton at the 1st and the halogen at the 2th position were important for MMP-12 inhibitory activity.

Mannino et al., [103] reported a 3-aza-6,8-dioxa-bicyclo[3,2,1]octane scaffold (BTA) to which they used a structure-based approach to design compounds having good MMP-12 inhibitory activity by screening from the virtual library. The molecule with the highest hit was synthesized and the binding site of the compound was identified by using NMR. The X-ray structure was also done to find out the ligand-enzyme interaction. The compound **6** (**Figure. 5**) had the highest inhibitory activity (MMP-12 IC_{50} = 149 μ M). It was observed that the N-hydroxyurea group in the 3rd position and the p-phenylbenzylcarboxy amide in the 7th position showed an improved affinity and selectivity towards MMP-12 and other MMPs.

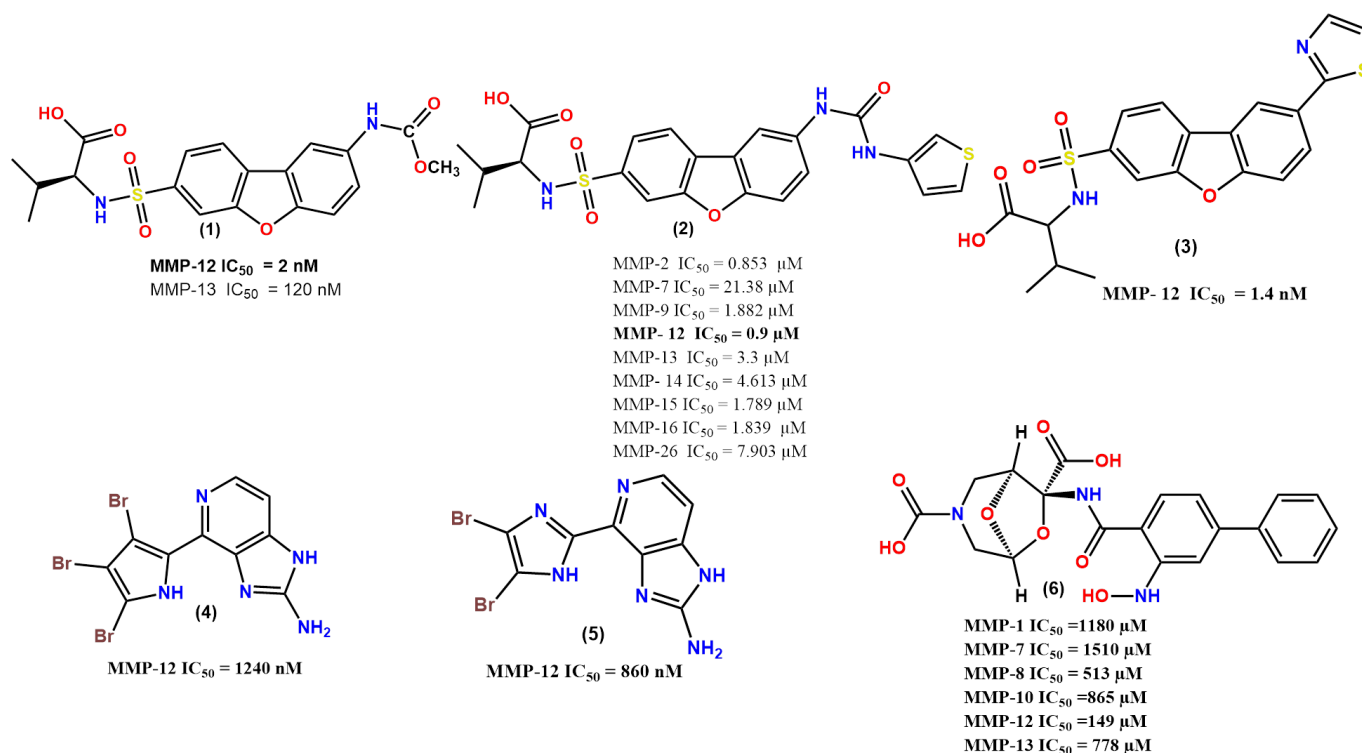


Figure 5: Some selective MMP-12 inhibitors.

Homes et al. [53] reported a β -hydroxy carboxylic acid derivatives as selective MMP-12 inhibitors were identified based on high throughput screening. Cross-screening was performed on a range of compounds, based on SAR studies compound **7** (**Figure. 6**) was selected as it had the highest MMP-12 inhibitory activity (MMP-12 IC_{50} = 0.062 nM). The X-ray crystallography was also performed to check the occupancy of the S1'pocket, compound **7** had better occupancy as compared to other compounds in the series.

Devel et al., [57] synthesized MMP-12 inhibitors without phosphinic zinc binding groups that can enter deep in the S1' cavity of the MMP-12 enzyme. Based on the MMP-12 inhibitory selectivity profile, two molecules were chosen. compound **8** and **9** (**Figure. 6**). The MMP-12 inhibitory activity of compound **8** was around 200 times better than MMP-8, whereas for compound **9** it had around 200 times better than MMP-3.

Ma et al., [104] reported tetrahydroisoquinoline based sulfonamide hydroxamates as potent matrix metalloproteinase inhibitors. The selective MMP-12 was selected based on the activity, as it had higher activity as compared to other MMPs. Compound **10** (**Figure. 6**) had potent MMP-12 inhibitory activity (IC_{50} = 0.170 μ M).

Jeng et al., [44] reported sulphonamide-based hydroxamic acid inhibitors having an MMP-12 inhibitory activity used for the treatment of chronic inflammation. Out of the three compounds that have been given, compound **11** (**Figure. 6**) was selected as it had the best MMP-12 inhibitory activity (MMP-12 IC_{50} = 0.9 μ M). Due to the presence of an optimal chain length and R-enantiomer, there was an increase in the MMP-12 inhibitory activity.

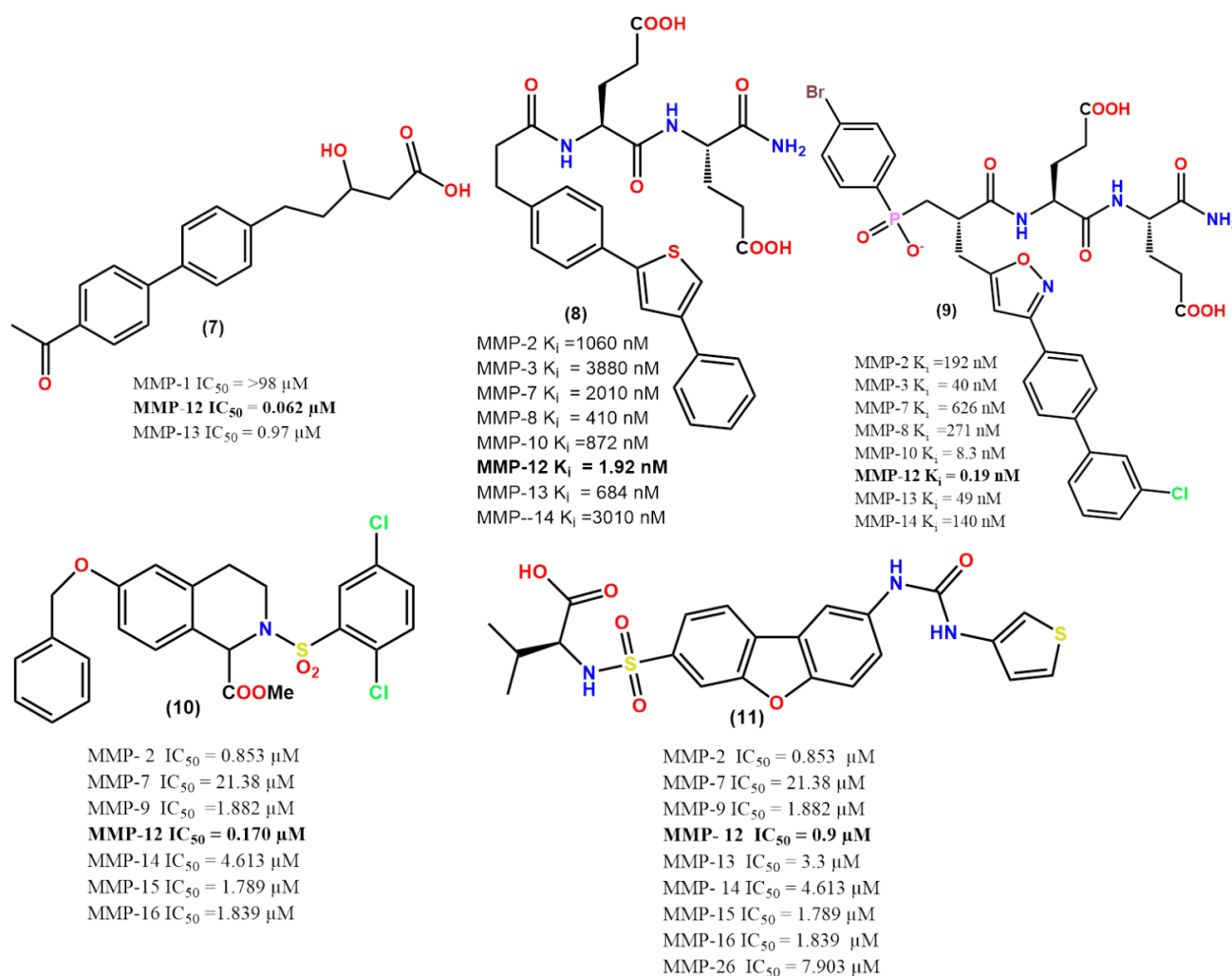


Figure 6: Some selective MMP-12 inhibitors.

Quement et al., [18] reported selective MMP-12 inhibitor AS111793 (MMP-12 IC_{50} = 20 nM) represented as compound **12** (**Figure.7**). The compound was used for the treatment of lung inflammation caused by cigarette smoking (CS) in C57BL/6 mice which were exposed to CS. It was found that compound **12** was able to reduce lung inflammation in CS exposed mice that had an MMP-12 inhibitory activity of (MMP-12 IC_{50} = 20 nM). In the Bronchoalveolar lavage

(BAL) fluid of the CS exposed mice compound **12** was able to suppress many inflammatory markers like TNF-1, MIP-1 γ , IL-6 and TIMP-1, CX3CL1, KC/CXCL1 and I-TAC/CXCL11 in lung parenchyma. As in the case of selectivity it had a selectivity of 1:30 over MMP-1, MMP-2 and 1:40 times over MMP-9.

Dublanche et al., [105] performed a structure-based designing method to a non-zinc chelating MMP-12 inhibitor. They have mainly used high throughput screening and molecular docking methods to design a compound having good MMP-12 inhibitory activity. The compound having the best MMP-12 inhibitory activity has been represented as compound **13** (**Figure. 7**) having a (MMP-12 IC₅₀= 0.014 μ M). The binding mode of compound **13** was confirmed by an X-ray crystal structure of MMP-12 having a catalytic domain complex. The information clearly shows that the biaryl moiety fits into the S1' pocket of the enzyme, where the majority of the binding interactions are hydrophobic.

Baggio et al., [106] reported compounds using techniques like NMR and structure-based guided optimization for the treatment of COPD. It is represented as compounds **14** and **15** in (**Figure. 7**). The compound **14** and **15** was further tested against various MMPs and found to be more potent than MMP408 represented as compound **2** [66] and better selective than pan-MMP inhibitor 6M6001 represented as compound **16** (**Figure. 8**). A preliminary pharmacokinetic analysis was performed by using Compound **14** in animals by intraperitoneal injections and the drug showed favourable plasma levels and half-life, it even resembled the FDA-approved proteasome inhibitor carfilzomib structurally.

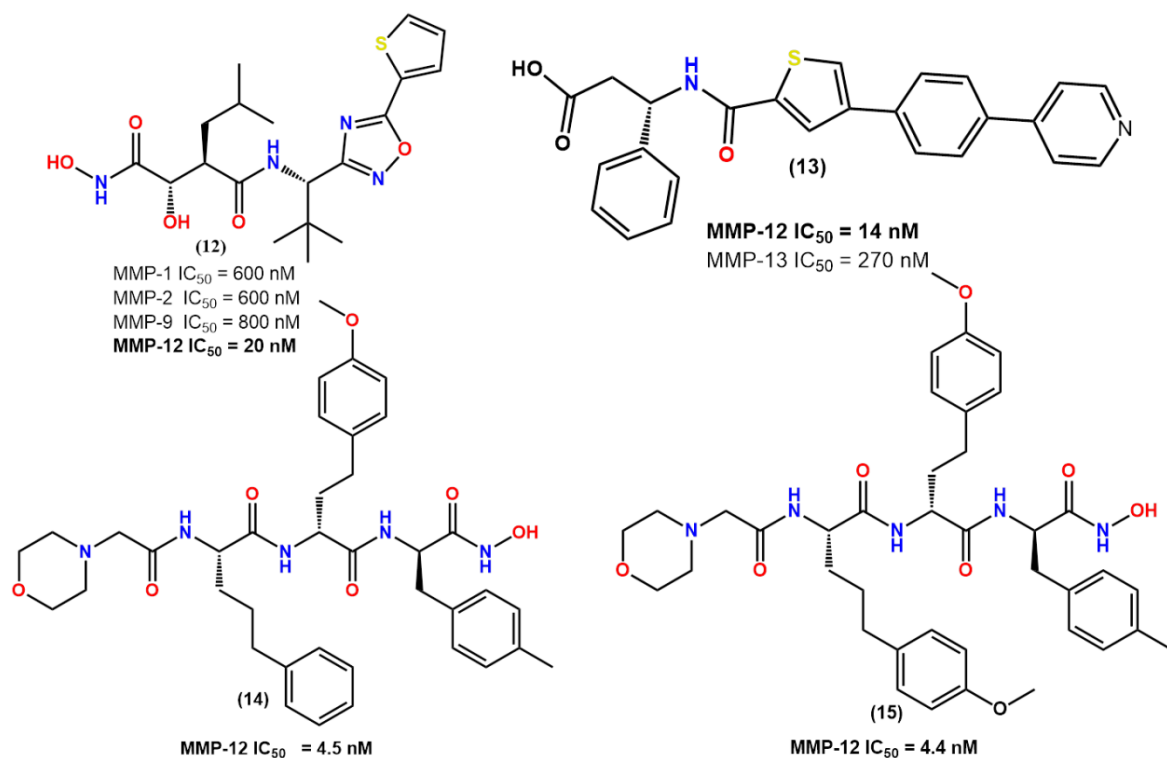


Figure 7: Some selective MMP-12 inhibitors.

Nuti et al., [107] synthesized a new class of MMP-12 inhibitors with arylsulfonamide carboxylates with improved hydrophilicity as a result of conjugation with a b-N-acetyl-d-glucosamine moiety for the development of new therapies in the treatment of lung and cardiovascular disease. The fluorimetric assay was used to assess their inhibitory activity on human MMPs, and a crystallographic analysis was carried out to find out their binding patterns. Compound **17** (**Figure. 8**) was selected based on the clogP value. The initial finding suggested that the sugar moiety, which was present in the P2, linked through a flexible linker not only improves the hydrophilicity but also improves the biological activity. Compounds **18** and **19** (**Figure. 8**) had an MMP-12 inhibitory activity of 18 nM and 12 nM respectively, and compound **18** was two-fold more selective than compound **17**.

Dragoni et al., [55] synthesised a biotin chain terminated (BCT) MMP-12 inhibitor having a high affinity for matrix metalloproteinase. Simultaneous formation of a highly stable ternary system Avidin-BTI-MMP has been assessed and the affinity of the developed BTI toward five different MMPs has been tested. Compound **20** (**Figure. 8**) having the highest MMP-12 inhibitory activity was selected, and the compound has an inhibitory value of (MMP-12 IC_{50} = 1.4 μ M).

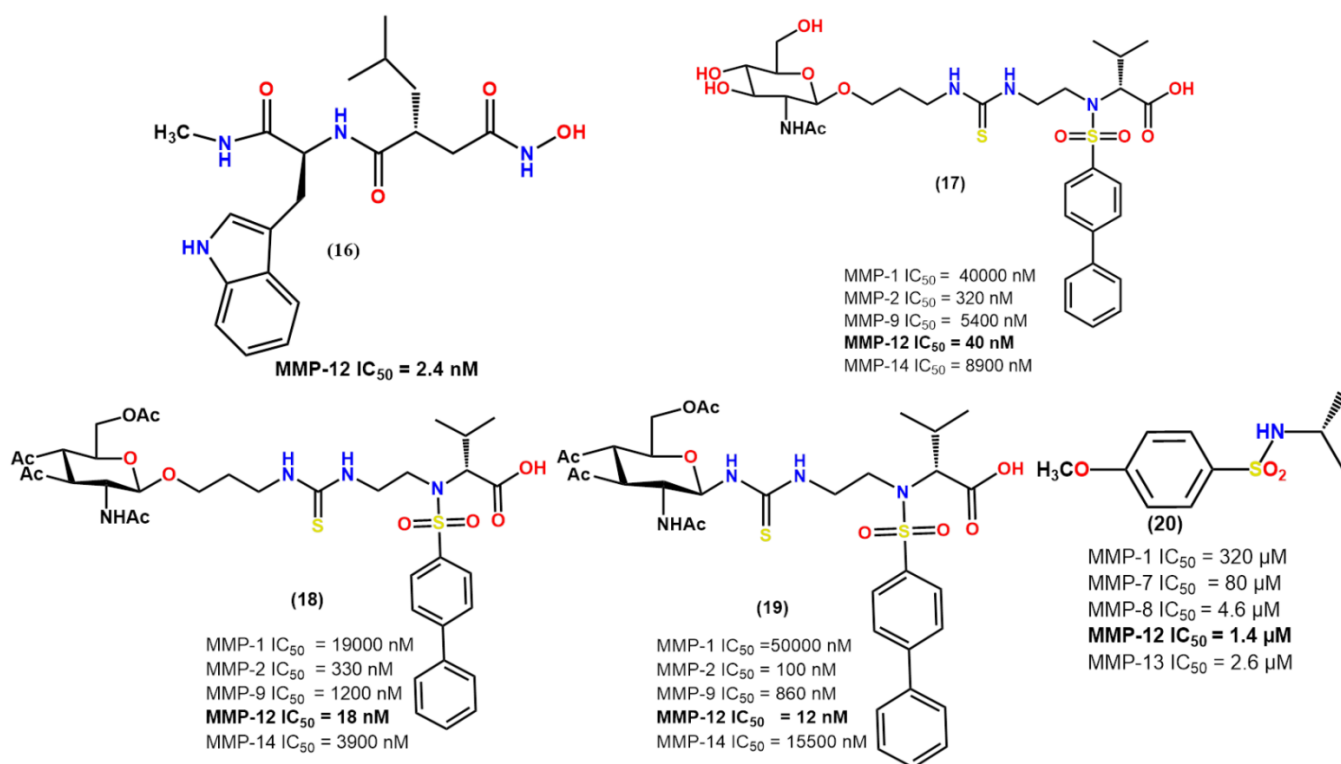


Figure 8: Some selective MMP-12 inhibitors.

Mori et al., [60] designed MMP inhibitors having an arylsulfonamide scaffold by structure-based optimization method. The compounds that were synthesized were studied using X-ray crystallography and fluorimetric assay and it showed high affinity for MMP-12. The compound **21** given in (**Figure. 9**) was selected, as it was characterized by a carboxylic acid zinc binding group which had low affinity for zinc and had strong inhibitory activity towards MMP-12. The compound **21** even had a good safety and toxicity profile and had (K_i) value of ($K_i = 7$). It was observed that compound **22** (**Figure. 9**) had a low (K_i) value of ($K_i = 1$) mainly due to the presence of the D-proline and the ethylene linker.

Aerts et al., [108] synthesized hydroxypyrrone-based matrix metalloproteinase (MMP) inhibitors and assayed their inhibitory property with other MMPs. Compound **23** (**Figure. 9**) had the selective MMP-12 inhibitory property assessed for in-vitro and in-vivo lipid-induced lethality (LPS) and inflammation-induced blood-cerebrospinal fluid barrier (BCSFB) disruption. It was found that compound **23** significantly reduced the LPS lethality and BCSFC permeability, which indicates it had anti-inflammatory activity.

Badland et al., [109] reported compounds with thiophene moiety having MMP-12 inhibitory activity. The toxicophore has been replaced by using different approaches like the replacement of the thiophene moiety. It was found that compound **24** (**Figure. 9**) where the thiophene core

was replaced with α florothiophene had good MMP-12 inhibitory activity. Further experiments were also conducted for the designing of new α florothiophene, it was found that compound **25** (Figure. 10) had even better MMP-12 inhibitory activity than compound **24**.

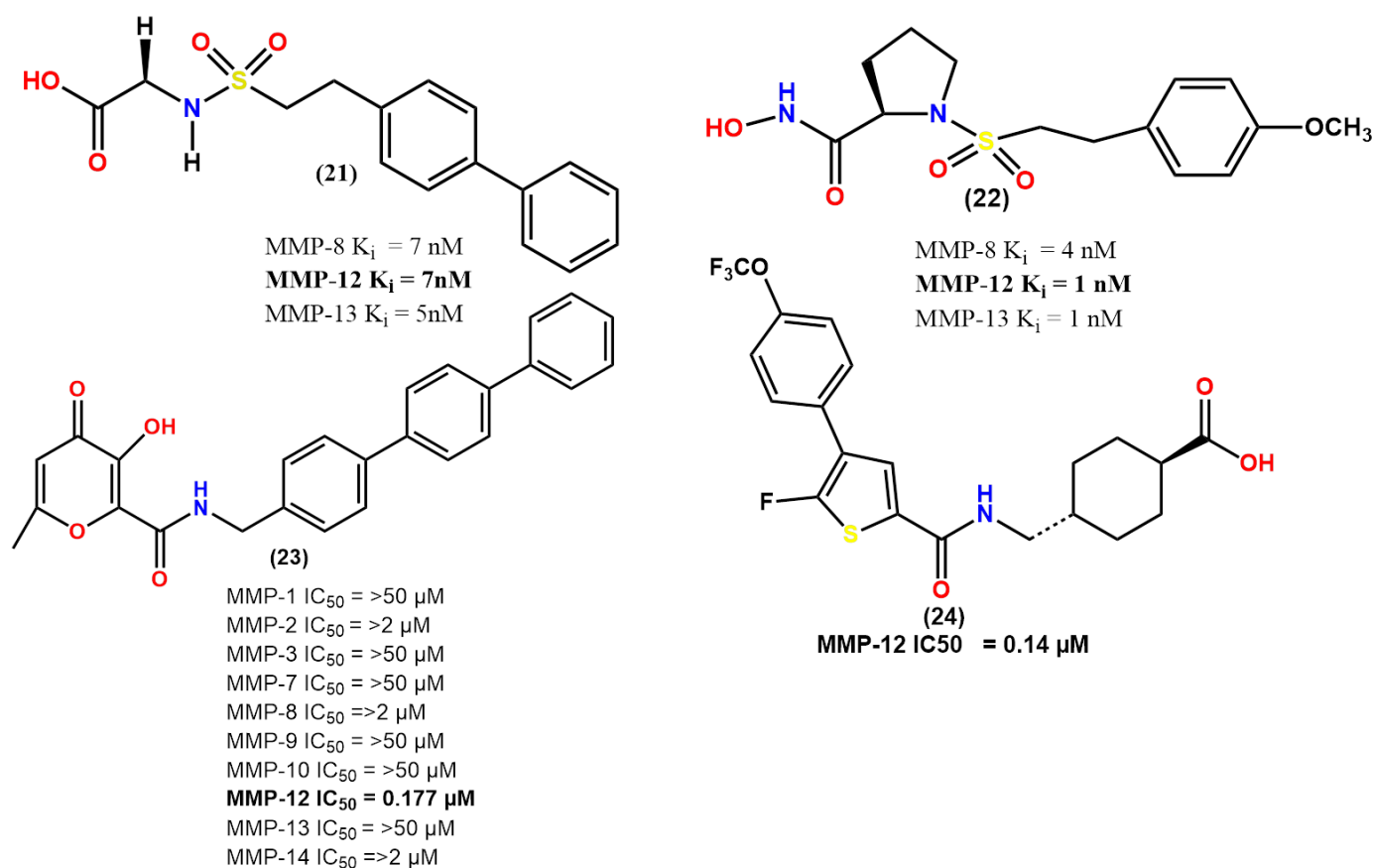


Figure 9: Some selective MMP-12 inhibitors.

Nuti et al., [110] designed and synthesised arylsulfonyl based MMP-12 inhibitors that have been linked to tissue remodelling and degradation in some inflammatory processes, such as COPD, emphysema, rheumatoid arthritis (RA), and atherosclerosis. Compound **26** (Figure. 10) was selected based on the in vitro evaluation and had MMP-12 inhibitory activity (MMP-12 IC_{50} = 0.2 nM). Compound **26** has around 17500-fold more selective than MMP-1 and 165-fold over MMP-14.

Nuti et al., [71] designed compounds having the thioaryl derivative from their earlier studies 4-methoxybiphenylsulfonyl hydroxamate and carboxylate-based inhibitors were modified to increase the selectivity for MMP-12, where they changed the zinc-binding group and the oxidation state of the sulphur. The compound **27** (Figure. 10) had an N-1-hydroxypiperidine-2,6-dione (HPD) group as ZBG. It was tested on human MMPs by using a fluorometric assay was selected based on activity and selectivity for MMP-12 (IC_{50} = 33 nM), as it was 1200 times

more selective than MMP-14, 176 times more selective than MMP-9, and 20 times more selective than MMP-2. The compound **27** was furthermore tested for cardiovascular or pulmonary pathologies in cell-based and in vivo models.

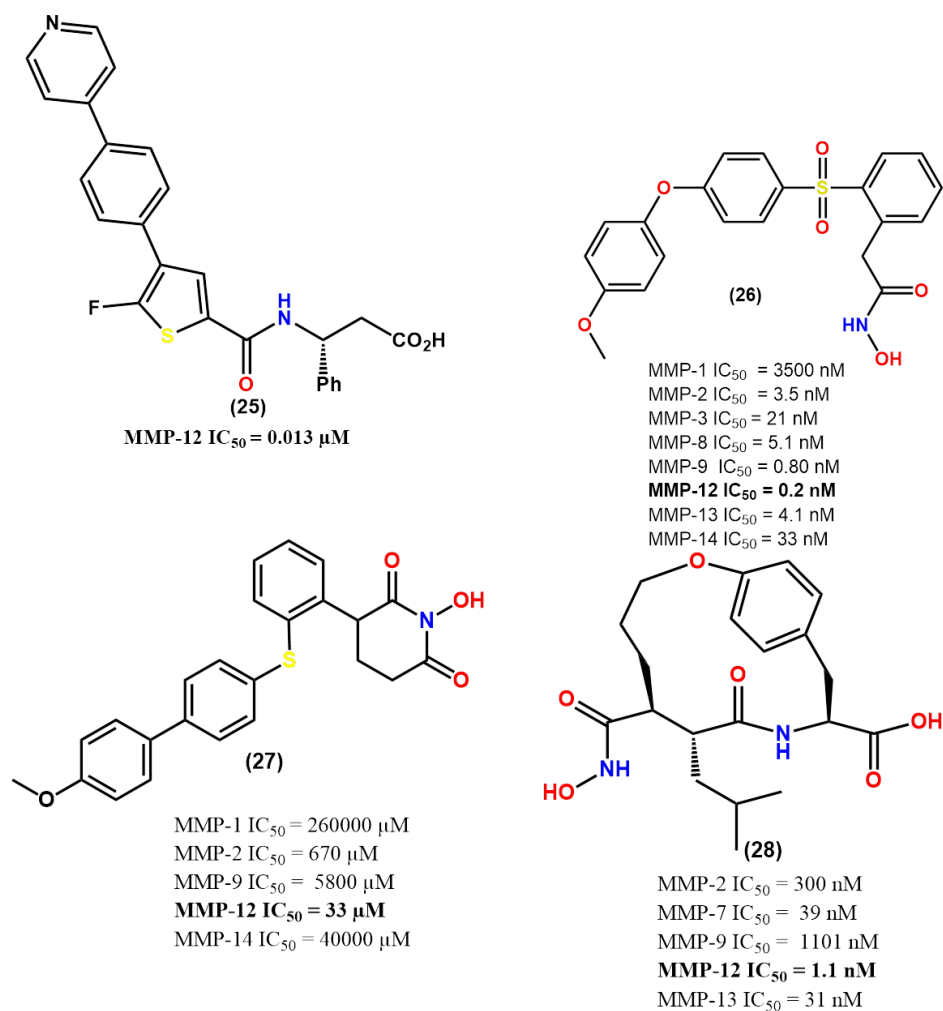


Figure 10: Some selective MMP-12 inhibitors.

Gona et al., [111] worked on MMP-12 target imaging so that it may be able to predict the abdominal aortic aneurysm (AAA) progression rupture risk and have developed three hydroxamate-based selective MMP-12 inhibitors. They are represented as compounds **28**, **29** and **30** in (Figure. 11). From compound **29** which was used as the deriving compound **31** (Figure. 10), a radiotracer ^{99m}TC-**31** was derived and was tested. The radiotracer ^{99m}TC-**31** showed faster blood clearance in mice and was radio-stable. It was also tested in murine AAA and ex vivo competition was used to demonstrate the tracer's precise binding to MMP-12.

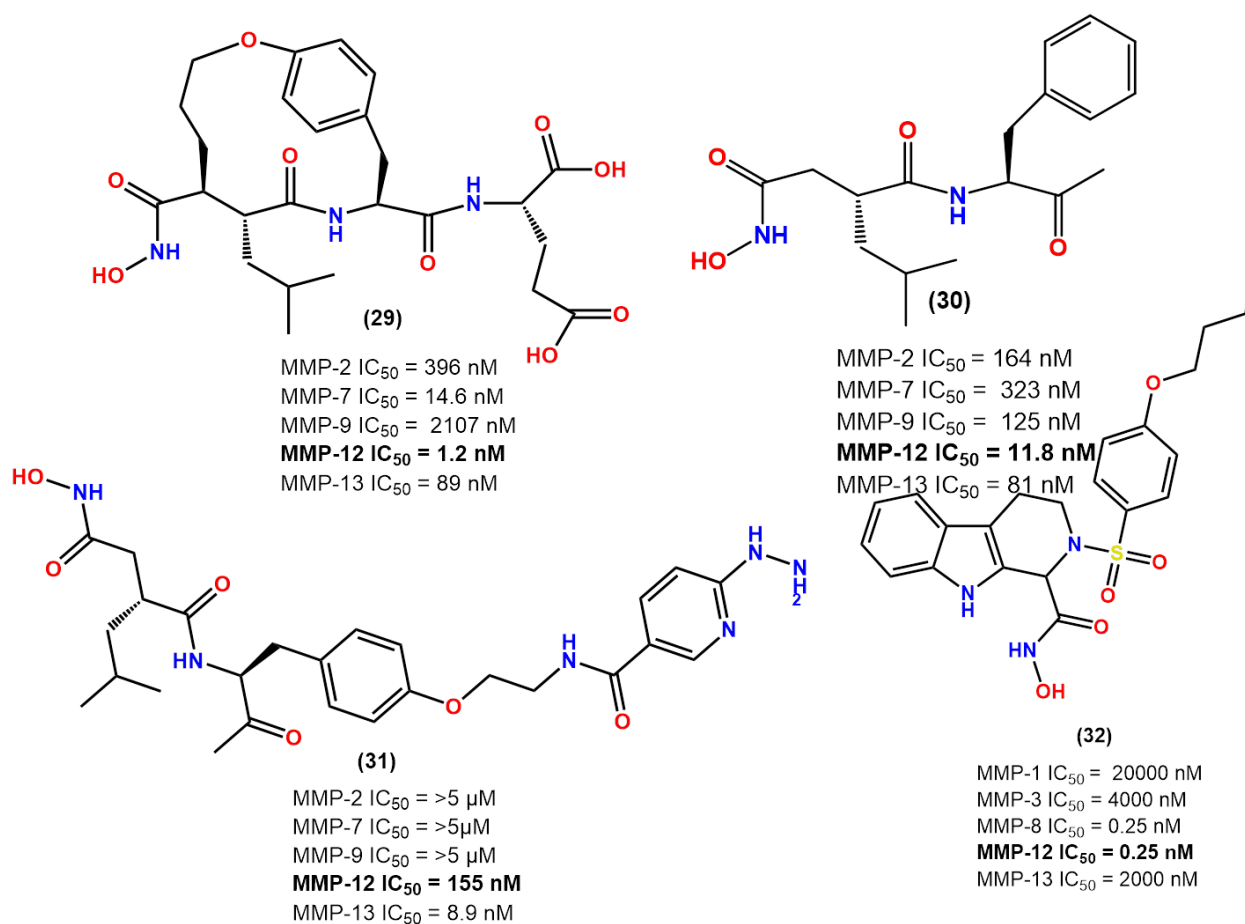


Figure 11: Some selective MMP-12 inhibitors.

Mangiatordi et al., [112] designed and synthesized some tetrahydro- β -carboline derivatives. It was observed that all the molecules showed good selective and sub-nanomolar gelatine inhibitors for the treatment of multiple sclerosis and cancer. Among these compounds, **32** (**Figure. 11**) (MMP-12 IC_{50} =0.25) and **33** (**Figure. 12**) (MMP-12 IC_{50} =0.25) showed more potent and selectivity towards MMP-12 over other MMPs.

Butsch et al., [113] designed and synthesized in vitro and in vivo evaluation of highly potent MMP-12 inhibitors. Positron Emission Tomography (PET) has been used for the diagnosis of diseases related to MMPs. Additionally, radiolabeled tracers such fluorine-18-labeled MMP inhibitors (MMPI) must be used for their specialized imaging in order to discriminate between the various roles and activities of individual MMPs in certain pathophysiological processes. As a result, fluorinated dibenzofuransulfonamide-based MMPIs were created, which exhibit superior MMP-12 inhibition and were highly selective MMP-12 over other MMPs. MMP-12 is a crucial enzyme in disorders including atherosclerosis and chronic obstructive pulmonary disease (COPD). Compound **34**, **35**, and **36** (**Figure. 12**) were selected based on high Human

Serum Albumin-binding and high metabolic stability upon incubation with mice and were selected for radiochemical resynthesis.

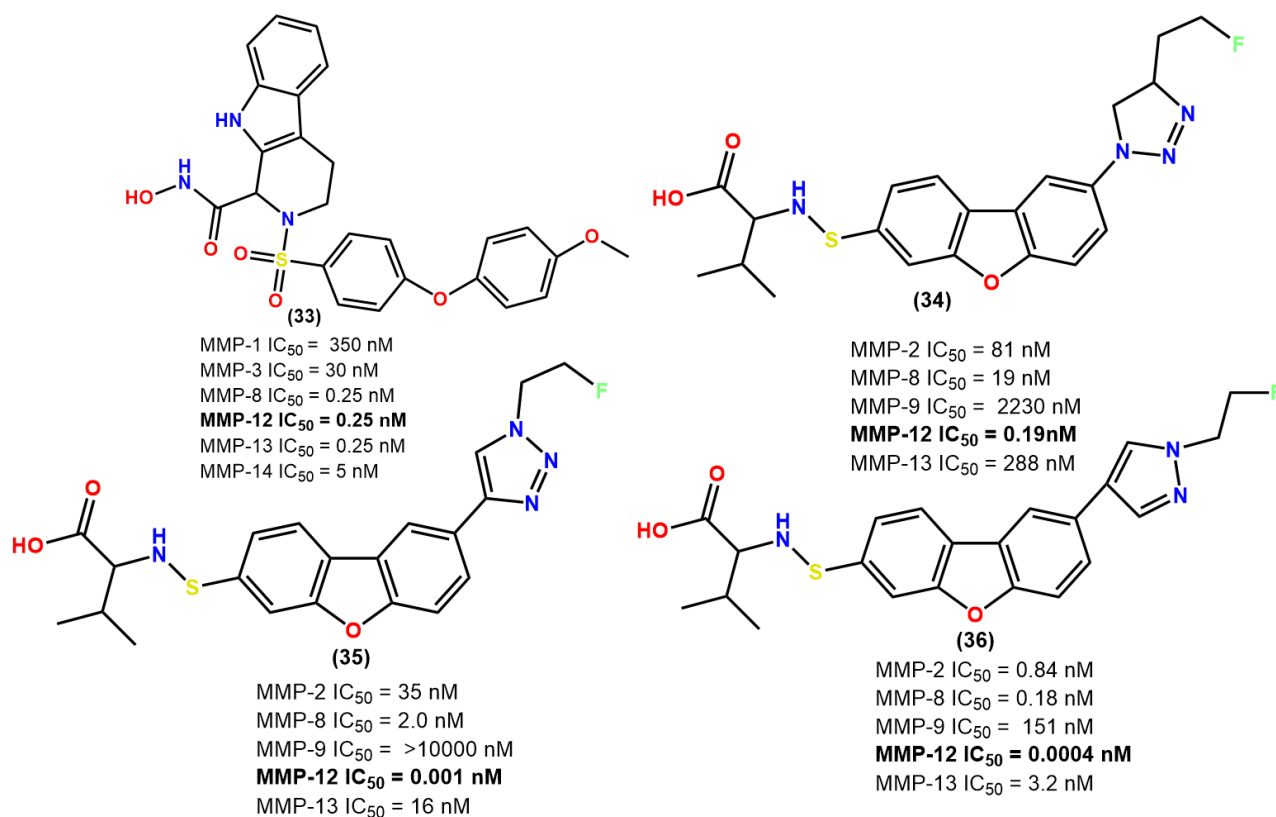


Figure 12: Some of the selective MMP-12 inhibitors.

2.2 Overviewing the QSAR studies performed on MMP-12 inhibitors

In recent years, computer-aided drug designing (CADD) techniques have been used which include ligand-based and structure-based approaches that have been used for the development of drugs. Using these strategies potent selective MMP-12 inhibitors can be designed. Some of the QSAR studies that have been conducted on compounds having an MMP-12 inhibitory activity as in the article by Shamsara et al., [114] performed a Hologram based QSAR (HQSAR) on a set of 35 molecules having an MMP-12 inhibitory activity. These molecules was divided into training ($n=26$) and the test ($n=9$) sets and the statistical performance of the model for the training set was represented by Q^2 , R^2 , and SEE , 0.697, 0.986, and 0.528 respectively. The model was externally validated using the test set having R^2_{pred} of 0.873. The colour code analysis was also represented to show the structural features of the compound. In the end, 5 new molecules were designed using the developed model. From the molecular docking studies, it was observed that the three compounds in which the docking studies were performed had a common chelation between the carboxylic and zinc binding group

heterocyclic ring did not interact with the binding pocket of MMP-12. The docked compound also had similar hydrogen bonding with the amino acid residues Leu181 and Ala 182 as well as π - π stacking with Tyr 240 and His 218 which has been given in **Figure 13**.

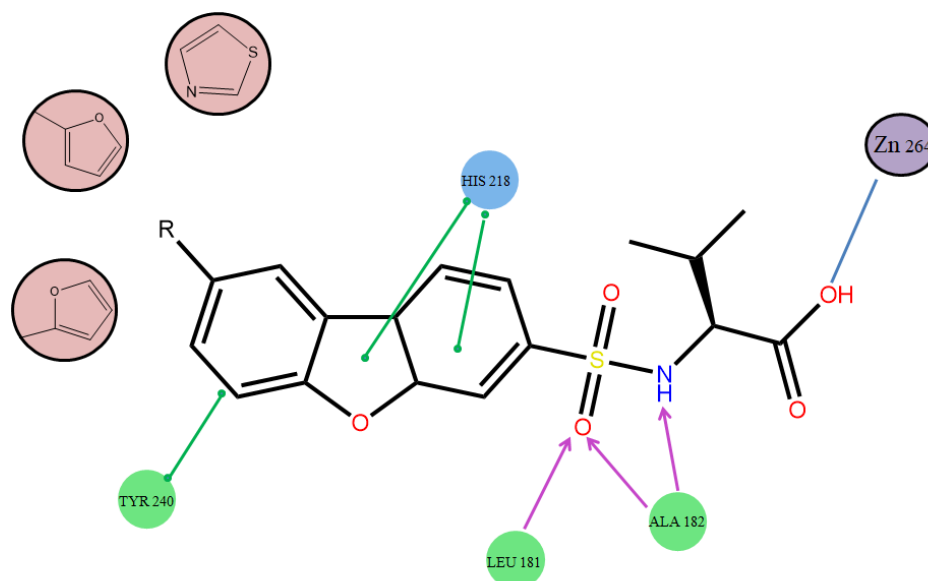


Figure 13: Similar amino acid residues observed on compounds having MMP-12 inhibitory activity.

Hadizadeh et al., [115] have performed 3D QSAR method mainly CoMFA and CoMSIA on compounds having an MMP-12 inhibitory activity. A total of 46 compound which were divided into training ($n = 38$) and test ($n = 8$) sets, the compounds were then aligned using four different methods. Using different alignment-based method the compound with the best statistical performance was selected. The contour maps for both CoMFA and CoMSIA was also represented which indicated the type of fields that have positive or negative impact on the structures. As these methods may help in the designing a potent MMP-12 inhibitor.

Singh et al., [116] performed a 3D QSAR pharmacophore based virtual screening and molecular docking study to identify potent MMP-12 inhibitors. There are 108 compounds in the data set which were divided into training ($n = 16$) and test ($n = 92$) sets. The best HypoGen pharmacophore model Hypo 1 that had two hydrogen bond acceptors, one hydrophobic aliphatic and one hydrophobic aromatic feature. The pharmacophore based virtual screening was also performed on the best model Hypo 1 which includes Specs, NCI and ChemDiv, to identify the new compounds that are presumably able to act as MMP-12 inhibitors. Molecular docking was performed on the hits of virtual screening with 20 compounds in the training set

it was found that the best compound had a docking score of -12.34. In the end, 4 novel compounds were selected for the designing of the potent MMP-12 inhibitors.

Zhang et al., [117] have performed different methods like Swarm Intelligence Optimization Algorithm-Based Machine Learning methods to increase the predictive accuracy of the LibSVM toolkit to identify the potential MMP-12 inhibitors. Six models were selected, and Y-randomization test was performed, it showed excellent and reliable results. Virtual screening was performed which helped to find out the predicted probability score of 100 molecules with a score greater than 7.9. In the end, Molecular Docking toxicological properties and MD simulation were also performed which helped in the generation of six non-toxic molecules.

Li et al., [118] have performed machine learning approaches on a set of MMP-12 inhibitors. A total of 142 inhibitors and 141 non-inhibitors were used which were divided into training ($n = 184$) and test set ($n = 99$) to which machine learning methods like supporting vector machine, k-nearest neighbour, C4.5 decision tree and random forest were employed. The model was evaluated based on the statistical performance and they had sensitivity, specificity, accuracy and Mathew's correlation coefficient in the range of 96.15-98.08%, 87.23-100.00%, 91.92-98.99% and 0.8401-0.9800 which indicated the model had a good statistical performance. The model also helped to differentiate the MMP-12 inhibitors from non-inhibitors and may eventually help in the designing of potent MMP-12 inhibitors.

Zhang et al., [119] have performed molecular modelling studies to explore the mechanism of some of the important crystal bound structures of the MMP-12 inhibitors. A total of 30 crystal structures having MMP-12 inhibitory activity were used from the protein data bank (PDB) and molecular docking was performed using the Glide software. The studies indicated the difference in the structure and other factors like the target protein, active pocket size, resolution, R-free and B factor that may be useful for choosing a crystal structure.

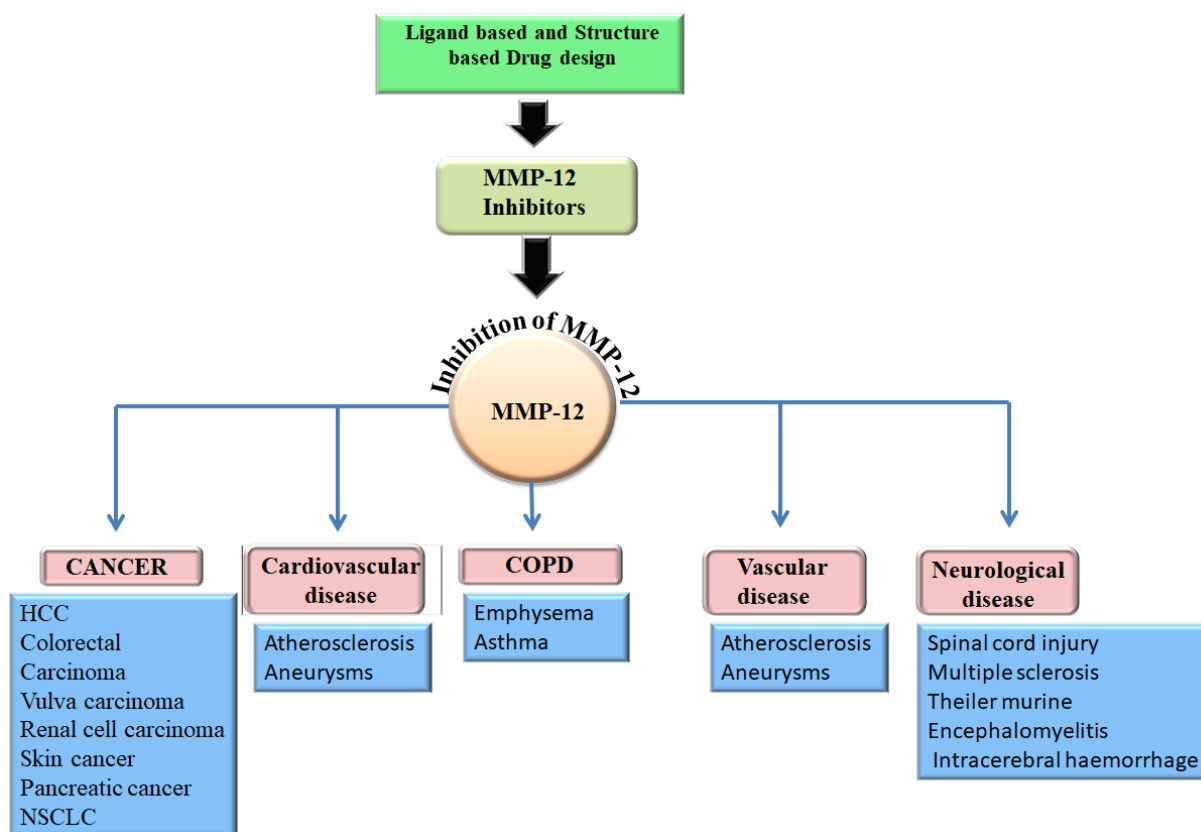


Figure 14: Structure based drug design for MMP-12 inhibitors.

Chapter 3: Rationale Behind the work

Rationale study Behind Selection of MMP-12 inhibitors

Over the years of research on MMP-12 showed the involvement of MMP-12 in different physiological and pathological conditions. MMP-12 in-vivo expression has previously been described in hepatocellular carcinoma, colorectal cancer, gastric cancer, renal cell carcinomas, pancreatic cancer, and esophageal carcinoma. However, the role of MMP-12 in cancer, whether beneficial or detrimental to tumor invasion and metastasis, appears to be tissue-type specific [120-121]. In fact, despite information associated with tumour, MMP-12 has a poor prognosis in various malignancies and there is rising evidence of MMP-12 "protective role" in tumor growth. Notably, MMP-12 overexpression is related to lower tumor growth rates in mice, resulting in a favorable outcome. Some researchers showed that the function of MMP12 is determined by cell type: when expressed by host macrophages it has a protective effect, however, when expressed by tumor cells, it does not [122]. Some MMPs, in addition to supporting tumor development and angiogenesis, can also prevent tumor vascularization. MMP-12 can degrade plasminogen to angiostatin, which effectively inhibits endothelial cell proliferation and angiogenesis, limiting tumor growth. In fact, MMP-12 gene transfer has recently been used in gene therapy in melanoma and colon carcinoma animal models [123]. Nonetheless, other substrates of MMP-12 include N-cadherin, plasminogen, tissue factor pathway inhibitor, α 1-antitrypsin, myelin basic protein (MBP), and pro- tumor necrosis factor α (TNF α) are known to play an important role in cancer and various other diseases [124]. In the case of esophageal squamous cell carcinoma immunohistochemistry of protein of MMP-12 was done. It was observed that the high expression of MMP12 in tumor tissues, but not in normal squamous epithelium. MMP-12 has been a valuable prognostic indicator for predicting the survival rate of cancer patients who have undergone surgical resection [125]. Beside all the significant roles of MMP-12 in cancer and tumors, they are involved in various diseases like COPD, skin diseases, arthritis, vascular diseases and neurological diseases [86]. In the case of COPD, the mechanism by which MMP-12 is induced is still unclear. Animal model data indicate that a decrease in transforming growth factor β 1 (TGF- β 1) or an increase in interleukin-13 (IL-13) or IFN- γ (interferon- γ) causes an increase in macrophage production MMP-12 [87].

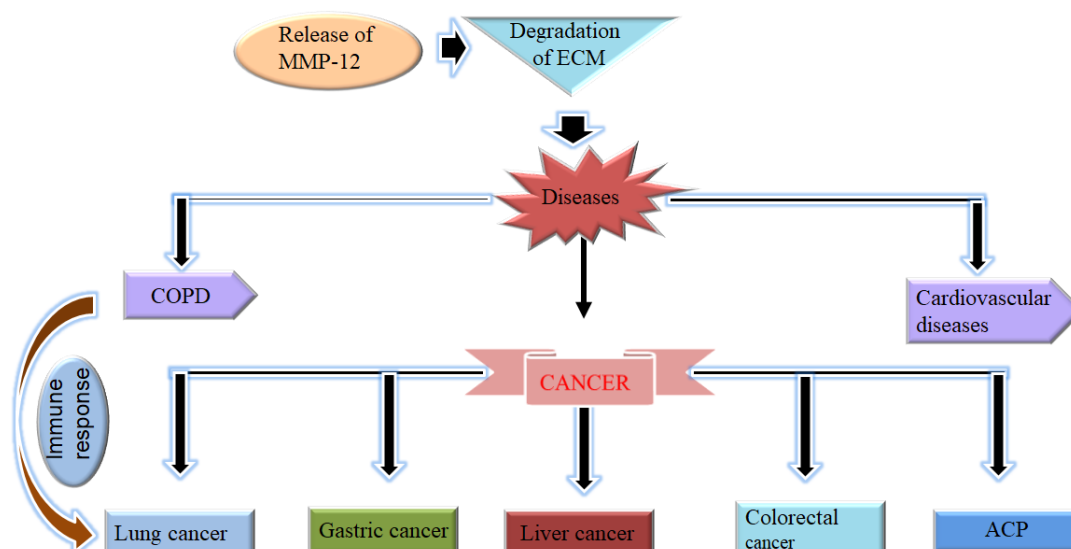


Figure 15: Role of MMP-12 in cancer and other diseases.

Beside the significant roles of MMP-12 in cancer and tumors, they are involved in various diseases like COPD skin diseases, arthritis, vascular diseases and neurological diseases [86]. In the case of COPD, the mechanism by which MMP-12 is induced is still unclear. Animal model data indicate that a decrease in transforming growth factor $\beta 1$ (TGF- $\beta 1$) or an increase in interleukin-13 (IL-13) [19] or IFN- γ (interferon- γ) causes an increase in macrophage production MMP-12 [87]. After considering all the contributions of MMP-12 in cancer and different pathophysiological conditions, the designing of the potent selective MMP-12 inhibitors is a major concern. Some studies have been conducted on MMP-12 and its inhibitors it was observed a zinc-binding group, hydrophobic moiety, and hydrogen bond donor and acceptor group are three important pharmacophoric properties. Among these three properties, the hydrogen bond donor and the hydrophobic group were essential for the MMP-12 inhibitory activity [126].

Chapter 4: Materials and Methods

Preparation of data set

To conduct the research, 87 dibenzofuran and dibenzothiophene-derived compounds having a wide range of MMP 12 inhibitory activity were selected from a variety of datasets. (Appendix Table A1) [98-100]. ChemDraw Ultra 5.0 was initially used to draw the 2D molecular structures of these compounds in the dataset and then ChemDraw Ultra 3D software was used to convert to their corresponding 3D structures [127]. These molecules' inhibitory activity against MMP-12 (IC₅₀ in nM) was transformed into the negative logarithmic scale using the formula ($\text{pIC}_{50} = \log \text{IC}_{50} * 1$) [128]. The geometry of the compounds was optimised as a final step in the molecule/dataset preparation procedure utilising the Discovery Studio 3.0 (DS) software's Prepare Ligands for QSAR protocol.[129].

Calculation of descriptors and dataset pre-processing

The statistical model generation process uses molecular descriptors, which are quantifiable structural characteristics, to correlate biological activity [127-129]. Here, the descriptor calculation in regression and classification-based QSAR has been performed using the PaDEL and DRAGON descriptor software. [130-131]. A dataset pre-treatment operation was also carried out to remove the redundant features and reduce the dimension of the dataset descriptors. The highly correlated and constant variables were eliminated using a correlation threshold of 0.9 and a covariance cut-off of 0.001, respectively [132-133] which left an array of 87 x 840 descriptors for further processing.

Selection of training and test datasets

The dataset division procedure is a crucial phase in the creation of QSAR models for assessing the effectiveness and predictability of the final models [132-133]. By using a Y-based ranking approach for regression-based, and Kennard Stone division for classification-based with the help of DTC lab software [134-135]. The dataset molecules were divided into the training (N_{Train} = 65) and the test (N_{Test} = 22) sets in accordance with the uniform distribution and the maintenance of structural diversity of the dataset compounds [133] where the training set contains the most active and the least active compound [132-133].

Regression-based 2D-QSAR studies

A. Multiple linear regression (MLR) analysis

One of the most widely utilised methods for developing QSAR/QSPR models is the multiple linear regression (MLR) analysis [134]. The benefit of MLR analysis is that it has a simple mathematical form with an understandable mathematical explanation [134-136]. For the

datasets' compounds, stepwise multiple linear regression (S-MLR) analysis was conducted using the training set, and its results were internally validated using leave-one-out (LOO) cross-validation molecules and externally validated from the test set [135-137]. The model was developed using the statistical parameters, such as squared correlation coefficient (R^2), adjusted R^2 (R^2_A), leave-one-out (LOO) cross-validated R^2 (Q^2), variance ratio (F), specified degrees of freedom (DF), standard error of estimate (SEE), and predicted residual sum of squares ($PRESS$) were assessed in addition to the r_m^2 matrices [133, 137]. Additionally, the Golbraikh and Tropsha parameters [138], Y -randomization and R^2_{pred} were used for validation [133].

B. Hologram QSAR (HQSAR) study

The hologram-based QSAR (HQSAR) study transforms the chemical representations of the molecules into holograms and connects them with the biological properties of the molecules via the construction of partial least square (PLS) models [139-140]. Here, the HQSAR study was conducted utilising 2D molecular holograms that describe some of the key properties, including atoms (A), bonds (B), connections (C), hydrogen atoms (H), chirality (Ch), and hydrogen bond donor and acceptor (DA) [141-142]. HQSAR study was performed using the SYBYL-X 2.0 software [143]. After constructing the HQSAR model on the training set, based on the leave-one-out cross-validation (Q^2) results, the best model was selected [144] where the final model's predictive power was assessed using the molecules from the test set.

Field-based 3D QSAR studies

Alignment of dataset molecules

The most important stage in the alignment-dependent 3D-QSAR investigation is the superimposition of the molecule groups with similar scaffolds. The model is validated based on the alignment of the molecules [133, 145]. Using the SYBYL-X 2.0 software, the dataset molecules in this study's dataset were molecularly aligned [143]. Initially, the molecules were minimised and then Gasteiger-Mersilli method was used to charge the molecules.[146]. Following the minimization procedure, the dataset's compounds were aligned using the Distill-Rigid alignment approach using the most potent MMP-12 inhibitor of the series [133, 146-147].

Comparative Molecular Field Analysis (CoMFA) study

In the comparative molecular field analysis (CoMFA) technique, the ability to predict the biological activity of the molecules in a 3D lattice is represented by the interaction between the steric and electrostatic forces [148]. After the alignment, the aligned molecules were placed

inside the 3D lattice of 2 Å grid points followed by the introduction of probes to determine the steric and electrostatic field of every molecule with the help of Lennard-Jones and Coulombic potential [149]. These field interaction energies are employed in the CoMFA study as the independent variables to compare the biological potency of the compounds in the dataset. [148-149]. Additionally, the PLS approach was used to establish a linear association between the CoMFA fields and the biological activity of MMP-12 inhibitors [146-150]. Cross-validation and leave-one-out techniques were used to assess the model's quality. The use of 5-fold and 20-fold bootstrap internal cross-validated R^2 (R^2_{5-CV} and R^2_{20-BS}) respectively were used to check the robustness of the model [151-152]. In the end, the R^2_{pred} value was evaluated using the test set compounds to predictive capability of the *PLS* model [152].

Comparative Molecular Similarity Indices Analysis (CoMSIA) study

Comparative molecular similarity indices analysis (CoMSIA) technique is similar to the method of CoMFA [153]. In the CoMFA technique, only two fields were calculated whereas CoMSIA can deal with five different field calculations such as steric, electrostatic, hydrophobic, hydrogen bond donor, and hydrogen bond acceptor [154]. A similar *PLS*-based method was used for establishing a relationship between the CoMSIA fields and the MMP-12 inhibitory property [154]. Where the same validation method that was used in the CoMFA technique was for the CoMSIA model 5-fold and 20-fold bootstrap internal cross-validated 5-fold and 20-fold used respectively in the training set and the R^2_{pred} was calculated for the test set validation. [152-153].

Topomer-CoMFA study

A 3D-QSAR approach called a "Topomer-CoMFA study" combines two techniques for alignment-free approaches, CoMFA and Topomer methodologies [155-157]. At first, the molecules were divided into two groups such as R_1 and R_2 [156-157]. Additionally, using sp³-hybridized carbon probes in the SYBYL-X 2.0 software, the interaction energies for the steric and electrostatic fields were calculated [143]. In the end, the model was developed using the *PLS* technique and the quality and robustness of the developed model were verified using similar approaches that were used for CoMFA and CoMSIA [157].

Classification Based QSAR study

Linear discriminant analysis (LDA) method

The utilization of Linear Discriminatory Analysis (LDA) method in QSAR study is to separate the *actives* and *inactives* with the help of the structural features by using a class or group-based modeling method [158]. It mainly acts by finding the linear combination of features and separating them into two or more classes [158]. At first, the descriptors generated from Dragon software were then imported into the STATISTICA 7.1 software for the construction of the model [131, 159-160]. The LDA analysis was done using a tolerance of 0.001, F of 4.0 for inclusion and F of 3.9 for exclusion. The model was selected based on the lowest Wilk's λ value, and the number of descriptors should be less than six [161]. The other validation parameters include p-level, sensitivity, specificity, accuracy, precision, MCC and F_1 . Whereas for comprehensible results two new additional parameters were calculated: the ROC graph euclidian distance (ROCED) and the ROC graph fitness function (ROCFIT).

$$\text{Sensitivity} = \frac{TP}{TP+FN} \quad (1)$$

$$\text{Specificity} = \frac{TN}{TN+FP} \quad (2)$$

$$\text{Accuracy} = \frac{TP+TN}{TP+TN+FP+FN} \quad (3)$$

$$\text{Precision} = \frac{TP}{TP+FP} \quad (4)$$

$$\text{MCC} = \frac{(TP*TN-FP*FN)}{\sqrt{(TP+FP)(TP+FN)(TN+FP)(TN+FN)}} \quad (5)$$

$$F1 = \frac{2 \times \text{precision} \times \text{sensitivity}}{\text{precision} + \text{sensitivity}} \quad (6)$$

$$di = \sqrt{(1 - \text{sensitivity})^2 + (1 - \text{specificity})^2} \quad (7)$$

$$\text{ROCED} = \{(d1 - d2) + 1\} (d1 + d2)(d2 + 1) \quad (8)$$

$$\text{fit}(\lambda) = \frac{(1-\lambda) \times (n-p-1)}{(n+p)^2 + \lambda} \quad (9)$$

$$\text{ROCFIT} = \frac{\text{ROCED}}{\text{FIT}\lambda} \quad (10)$$

Bayesian classification study

The Bayesian classification model was developed on compounds with dibenzofuran and dibenzothiophene structures having MMP-12 inhibitory activity, using Discovery studio (DS) [162-163]. The model was developed by using various molecular properties like Extended Connectivity of the Fingerprint of diameter 6 (ECFP_6), molecular weight (MW), number of hydrogen bond donors (nHBD), number of hydrogen bond acceptors (nHBA), number of rotatable bonds (nRB), number of aromatic rings (nAR), number of rings (nR) AlogP, molecular fractional polar surface area (MFPSPA), etc. [164-165]. The characteristics of the model were evaluated by the quality of true positive (TP), true negative (TN), false positive (FP), and false negative (FN), which provided the statistical validation of the model namely sensitivity, specificity, accuracy, precision, Matthew's correlation coefficient (MCC) and F-measure (F_1) [166]. The model validation was also done by using 5-fold cross-validation of the training set and ROC, along with the external validation with the statistical validation metrics provided below and was done using the test set [167]

Recursive partitioning (RP) study

Recursive partitioning (RP) study is also a classification-based QSAR method that classifies compounds by constructing a decision tree, which explores the relationship between the biological activity and molecular fingerprints [168]. The model was built using different types of molecular properties like Functional Class Molecular Fragment descriptors at diameter 6 (FCFP_6), MW, nHBD, nHBA, nRB, nR, MFPSPA, AlogP, etc., using Discovery Studio (DS) [162-169]. The same statistical validation that was used in the Bayesian classification study was also used in the RP model for validation.

SARpy analysis

The SARPY (Structure-activity relationship in Python) analysis method was used to determine the structure of the molecules of the dataset. This tool uses an active ruleset and it validates the substructures of compounds in the training set using the SMILES string [170]. Here, SARpy analysis was also applied to MMP-12 inhibitors having dibenzofuran and dibenzothiophene moieties. Initially, the training set was used for identifying the active structure using atom numbers between 2 and 18 that produced structural alerts responsible for producing the high MMP-12 inhibitory activity. This was subsequently validated on the test set population [171]. Using the training set, it produced the substructures of the chemicals and then the robustness of the ruleset was validated by using the sensitivity, specificity, accuracy, precision, MCC and F_1 [172].

Molecular Docking Study

For the molecular docking study at the active site of the MMP-12 enzyme (PDB ID: 1RMZ), the binding orientation of these molecules at the active site of the two most active compounds, 69 and 70, were observed. The Maestro v12.1 software from the Schrodinger suite performed the molecular docking analysis of these compounds.[173].

Ligand preparation

Here, in this study, the *Ligprep* module from the Schrodinger Maestro v12.1 [173] was used for the energy minimization of the molecules by the optimized potential for liquid simulations (*OPLS_2005*) force field.

Protein preparation

Initially, the 3D crystallographic structure MMP-12 (**PDB ID: 1RMZ**) [174] was used. The *Protein preparation* module of the Schrodinger Maestro v12.1 software was used in the next stage to refine and optimise the 3D protein structure, including the insertion of hydrogens, removal of water molecules, bond order assignment, and inclusion of side chain missing atoms. [173].

Generation of receptor grid

The *receptor grid generation* module from the Schrodinger Maestro v12.1 [173] software was used to create a rigid grid around the active site of the MMP-12 enzyme. The default 10Å grid box was used to generate the receptor grid keeping the inbound ligand at the centroid.

Ligand docking

To procure the binding poses, these inhibitors were predicted in an ‘*extra precision (XP)*’ method with *OPLS2005* forcefield, flexible ligand sampling with the help of grid-based Ligand Docking and Sampling (*GLIDE*) module by using the *Ligand Docking* protocol of Schrodinger Maestro v12.1 [173]. Additionally, in this molecular docking process, the interaction scores of the ligands/molecules per residue of the active site were calculated within a 12Å radius from the grid center for further analysis.

Molecular Dynamic (MD) Simulation study

The GROMACS (Version 2022.1) software package [175-176] was employed for the docked complexes of molecules 69 and 70 bound to MMP-12 in a 100 nanoseconds (ns) all-atom MD simulation analysis (PDB ID: 1RMZ). The CHARMM36 force field [177] with CHARMM-

modified TIP3P water model (*TIP3P_CHARMM*) [178] was taken into account for the complexes' MD simulation study. The ligand topology was constructed by the CHARMM general force field (*CGenFF*) program in the CGenFF webserver [179]. The MD simulation of the complexes was done under a neutral (pH = 7.0) condition and the whole complexes were neutralized by sodium (Na^+) and chloride (Cl^-) ions. 5000-step energy minimization was imposed in the *Steepest descent* method to resolve the bad contacts and clashes followed by a two-step equilibration process. A 100 picosecond (ps) *NVT* and 100 ps *NPT* equilibrations were executed for each stage by the modified Berendsen thermostat [180-181] and Parrinello-Rahman barostat. Also, for the MD simulation, a 300 K temperature was maintained for the system with LINCS, and particle-mesh Ewald (PME) algorithms [182-183] were used for covalent bond length constrain and long-range electrostatic interaction calculation, respectively allowing a 2 femtosecond (fs) integration time step size. The CHARMM36m all-atom force field was applied throughout the MD simulation. The radiuses of gyration (R_g), root mean square deviation (RMSD), root mean square fluctuation (RMSF), and hydrogen bond (H-bond) occupancy were derived from the simulation study for further analysis.

Chapter 5: Results and Discussion

2D QSAR studies

Multiple linear regression (MLR) analysis

The final MLR model consists of 8 descriptors developed using the S-MLR-based method, evaluated based on the R^2 , Q^2 , and R^2_{pred} values. The MLR equation (*equation 11*) is given

below. The descriptors used in the development of *equation 11* and the predicted activity are shown in (Appendix Table A2). Additionally, the statistical performance of the MLR model (*equation 11*) is shown in Table 3.

$$pIC_{50} = -22.85613 (\pm 3.84397) + 0.89485 (\pm 0.09998) nHBint5 - 0.71295 (\pm 0.10719) nN + 0.01962 (\pm 0.00408) ATSC6s - 0.01812 (\pm 0.00251) AATS0m + 4.84815 (\pm 0.56459) piPC6 + 0.10212 (\pm 0.02372) VE3_Dzi - 1.37207 (\pm 0.37546) ATSC1e - 0.05678 (\pm 0.02293) VE3_Dzp \quad (11)$$

where *nHBint5* represents the count of E-State descriptors of strength for potential hydrogen bonds of path length 5, *nN* indicates the number of nitrogen atoms present in the molecules, *ATSC6s* signifies centered Broto-Moreau autocorrelation-lag 6/weighted by I-state, *AATS0m* is the average centered Broto-Moreau autocorrelation - lag 0/weighted by mass, *PiPC6* is the conventional bond order ID number of order 6, *VE3_Dzi* represents the logarithmic coefficient sum of the last eigenvector from Barysz matrix/weighted by first ionization potential, *ATSC1e* signifies the centered Broto-Moreau autocorrelation-lag 1/weighted by Sanderson electronegativities, and *VE3_Dzp* defines the logarithmic coefficient sum of the last eigenvector from Barysz matrix/weighted by polarizabilities.

Table 3. Statistical performance calculated for the MLR model (*equation 11*)

<i>Parameters</i>	<i>equation 11</i>
<i>N_{Training}</i>	65
<i>R²</i>	0.840
<i>R²_A</i>	0.817
<i>SEE</i>	0.449
<i>F</i>	36.809 (DF: 8, 56)
<i>Q²</i>	0.789
<i>PRESS</i>	11.303
<i>Average r_m² (LOO)</i>	0.704
<i>Delta r_m² (LOO)</i>	0.139

cR_p^2	0.775
N_{Test}	22
r^2	0.626
r_0^2	0.604
$RMSE_p$	0.671
R^2_{pred}	0.603
Q^2f_2	0.601
Average r_m^2 (test)	0.504
Delta r_m^2 (test)	0.081

The above *equation 11* explains 81.7 % and predicts 78.9 % of the MMP-12 inhibitory activity. Also, the R^2_{pred} of the test set compounds was found to be 0.603. The observed versus predicted activity for *equation 11* is given in **Figure 16A**. The model has also passed the p -level ($p < 0.05$) and the Golbraikh and Tropsha model acceptability criteria (**Appendix Table A3**) [1]. Also, after the MLR model was developed, The MLR model's application domain was tested. The Euclidean distance-based normalized mean distance values for these compounds are given in **Figure 16B**. Additionally, the correlation matrix for the training set and the Y -randomized models for *equation 11* are shown in **Figures 16C** and **16D**, respectively.

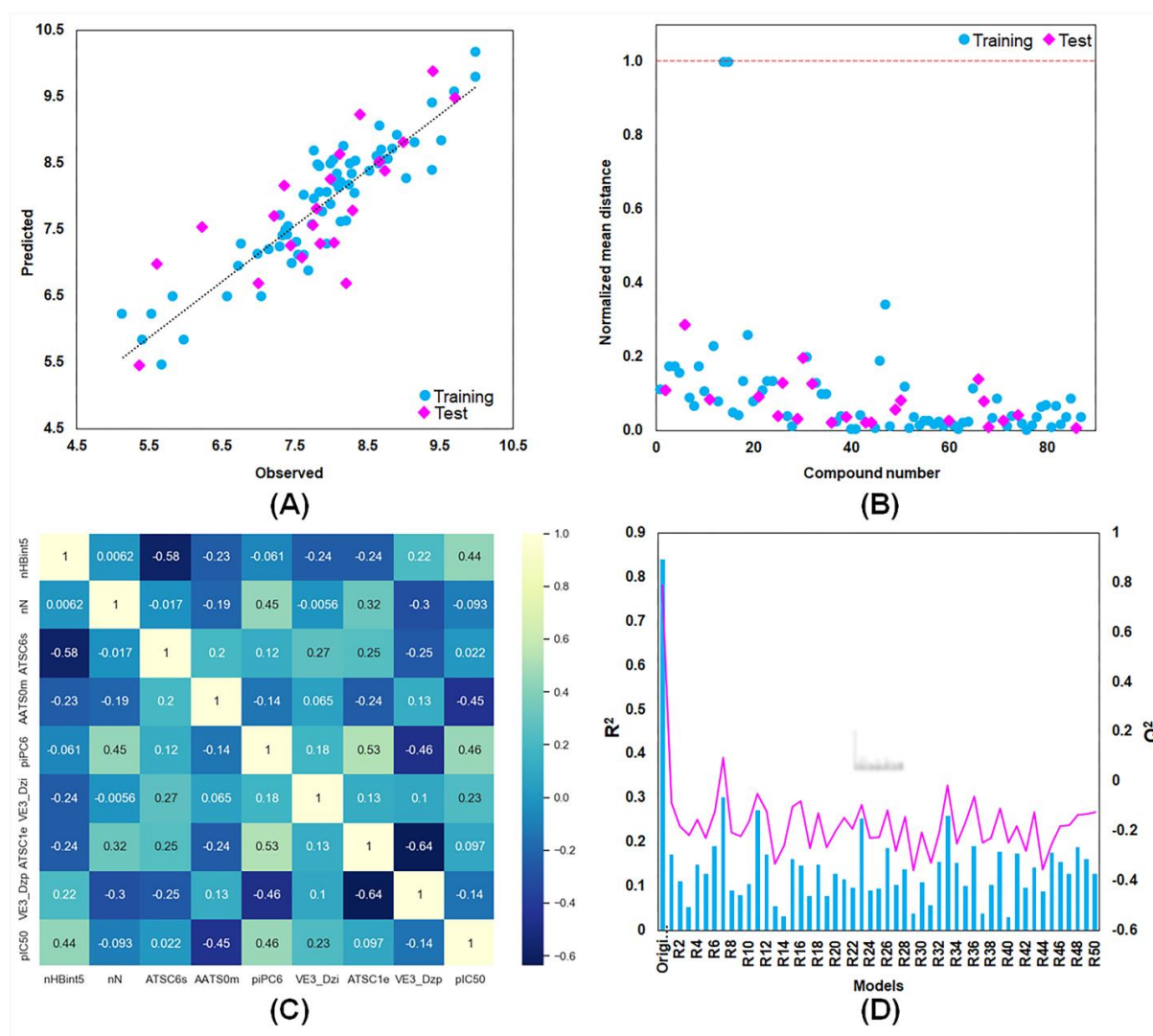


Figure 16. (A) The observed vs predicted activity for the MLR model (*equation 11*); (B) The normalized mean distance values for the dataset compounds for the training and the test sets; (C) The training set correlation matrix for the MLR model (*equation 11*); (D) The R^2 (blue bars) and Q^2 (magenta bars) values of the MLR model (*equation 11*) and the Y-randomized models

Interpretation of descriptors in MLR analysis

According to MLR *equation 11*, the molecular descriptors nHBint5, ATSC6s, piPC6, and VE3 Dzi positively contributed to the MMP-12 inhibitory activity of these dataset compounds, whereas the characteristics nN, AATS0m, ATSC1e, and VE3 Dzp negatively contributed. Among these features, the electrotopological state atom type descriptor *nHBint5* indicates the count of E-State descriptors of strength for potential hydrogen bonds of path length 5. Following analysis of the dataset compounds, it was observed that the more potent MMP-12 inhibitors had the higher values of nHBint5 (nHBint5 3), but the less potent MMP-12 inhibitors

(Compounds 1–7, 10-15, 30-31, and 34–35) have the lower values of nHBint5. The atom count descriptor *nN* signifies the number of nitrogen atoms present in the molecule and showed the negative contribution to the MMP-12 inhibitory activity. It is observed that among these molecules containing only the single sulfonamido nitrogen atom (Compounds 1-2, and 68-72), mostly (Compounds 68-72), are the highly potent MMP-12 inhibitors of the series. The autocorrelation descriptor *ATSC6s* (Centered Broto-Moreau autocorrelation-lag 6/weighted by I-state) indicated its positive correlation with MMP-12 inhibitory activity. Interestingly, the autocorrelation descriptor *AATSC0m* (Average centered Broto-Moreau autocorrelation - lag 0/weighted by mass) showed the negative contribution to the MMP-12 inhibition where compounds 9, 14-15, and 30-33 containing the *AATSC0m* value >150 are mostly least active inhibitors of MMP-12 (Compounds 14-15, and 30-31). The feature suggested the negative influence of the high molecular weight can be detrimental to MMP-12 inhibition of these compounds. Interestingly, compounds 14 and 15 both contain the bromine (Br) atom whereas compound 13 of this series without any Br atom in it was a more potent MMP-12 inhibitor. The Path Count descriptor *PiPC6* (Conventional bond order ID number of order 6) and the Barysz Matrix descriptor *VE3_Dzi* (logarithmic coefficient sum of the last eigenvector from Barysz matrix/weighted by first ionization potential) both correlated positively with the biological activity. Interestingly, these molecules (Compounds 54, 64, 68-71, 73-74, and 76) having the *VE3_Dzi* value between -4.0 to -5.0 all are highly active inhibitors of MMP-12 while having mostly sub-nanomolar range inhibitory activity against MMP-12. Similarly, the negative correlation of the autocorrelation descriptor *ATSC1e* (Centered Broto-Moreau autocorrelation-lag 1/weighted by Sanderson electronegativities) as well as Barysz Matrix descriptor *VE3_Dzp* (Logarithmic coefficient sum of the last eigenvector from Barysz matrix/weighted by polarizabilities) may indicate the possible negative contributions of electronegativity and polarizability of these MMP-12 inhibitors toward their biological activity.

Hologram QSAR (HQSAR) study

HQSAR study was performed using different fragment distinctions such as atom (*A*), bonds (*B*), connection (*C*), chirality (*Ch*), donor and acceptor (*DA*), and hydrogen (*H*). These features were used in different combinations for the generation of 50 models (**Appendix Table A4**). The best model was selected initially based on the Q^2 value. The model with $Q^2 > 0.500$ was considered for further optimization using the atom count. The HQSAR model **I-f** was created by utilizing the atom (*A*) fragments, an atom count of 6 to 9, and a hologram length of

353 had been selected as the best HQSAR model (**Table 4**). Besides showing the Q^2 and R^2 values of 0.698 and 0.898, respectively, the HQSAR model **1-f** delivered the externally predicted R^2 (R^2_{pred}) of 0.723. The observed versus predicted activity for the final HQSAR model is given in **Figure 17A**.

Table 4. Summary of the HQSAR models developed based on atom fragments

Model	Atom Count	R^2	R^2_{cv}	SE	Length	Component
1-a	1 to 4	0.643	0.43	0.660	61	6
1-b	2 to 5	0.712	0.483	0.587	353	5
1-c	3 to 6	0.867	0.630	0.403	307	6
1-d	4 to 7	0.883	0.686	0.377	151	6
1-e	5 to 8	0.883	0.683	0.378	401	6
1-f	6 to 9	0.898	0.698	0.353	353	6
1-g	7 to 10	0.890	0.688	0.367	257	6

best model is shown in bold face

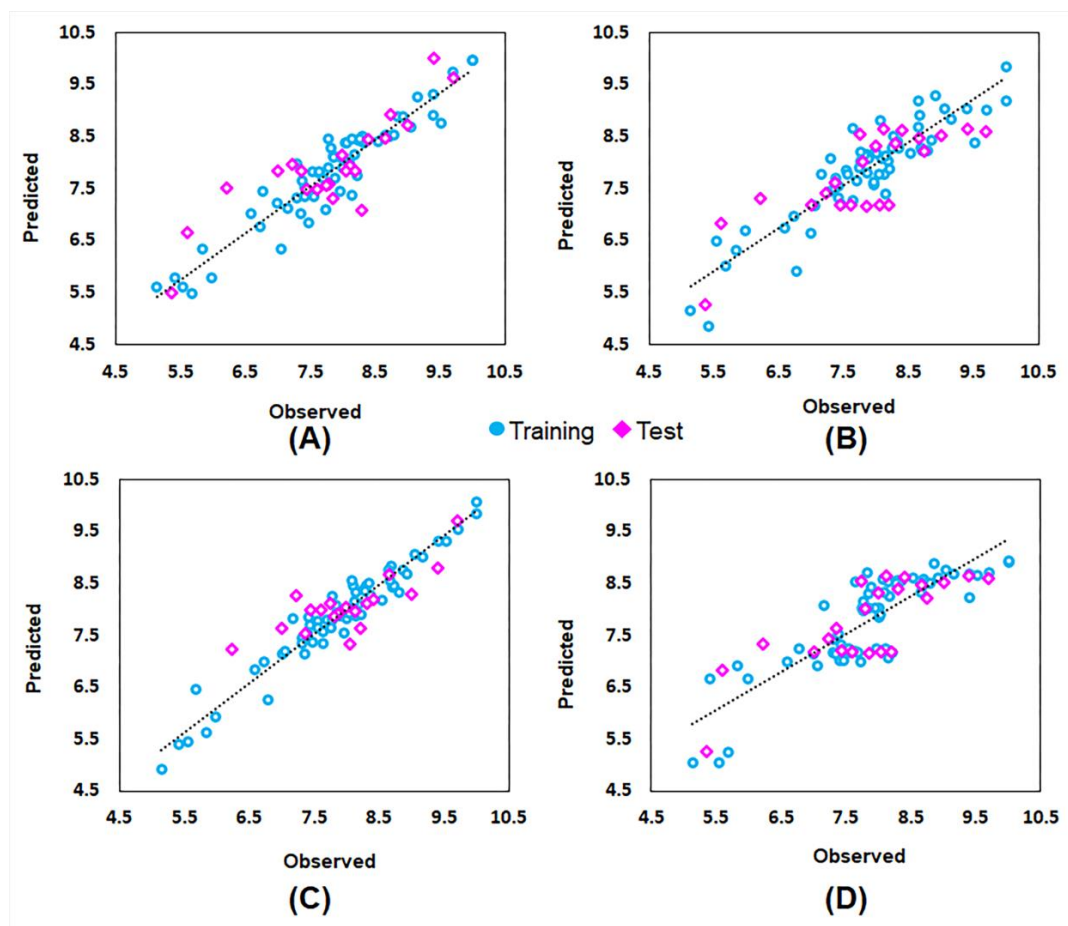


Figure 17. The observed versus predicted activity plots for the (A) HQSAR model; (B) CoMFA model; (C) CoMSIA model; (D) Topomer-CoMFA model

Interpretation of HQSAR study

In addition to the statistical results, the HQSAR model successfully detected significant structural fragments of all these MMP-12 inhibitors using various colour coding, with the poor fragments being indicated by the colours red (-0.1855325) and red-orange (-0.1855325 to -0.1113195). The moderately bad fragments were coloured orange (-0.1113195 to -0.074213) whereas the moderate fragments are shown in white (-0.074213 to 0.12524067). Additionally, good fragments are shown in green (≥ 0.31310167) and green-blue (0.187861 to 0.31310167) colours along with moderately good fragments in yellow (0.12524067 to 0.187861). The HQSAR model identified fragments for the most active (Compounds 69 and 70), moderately active (Compound 7), and least active (Compound 35) molecules are shown in **Figure 18**.

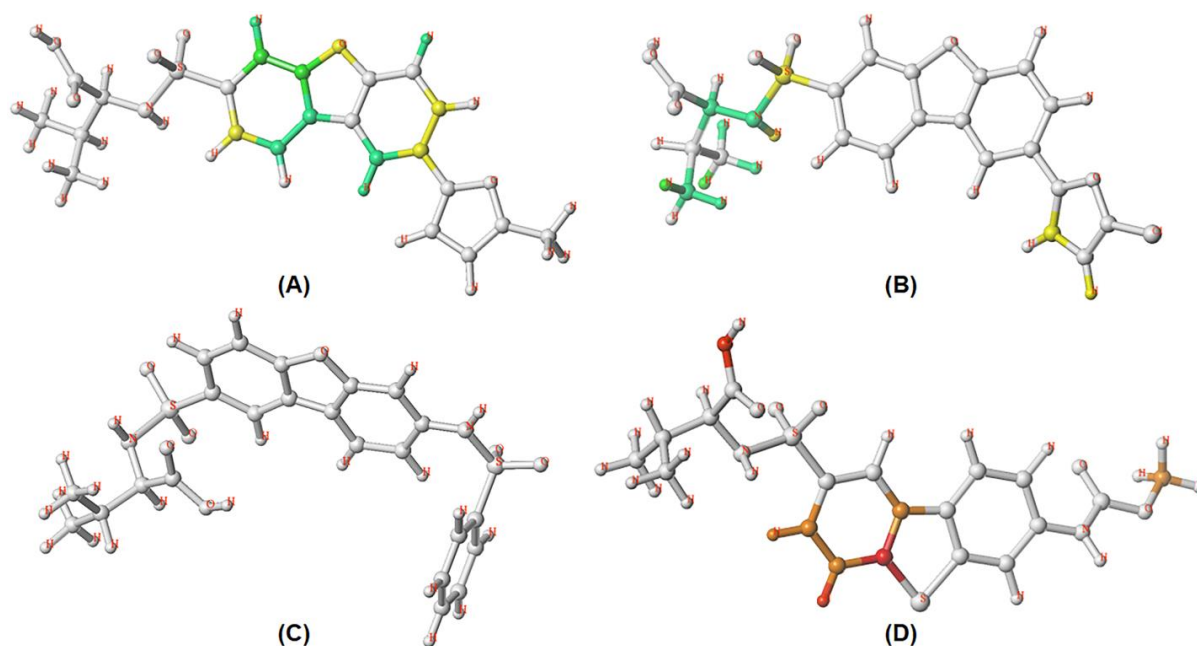


Figure 18. HQSAR contours with colour-coded fragments for (A) Compound **69**; (B) Compound **70**; (C) Compound **7**; (D) Compound **35**

From the contours provided by the HQSAR model (**Figure 18**), it is observed that the dibenzofuran moiety of the compound **69** (**Figure 18A**) and the isopropyl sulfonamido carboxylic acid function of the compound **70** were identified to have moderate to highly positive influence on their MMP-12 inhibitory activity (**Figure 18A** and **18B**, respectively). Notably, one of the hydrogen and carbon atoms from the 5-chloro furan ring of compound **70** was also identified as a moderately good contributor to the compound's MMP-12 inhibitory activity (**Figure 18B**). Also, no good or bad contributors were noticed in the case of moderately active compound **7** (**Figure 18C**) whereas the four carbon and two hydrogen atoms from the fused phenyl ring, present between the thiophene and the sulfonamide moieties of compound **35** were indicated as negative contributors for the inhibitory activity and are shown in red and red-orange colours (**Figure 18D**). Also, the terminal methyl carbon atom present at the end of the dibenzothiophene ring of compound **35** and the carboxylic oxygen atom are suggested to have a detrimental effect on the biological activity (**Figure 18D**). This might have indicated the favourability of furan-substituted dibenzofuran moiety over acetamide-substituted dibenzothiophene ring for the MMP-12 inhibitory potency while binding to the S1' pocket of the enzyme.

Field-based 3D-QSAR studies

CoMFA Study

The CoMFA model was created utilising the CoMFA steric, CoMFA electrostatic, and molecular weight (*MW*) which yielded the Q^2 value of 0.529 with 4 components while considering compound **37** with the high residual error as the outlier. The CoMFA model has delivered an R^2 value of 0.822 with the standard error (*SE*) of 0.454. The other validation parameters for the CoMFA model are provided in **Table 5**. Also, the observed versus predicted activity for the final CoMFA model is shown in **Figure 17B**.

Table 5. Statistical validation parameters for the CoMFA and CoMSIA models

<i>Parameters</i>	<i>CoMFA</i>	<i>CoMSIA</i>
<i>Features</i>	<i>S, E, MW</i>	<i>S, E, H, D, A</i>
Q^2	0.529	0.552
<i>Component</i>	4	6
R^2	0.822	0.942
<i>SEE</i>	0.454	0.263
R^2_{5-cv}	0.527	0.577
R^2_{20-BS}	0.870	0.959
<i>F</i>	68.170 (4, 59)	155.715 (6, 57)
Q^2_{scr}	0.322	0.330
<i>CSDEP</i>	0.869	0.896
dq^2/dr_{yy}^2	0.573	0.633
R^2_{pred}	0.507	0.610
<i>Field</i>	<i>Field distribution (%)</i>	
<i>Steric</i>	49.7	11.1

<i>Electrostatic</i>	46.8	25.9
<i>Molecular weight</i>	3.5	--
<i>Hydrogen bond acceptor</i>	--	11.3
<i>Hydrogen bond donor</i>	--	24.2
<i>Hydrophobic</i>	--	27.5

The steric and electrostatic field influence for the most and least active compounds was discernible from the CoMFA 3D-field-based contours for these compounds. The *Distil-Rigid* alignment of the dataset compounds is represented in **Figure 19A**.

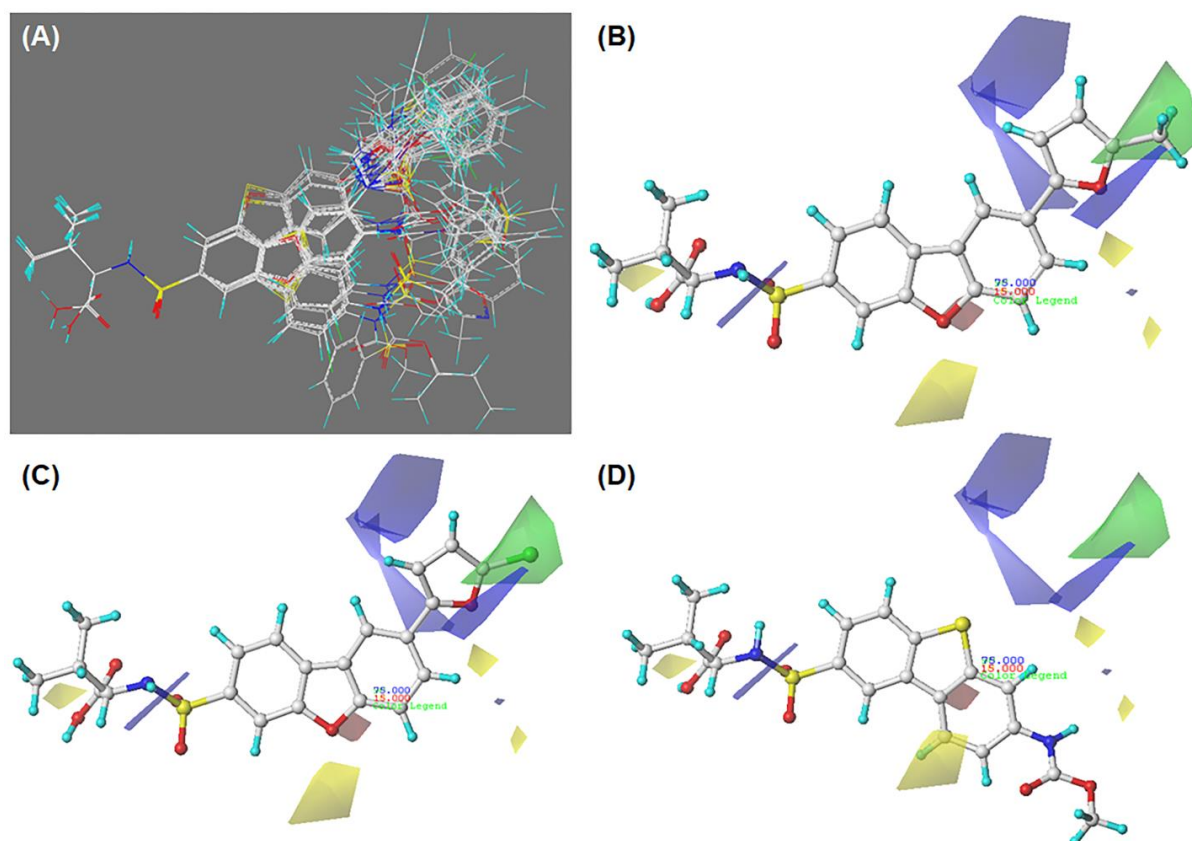


Figure 19. (A) Distil-Rigid alignment of the dataset compounds; CoMFA contours for (B) Compound **69**; (C) Compound **70**; and (D) Compound **35**

From the steric and electrostatic field maps, a steric favorable (green) region was observed near the furan ring of the higher active compounds proximal to the methyl function of compound **69** and the chlorine atom of compound **70** (**Figure 19B** and **19C**) respectively. Also, an

electrostatic favorable (blue) region near the substituted furan ring was observed suggesting the favourability of electrostatic substituents at the end of the MMP-12 S1' pocket that can increase the interactions between the molecule and the receptor, further increasing the inhibitory activity. An electrostatic unfavorable (red) region was observed close to the heterocyclic oxygen atom of the compounds **69** and **70**, suggesting the unfavorability of electrostatic functions inside the hydrophobic S1' pocket of MMP-12 enzyme (**Figure 19B** and **19C**, respectively). On the other hand, the orientation of the least active compound **35** led to a drift of the substitution on the dibenzothiophene ring from the electrostatic and steric favourable region (**Figure 19D**) toward the space surrounded by steric unfavorable (yellow) region. This may indicate that the steric movement of the linear/branched substitution at the end of the fused heterocyclic P1' moiety of these molecules may interfere with a rigid binding of the P1' substituent at the S1' pocket of the enzyme.

CoMSIA study

The CoMSIA model showed the Q^2 value of 0.519 for 6 components and the R^2 value of 0.942. The 5-fold and 20-fold bootstrap internal cross-validated R^2 (R^2_{5-CV} and R^2_{20-BS}), for the training set compounds are 0.577 and 0.959, respectively while considering compound **37** as the outlier. The external validation for the CoMSIA model showed the R^2_{pred} of 0.610 for the test set of compounds as the outliers with high residual values (Compounds **6**, **30**, and **36**) were removed. The calculated statistical parameters for the CoMSIA model are provided in **Table 5**. The observed versus predicted activity for the final CoMSIA model is given in **Figure 17C**.

The CoMSIA contour plots for the most effective and the least effective compounds (**Figure 20**) showed several similar results to that of the CoMFA study (**Figure 19**). A similar steric favorable region (green) is observed near the methyl and the chlorine substitutions of the compounds **69** and **70** (**Figures 20A** and **20B**) respectively along with a steric unfavorable (yellow) region near the acetamido group of the compound **35** (**Figure 20E**).

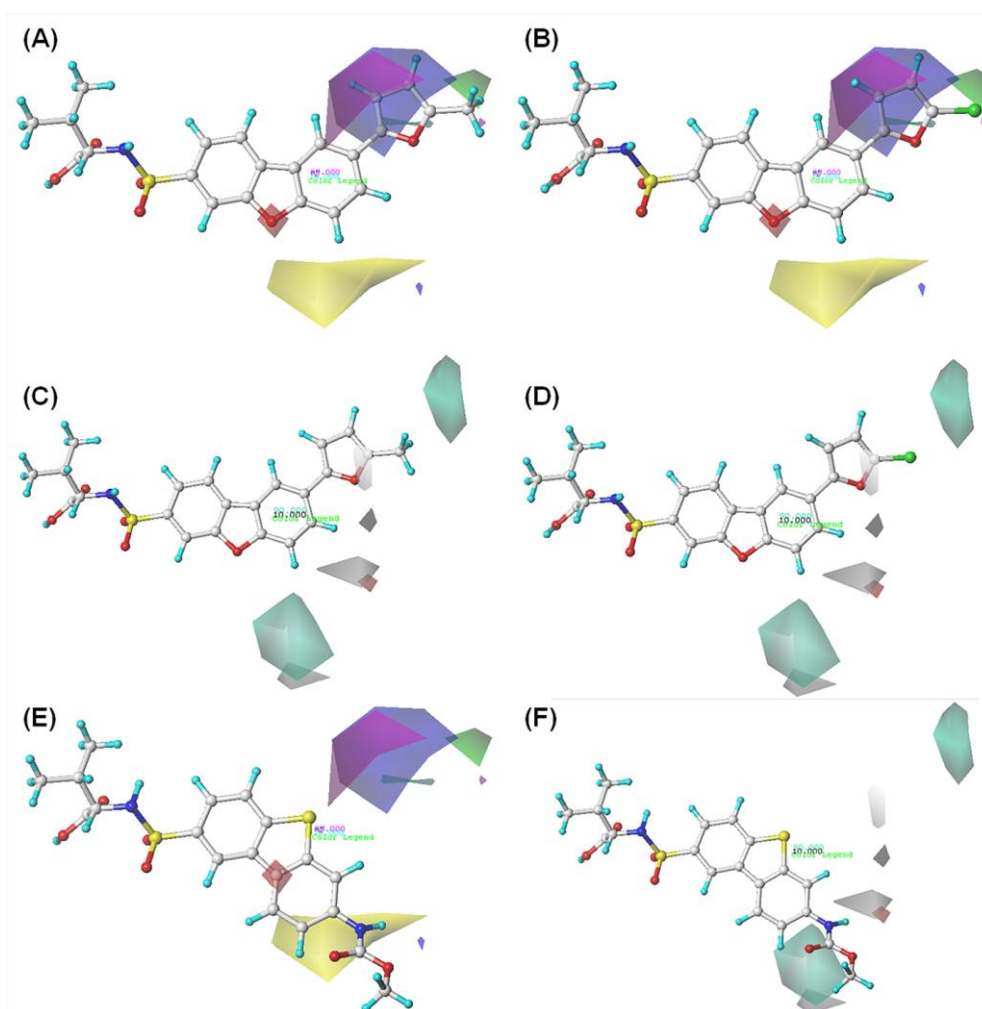


Figure 20. (A) CoMSIA steric, electrostatic, and hydrophobic contours of Compound **69**; (B) CoMSIA steric, electrostatic and hydrophobic contours of Compound **70**; (C) CoMSIA hydrogen bond acceptor and donor contours of Compound **69**; (D) CoMSIA hydrogen bond acceptor and donor contours of Compound **70**; (E) CoMSIA steric, electrostatic and hydrophobic contours of Compound **35**; (F) CoMSIA hydrogen bond acceptor and donor contours of Compound **35**

Similar electrostatic unfavorable (red) and favorable (blue) regions are also observed in the CoMFA study where an electrostatic unfavorable region is noticed near the dibenzofuran heterocyclic oxygen atom of compounds **69** and **70** (**Figures 20A** and **20B**) respectively. Also, for the CoMSIA model, though no hydrophobic unfavorable (cyan) region was noticed but the hydrophobic favorable fields (magenta) were observed near the furan rings of these compounds (**Figure 20C** and **20D**) respectively. Interestingly, the acetamido function of the least active compound **35** was located away from the hydrophobic favorable region which might be one of the prime reasons for the unstable binding of the compound at the hydrophobic S1' pocket of

MMP-12, therefore, diminishing the inhibitory activity of the compound (**Figure 20E**). Besides, regarding the CoMSIA donor and acceptor fields, hydrogen bond donor unfavorable (brown) regions were found away from the molecule whereas hydrogen bond donor favorable (white) fields were detected near the heterocyclic oxygen atom of the substituted thiophene ring of the most active compound **69** and **70** (**Figure 20C** and **20D**) respectively. This suggests the possibility of forming hydrogen bond interactions by the heterocyclic oxygen atom from the terminal furan ring of the most active compounds at the MMP-12 active site. Regarding the hydrogen bond acceptor favorable (aquamarine) region, the unfavorable acceptor region is found at a distance from the dibenzofuran ring of compounds **69** and **70** (**Figure 20C** and **20D**) respectively while the conformation of the least active compound **35** allowed the acetamido dibenzothiophene moiety to become proximal to the acceptor favorable region near the acetamide function (**Figure 20F**). For the acceptor unfavorable (black) region, the hydrogen bond acceptor unfavorable field was seen near the amide group of the substituted acetamido moiety of compound **35** (**Figure 20F**), suggesting the probable hydrogen bond donor function of the amide group for the molecule while binding at MMP-12 active site.

Topomer-CoMFA study

The Topomer-CoMFA study is an alignment-independent CoMFA study that utilizes the Topomer conformation generation of compounds before the CoMFA study. The Topomer-CoMFA model showed the Q^2 of 0.519 with 3 components

the R^2 of 0.711 and the standard error (SE) of 0.570 for the PLS analysis. The Topomer-CoMFA model also delivered the R^2_{pred} of 0.642 for the test set. The observed versus predicted activity for the Topomer-CoMFA model is shown in **Figure 17D**.

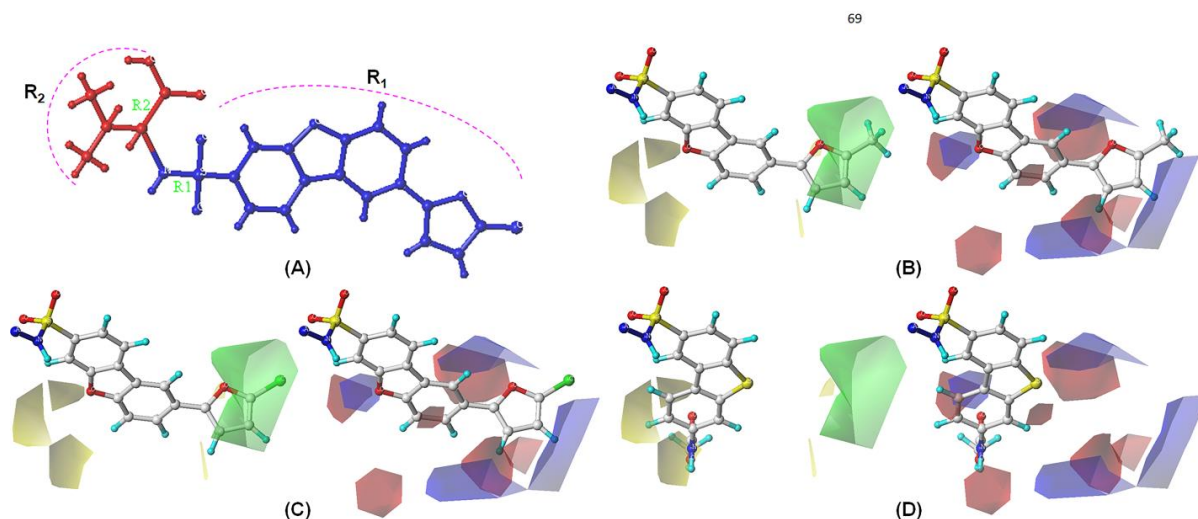


Figure 21. (A) The R₁ and R₂ groups selected for the Topomer-CoMFA study; the Topomer-CoMFA contours for the R₁ group of (B) compound 69; (C) Compound 70; (D) Compound

35

During the development of the Topomer-CoMFA model, the compounds were divided into two coloured groups such as the blue fragment (R₁) and the red fragment (R₂) (**Figure 21A**). Although no favorable and/or unfavorable fields are noticed near the R₂ fragment of the compound, the steric and electrostatic favorable and unfavorable regions for the R₁ fragment are shown in (**Figure 21B-21D**). For the most active compound **69** and **70**, a steric favorable (green) region like CoMFA and CoMSIA studies are observed at the terminal methyl group of the furan ring and chloro furan rings whereas the steric unfavorable (yellow) region is noticed near the dibenzofuran ring (**Figure 21A** and **21B**) respectively). Interestingly, for the R₁ group of the least active compound **35**, the acetamido function of the molecule is in proximity to the steric unfavorable region (**Figure 21D**). Regarding the electrostatic field contours provided by the Topomer-CoMFA study, it is noticed that an electrostatic favorable (blue) region near the heterocyclic oxygen atom of the dibenzofuran ring of the most active compounds (**Figure 21B** and **21C**) whereas the electrostatic unfavorable (red) region is noticed near the acetamido function of the least active compound **35** (**Figure 21D**). **Classification based QSAR study**

Linear discriminate analysis (LDA) method

The LDA model was developed using the dragon software and 6 descriptors were used Mor28m, H6m, IC2, nCt, F05[C-N], F05[C-C] with the help of these descriptors, the equation was constructed, that had the positive or negative impact on the MMP-12 inhibitory activity.

$$DF = - 671.544 - 17.577 \text{ Mor28m} + 277.514 \text{ IC2} - 106.490 \text{ H6m} + 43.631 \text{ nCt} - 5.934 \text{ F05[C-N]} + 5.029 \text{ F05[C-C]} \quad (12)$$

The **equation 12** had a Wilks lambda value of 0.393 and exhibited sensitivity, specificity, accuracy, precision and MCC and F_1 of 93.1%, 88.8%, 90.7%, 87%, 0.82 and 0.89 respectively. For the test set, it had sensitivity, specificity, accuracy, precision, MCC and F_1 of 83.3%, 100%, 90.9%, 100%, 0.83 and 0.91 respectively. The ROC score was 0.906 for the training and 0.917 for the test set. The ROC curve for the LDA model was also constructed which is represented in **(Figure 22A)**. The model exhibited a ROCED and ROCFIT of 0.471 and 0.531 for more comprehensible results.

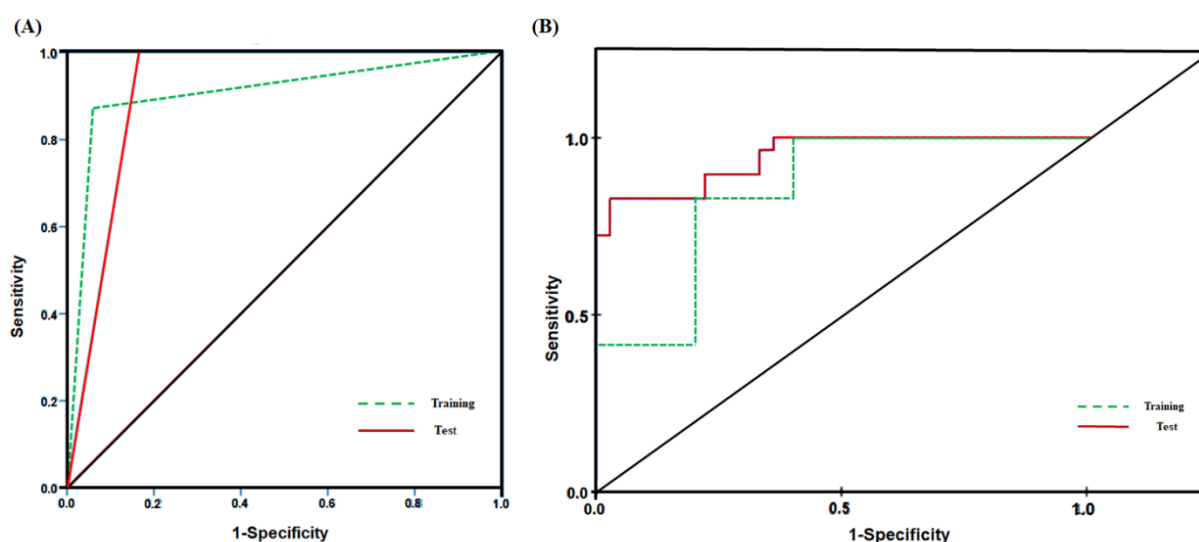


Figure 22: The ROC plot for true positive rate and the false positive rate for training and test represented by green and red for (A) LDA (B) Bayesian classification

Interpretation of LDA model

The above **equation 12** was constructed using the LDA analysis method that consisted of 6 descriptors that had either the positive or negative impact on the biological activity. The descriptors IC2, nCt and F05[C-C] had positive impacts, while the other descriptors Mor28m, H6m and F05[C-N] had negative impacts on the MMP-12 inhibitory activity. The first descriptor Mor28m (signal 28 / weighted by mass) had the negative contribution toward the MMP-12 inhibitory activity, these were observed in compounds **3, 4, 6, 7, 30, 31, 32**, and **33** which had signal 28/weighted by mass of more than 0.4. The other descriptor IC2 [Information Content index (neighbourhood symmetry of 2-order)] has the positive contribution which means

that the higher the value of the descriptor, the greater will be the MMP-12 inhibitory activity. The H6m (H autocorrelation of lag 6 / weighted by mass) belongs to the GATEWAY class of descriptor which has the negative contribution. This indicates that the higher the degree of interaction between the atoms, the lesser will be MMP-12 inhibitory activity. The descriptor nCt [number of total tertiary C (sp³)] has the positive contribution towards MMP-12 inhibitory activity. These properties were mainly observed in compounds **19**, **46**, **78**, **80**, **83**, **84**, **85** and **87** which have a greater number of tertiary carbon atom; hence, more the tertiary carbon atom the higher the inhibitory activity and vice versa. The fingerprint descriptor F05[C-N] (Frequency of C-N at topological distance 5) has a negative contribution, which means the greater the number of C-N bonds at topological distance 5 lesser the MMP-12 inhibitory activity. The other fingerprint descriptor F05[C-C] (frequency of C-C at topological distance 5), observed in compounds **27**, **66**, **69**, **72**, **79**, **85** and **86**, more the number of C-C bonds at a topological distance of 5 due to which higher will be the MMP-12 inhibitory activity. Statistical performance of the classification-based model is given in **Table 6** and the ROC plot of the training and the test sets of the LDA model are represented in **Figure. 22A**.

Table 6: Statistical performance of the classification-based model

Model	Set	ROC	ROCcv	TP	TN	FP	FN	Se	Sp	Acc	Pr	MCC	F ₁
Bayesian	Training	0.838	--	23	35	1	6	0.79	0.97	0.89	0.95	0.79	0.86
	Test	0.85	--	9	8	2	3	0.75	0.8	0.77	0.81	0.54	0.77
Recursive	Training	0.838	0.697	19	34	2	10	0.65	0.94	0.81	0.9	0.64	0.76
	Test	0.933	--	10	10	0	1	0.83	1	0.91	1	0.83	0.91
SARpy	Training	--	--	24	26	10	5	0.83	0.72	0.77	0.7	0.55	0.76
	Test	--	--	6	10	0	6	0.56	0.5	1	0.73	0.56	0.63
LDA	Training	0.906		27	32	4	2	0.93	0.88	0.91	0.87	0.82	0.89
	Test	0.917		10	10	0	2	0.83	1	0.91	1	0.83	0.91

Bayesian Classification study

The Bayesian classification model was developed using eight molecular properties and the constructed model had a LOO-cross-validation ROC score (ROC_{loo} = 0.838), 5-fold cross-validation ROC score for the training set (ROC_{5cv} = 0.825), and external validation ROC score

for the test set ($ROC_{ECV} = 0.850$), respectively. The characteristics of the model both internally and externally were judged by using sensitivity, specificity, precision, accuracy, MCC and F_1 values which are 0.793, 0.972, 0.958, 0.892, 0.790 and 0.860 respectively for the training set, whereas for the test set 0.750, 0.800, 0.818, 0.773, 0.540 and 0.770 respectively. The ROC curve for the training set and test set are shown in **Figure 22B**.

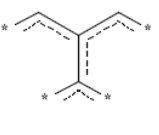
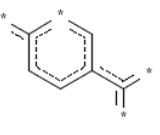
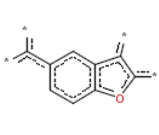
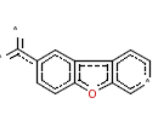
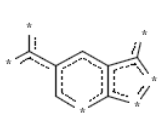
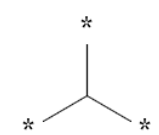
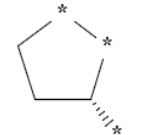
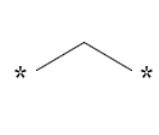
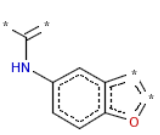
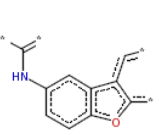
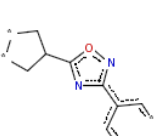
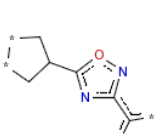
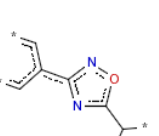
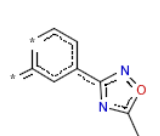
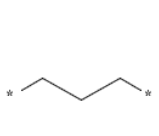
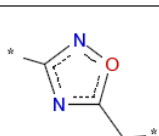
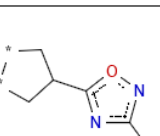
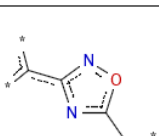
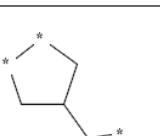
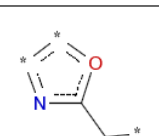
 G1: -181568884 10 out of 11 good Bayesian Score: 0.592	 G2: -219423964 10 out of 11 good Bayesian Score: 0.592	 G3: 125741795 10 out of 11 good Bayesian Score: 0.592	 G4: -1405707920 10 out of 11 good Bayesian Score: 0.592	 G5: -2077583328 10 out of 11 good Bayesian Score: 0.592
 G6: -167460056 4 out of 4 good Bayesian Score: 0.563	 G7: -1331450522 4 out of 4 good Bayesian Score: 0.563	 G8: -992506539 7 out of 8 good Bayesian Score: 0.533	 G9: -2086808075 10 out of 12 good Bayesian Score: 0.519	 G10: 121770370 10 out of 12 good Bayesian Score: 0.519
 G11: -1977227648 3 out of 3 good Bayesian Score: 0.517	 G12: 2133386757 3 out of 3 good Bayesian Score: 0.517	 G13: 896029710 3 out of 3 good Bayesian Score: 0.517	 G14: -623367261 3 out of 3 good Bayesian Score: 0.517	 G15: -1332781180 3 out of 3 good Bayesian Score: 0.517
 G16: 462432231 3 out of 3 good Bayesian Score: 0.517	 G17: -1638039391 3 out of 3 good Bayesian Score: 0.517	 G18: 1947000012 3 out of 3 good Bayesian Score: 0.517	 G19: -2097294478 3 out of 3 good Bayesian Score: 0.517	 G20: 1093505570 3 out of 3 good Bayesian Score: 0.517

Figure 23: Bayesian classification good fingerprints.

The Bayesian classification model was developed based on the good and bad fingerprints. The model recognized 20 good and bad fragments, each of these fragments has their own contribution towards the MMP-12 inhibitory activity. The good fingerprints from (G1 to G20) are given in **Figure 23**. The fused ring structure mainly dibenzofuran scaffold was observed in G1 to G5, G9 and G10, as compounds with these substructures showed better MMP-12

inhibitory activity. The oxadiazoles ring structure in the G11 to G14, G16 to G18 and G20 fragments is mainly observed in compounds **76-87** in **Figure 24**. It was observed that molecules having these substructures have high MMP-12 inhibitory activity with an average pIC_{50} of 8.488. The fragments observed in G6, G8 and G15, that is the isopropyl substructure are present in most of the molecules in the data set and these have a positive contribution towards the MMP-12 inhibitory activity. However, fragments G7 and G19 indicated the substitution furan ring substructure at positions 7 and 8, and showed good MMP-12 inhibitory activity. Finally, the presence of a dibenzofuran scaffold, isopropyl group, oxadiazoles and furan substitution increased the MMP-12 inhibitory activity. Structures of some MMP-12 inhibitors containing good Bayesian fingerprints are represented in **Figure 24**.

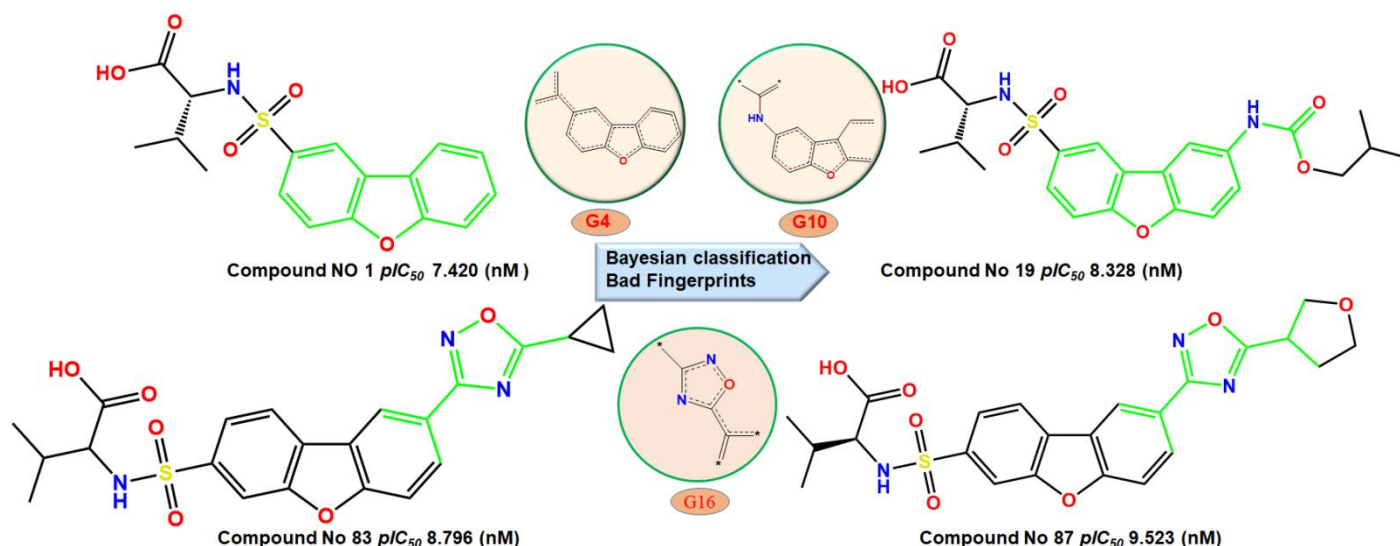


Figure 24: Structure of some of the MMP-12 inhibitors containing good Bayesian fragments.

In Bayesian classification model, the structures that have been exhibited in the **Figure 25** represented 20 bad fingerprints that had negative contribution towards the MMP-12 inhibitory activity. It was observed most of the fingerprints from B1 to B20 had a sulphonamide group that had either directly or indirectly attached to the scaffold.

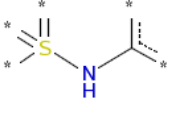
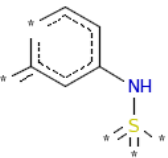
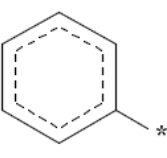
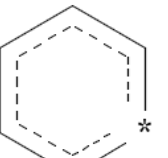
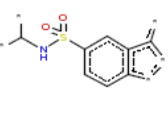
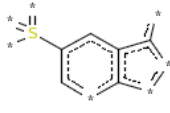
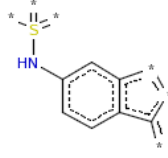
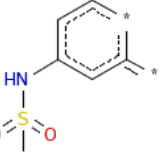
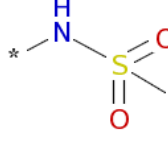
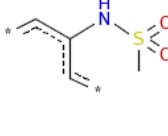
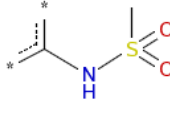
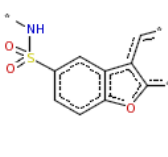
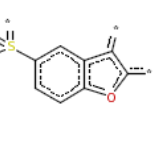
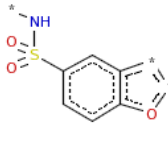
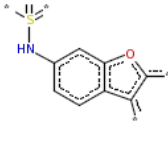
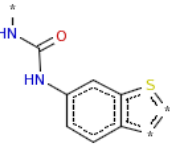
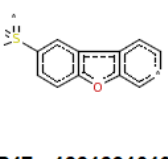
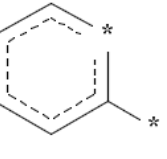
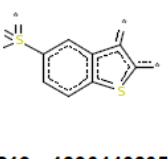
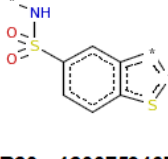
 B1: -1238602038 0 out of 9 good Bayesian Score: -1.641	 B2: 1431901335 0 out of 9 good Bayesian Score: -1.641	 B3: -281505363 0 out of 7 good Bayesian Score: -1.443	 B4: 1571214559 0 out of 7 good Bayesian Score: -1.443	 B5: 1/13818546 1 out of 15 good Bayesian Score: -1.378
 B6: 1458676750 1 out of 15 good Bayesian Score: -1.378	 B7: -27783487 0 out of 5 good Bayesian Score: -1.197	 B8: 441864219 0 out of 5 good Bayesian Score: -1.197	 B9: -1771138410 0 out of 5 good Bayesian Score: -1.197	 B10: -2014712459 0 out of 5 good Bayesian Score: -1.197
 B11: -1097828263 0 out of 5 good Bayesian Score: -1.197	 B12: -213517394 1 out of 12 good Bayesian Score: -1.186	 B13: -1883426837 1 out of 12 good Bayesian Score: -1.186	 B14: -18607838 1 out of 12 good Bayesian Score: -1.186	 B15: 1660685101 0 out of 4 good Bayesian Score: -1.047
 B16: 1660359389 0 out of 4 good Bayesian Score: -1.047	 B17: -1331391019 1 out of 10 good Bayesian Score: -1.033	 B18: 1564392544 1 out of 10 good Bayesian Score: -1.033	 B19: -1396440365 0 out of 3 good Bayesian Score: -0.870	 B20: -1200759467 0 out of 3 good Bayesian Score: -0.870

Figure 25: Bayesian classification Bad fingerprint .

In fragments B1, B2, B3, B7 to B11 and B15 it was observed that due to the presence of the sulphur dioxide group, which is indirectly attached to the fused ring structure along with the secondary amine group showed low MMP-12 inhibitory activity and is represented in **Figure 26**. On the other hand, a dibenzothiophene scaffold was observed in fingerprints B6, B12, B14 and B17 the presence of the sulphur atom lowered the MMP-12 inhibitory activity. The fingerprints B3 B4 and B18 indicated the presence of a six-membered ring structure directly attached to the fused ring structure and isopropyl sulfonamido carboxylic acid function showed less MMP-12 inhibitory activity. Finally, fingerprints B2, B19 and B20, which have a dibenzothiophene structure directly attached to the isopropyl sulfonamido carboxylic acid

function given in **Figure 26** had two sulphur atoms, one in the fused ring structure and other in the isopropyl sulfonamido carboxylic acid function, due to which compound with these substructures had low MMP-12 inhibitory activity. It was noted that the presence of the sulphur atom directly or indirectly attached to the fused ring structure had lowered MMP-12 inhibitory activity. The structure of some MMP-12 inhibitors containing bad bayesian fingerprints is given in **Figure 26**.

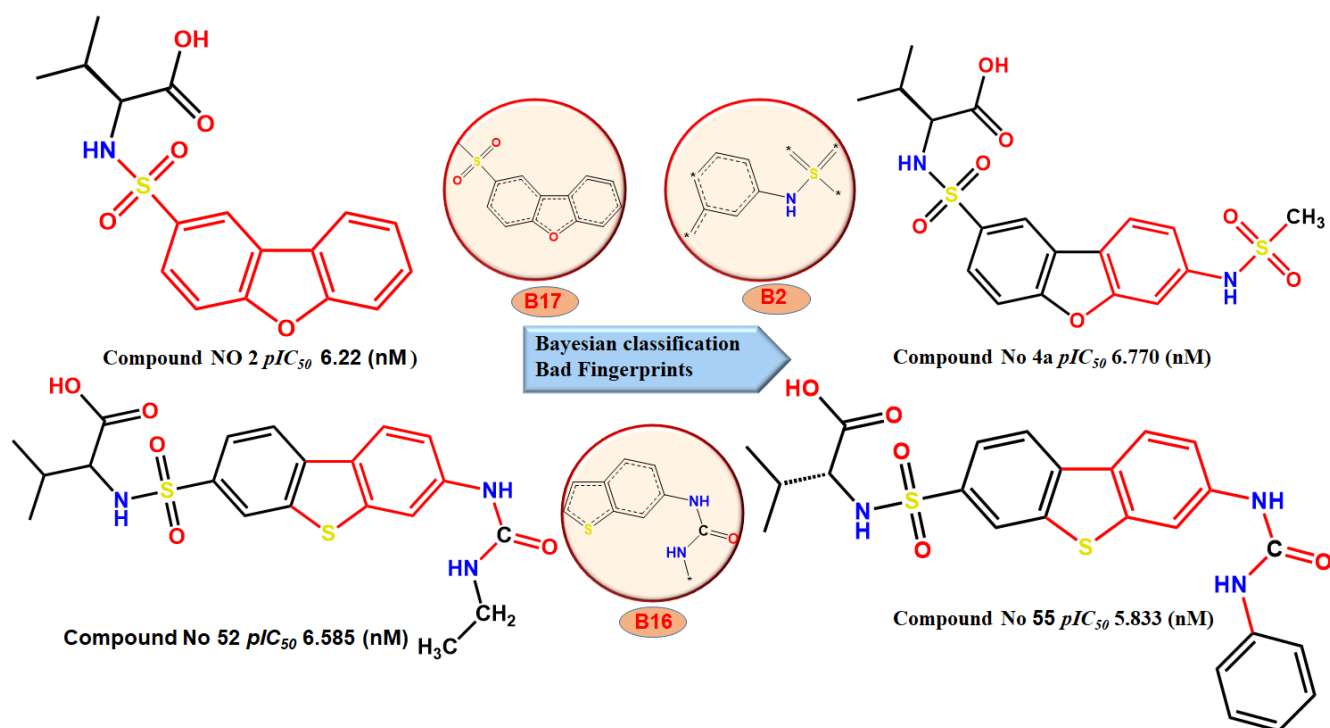


Figure 26: Structure of some of the MMP-12 inhibitors containing bad Bayesian fragments.

Recursive partitioning study

In the recursive partitioning method, a decision tree was constructed that classified compounds based on the actives and inactive using molecular properties like Functional Class of Molecular Fragment Descriptor of Diameter 6 (FCFP_6) MW, nHBD, nHBA, nRB, nR, MFPSA and AlogP. Two decision trees were developed; it was selected based on the predictive performance. Tree 1, having 4 leaves with the highest ROC score of 0.839 and ROC cross-validation of 0.697, was selected on the basis of better statistical performance over Tree 2, with 2 leaves, had a ROC score of 0.761 and an ROC cross-validation of 0.697. The external validation was also done using the test set, and the ROC score of trees 1 and 2 were 0.933 and 0.808 respectively.

Tree 1 given in **Figure 27A** was selected based on the higher predictive performance, the training set molecules have sensitivity, specificity, accuracy, precision, MCC and F1 of 65.5%, 94.4%, 81.5%, 90.4 %, 63.7% and 75.9 respectively. At the same time, the test set had sensitivity, specificity, accuracy, precision, MCC and F₁ of 83.3%, 100%, 90.9%, 100%, 83.3% and 90.7 respectively. Tree 1 had three substructures, mainly 6-amino benzofuran (FP-1), dibenzofuran (FP-2) and ester (FP-3). The use of mainly dibenzofuran structure has been used for the decision tree, and they have been discriminated into substructures as these play crucial

roles in MMP-12 inhibitory activity. The statistical performance of the recursive portioning (RP) model is shown in **Table 6B** and the radar graph is represented in **Figure 27B** and **27C**.

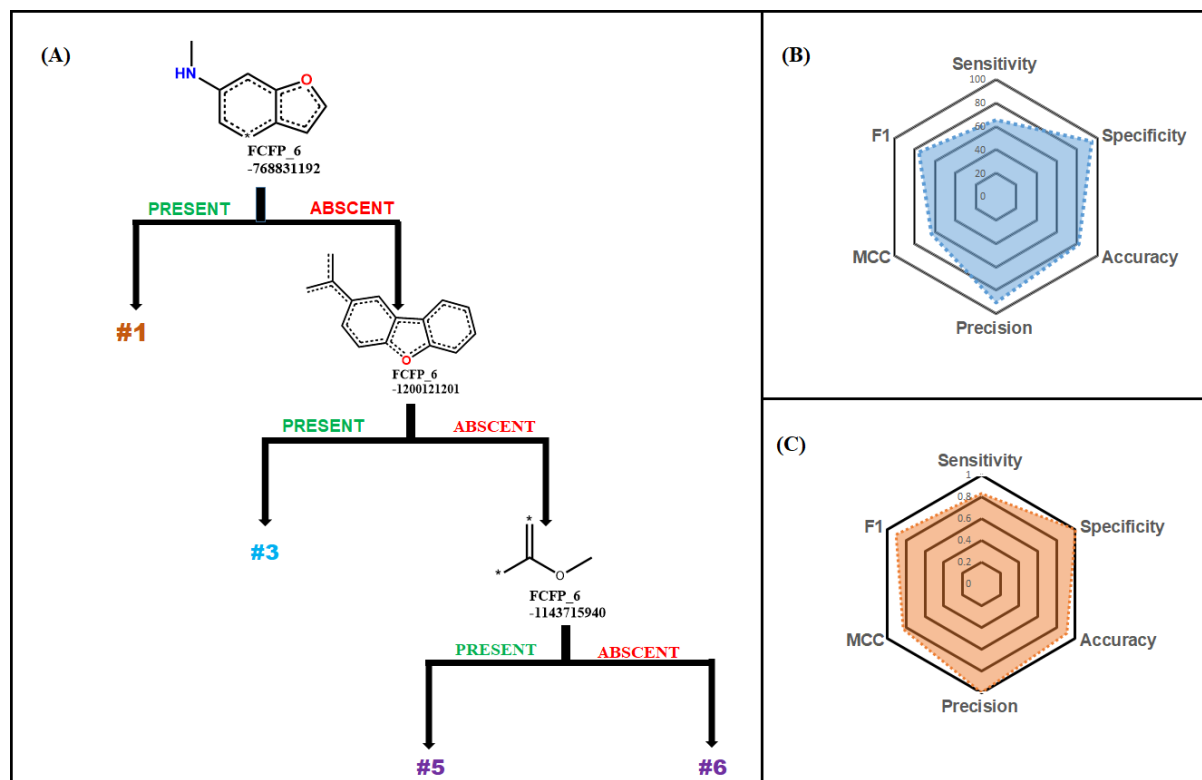


Figure 27: Decision tree schematic representation for recursive portioning.

Table 7: Statistical performance of the Recursive Portioning (RP) model

Tree no	Leaves	Set	ROC	ROCcv	TP	TN	FP	FN	Se	Sp	Acc	Pr	MCC	F ₁
1	4	Training	0.838	0.697	19	34	2	10	0.655	0.944	0.815	0.904	0.637	0.759
		Test	0.933		10	10	0	1	0.833	1	0.909	1	0.833	0.907

2	2	Training	0.761	0.697	24	25	11	5	0.827	0.694	0.753	0.685	0.52	0.748
		Test	0.808	-----	11	7	3	1	0.916	0.7	0.818	0.785	0.638	0.845

SARpy analysis

The fragment-based analysis provided the curtail structures in the form of SMILES, the MMP-12 dataset contributed to the generation of four active rulesets for the training sets given in **Figure 28** and was externally validated by using the test sets. The four active rule set that was obtained using the training set are c1ccc2c(c1)oc1c2cc(cc1)NC(=O)OC (methyl

dibenzo[b,d]furan-2-ylcarbamate) (LR = ∞) that were observed in compounds (**16** to **24**), S(=O)(=O)c1ccc2c(c1)oc1c2cc(cc1)NC (7-hydrosulfonyl-N-methyldibenzo[b,d]furan-2-amine) (LR = 7.45) that were observed in compounds (**8,9** and **25** to **29**), 1ccc2c(c1)oc1c2cc(cc1)c1nc(on1)CC (3-(dibenzo[b,d]furan-2yl)-5ethyl-1,2,4-oxadiazole) (LR = 6.21) that were observed in compounds (**76** to **87**), S(=O)(=O)c1ccc2c(c1)oc1c2cc(cc1) (3-hydrosulfonyldibenzo[b,d]furan) (LR = 2.80) that were observed in compounds (**62** to **75**) which have been represented in **Figure 28**.

For the training set, the SARpy analysis provided sensitivity, specificity, accuracy, precision, MCC and F₁ of 82.7%, 72.2%, 76.9%, 70.5%, 0.55 and 0.76 respectively. The test set had a sensitivity, specificity, accuracy, precision and MCC and F₁ of 50%, 100%, 72.7%, 100%, 0.56 and 0.63.

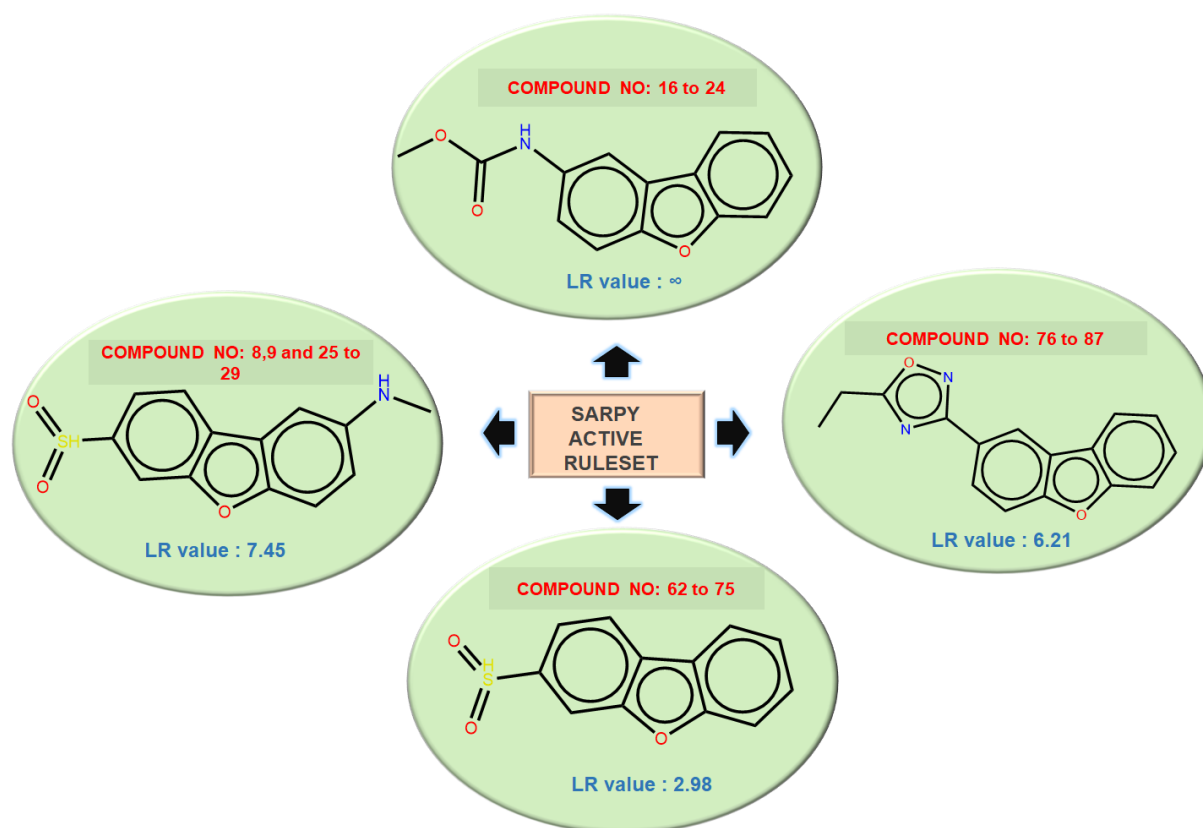


Figure 28: SARpy four active rulesets.

After applying the four structural alerts that were present in the active ruleset, the structural features OC(=O)C(C(C)C)NS(=O)(=O)c1ccc2c(c1)oc1c2cc(cc1)NC(=O)OCC(C) that [8-(propoxycarbonyl)amino)dibenzo[b,d]furan-3-yl)sulfonyl]valine was similar to the structural

alert having an LR value of infinity. In this compound, both carbamate as well as amine-type substructures were present which has a positive impact on MMP-12 inhibitory activity. These types of structures were also observed in compound numbers **16** to **24**. The other structure OC(=O)C(C(C)C)NS(=O)(=O)c1ccc2c(c1)oc1c2cc(cc1)c1nc(on1)C1CCC1 is [8-(5-cyclobutyl-1,2,4-oxadiazole-3-yl)dibenzo[b,d]furan-3-yl)sulfonyl]valine was also similar to the structural features having a LR value of 6.21. Due to the presence of 1,2,4-oxadiazole at the 8th position this has a positive contribution towards the MMP-12 inhibitory activity. These types of structures are usually seen in compounds 76 to 87. The other alert having LR value of 7.45 and 2.98 has similar types of structural features that are the presence of the sulfonyl group at the 3rd position. The only difference is the presence of the amine group at the 8th position. The structural alert having LR value of 7.45 was observed in the structure OC(=O)C(C(C)C)NS(=O)(=O)c1ccc2c(c1)oc1c2cc(cc1)NC(=O)c1ccsc1 is [8-(thiophene-3-carbonyl)dibenzo[b,d]furan-3-yl)sulfonyl] valine and were found in compounds **8,9** and **25** to **29**. In the end, structural alert having LR value of 2.98 seen in the structure OC(=O)C(C(C)C)NS(=O)(=O)c1ccc2c(c1)oc1c2cc(cc1)c1cocc1 is [8-(furan-3-yl)dibenzo[b,d]furan-3-yl)sulfonyl]valine and these types of structural alert were also seen in compounds (**62** to **75**).

Out of the 65 compounds in the training set, only 18 compounds did not match the 4 active ruleset due to the structural difference and had dibenzothiophene moieties in their structure. At the same time, the rest of the compounds in the training set matched with the active ruleset. For the test set, 7 out of 22 compounds did not match with the active structural alert, whereas the rest of the 15 structures matched with the active ruleset.

3.4. Molecular docking and molecular dynamic (MD) simulation studies

The molecular docking study of the most active compounds of these MMP-12 inhibitors has represented the chelation between the carboxylic acid zinc binding group (ZBG) of these compounds while the substituted dibenzofuran moiety strongly bound at the S1' pocket of the enzyme **Figure. 29**. The docking scores and the important amino acid residues have been tabulated in **Table 8**.

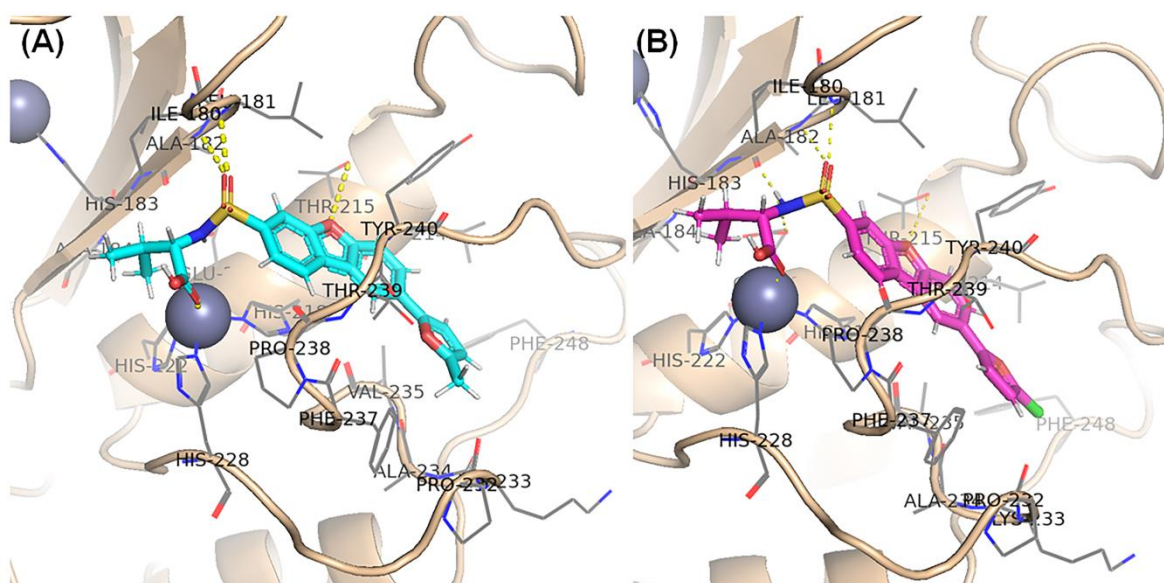


Figure 29. The docking interactions of (A) compound **69**; and (B) compound **70** at the active site of MMP-12 (PDB ID: 1RMZ)

Table 8. Summar of molecular docking study of compounds **69** and **70**

Cpd.	Docking score	Glide XP GScore	Glide gscore	Glide energy	Key Interacting Residues	Residues with H-Bonding	Residues with π - π interaction
69	-13.0687	-13.0688	-13.0688	-55.9501	Leu181, Ala182, Thr215, His218, Tyr240	Leu181, Ala182, Thr215	His218, Tyr240
70	-13.2918	-13.2919	-13.2919	-62.9682	Leu181, Ala182, Thr215, His218, Tyr240	Leu181, Ala182, Thr215	His218, Tyr240

From the molecular docking study, it was observed that both compounds **69** and **79** showed identical interactions at the active site of MMP-12 (PDB ID: 1RMZ). Both these compounds formed hydrogen bonding interactions with amino acid residues Leu181, Ala182, and Thr215 furthermore π - π stacking interactions with His218 and Tyr240 amino acid residues (**Appendix Figure A1**).

The MD simulation study of the docked complexes has also exhibited promising results. The RMSD calculation for the protein (black), and the complexed MMP-12 inhibitors (red) have shown a low RMS deviation **Figure. 30**.

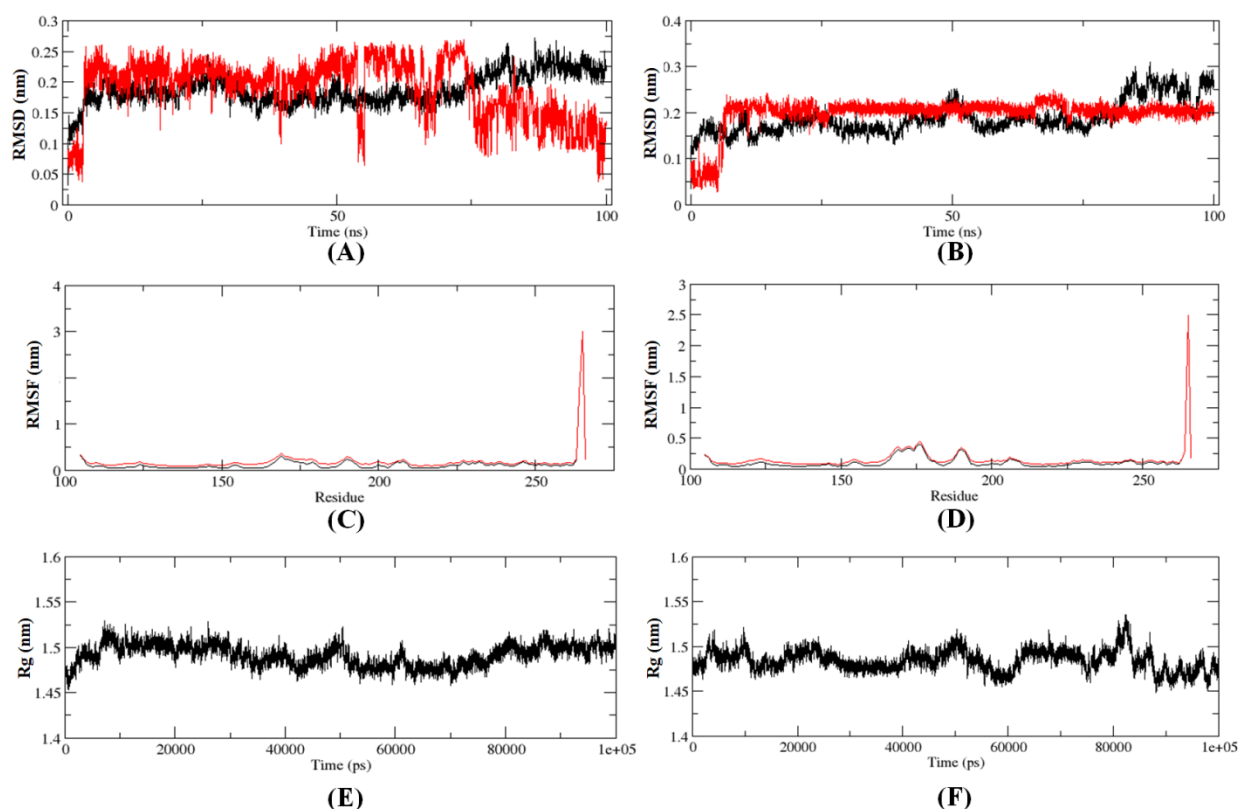


Figure. 30. (A) The RMSD plots for the C- α chain (black), and compound **69**; (B) The RMSD plots for the C- α chain (black), and compound **70**; (C) The RMSF plots for the C- α (black) chain and C- α -compound **69** complex (red); (D) The RMSF plots for the C- α (black) chain and C- α -compound **70** complex (red); (E) The R_g plots of the main chain for C- α -compound **69** complex; (F) The R_g plots of the main chain for C- α -compound **70** complex.

For the MD simulation study, it is noticed that although the C- α chain of the protein represented almost identical RMSD while complexing with both compounds **69** and **70**, compound **70** (**Figure. 30B**) showed comparative more stable binding compared to compound **69** (**Figure. 30A**) at MMP-12 active site. For compound **69**, the average RMSD value was 0.588 nm whereas the average RMSD of compound **70** was found to be 0.421 throughout the 100 ns MD run. For both compounds, the low RMSD values proposed stable interaction at the MMP-12 catalytic site.

On the other hand, in regard to the RMS fluctuation of the amino acid residues, comparatively less fluctuation in the residue movement was observed in the case of compound **69** (**Figure. 30C**) in comparison to compound **70** (**Figure. 30D**). From the analysis of the RMS fluctuation values of the protein residues, it was observed for compound **69** that apart from the structural

and catalytic Zn²⁺ ions (RMSF values of 3.01 nm and 1.62 nm, respectively) all the residues displayed a lower fluctuation (RMSF ranging between 0.092 nM and 0.367 nM). Interestingly, in the case of compound 70, only structural Zn²⁺ ion was found to exhibit high RMS fluctuation (2.491 nm). However, for both compounds **69** and **70**, the average RMS fluctuation values were assessed to be 0.189 nm and 0.157 nm, respectively, suggesting effective binding with less fluctuation.

The radius of gyration (Rg) for the main chain also exhibited a gyration between 1.45 nm and 1.55 nm (**Figures 30E** and **30F**). Therefore, these observations indicate stable binding of these molecules at the MMP-12 (PDB ID: 1RMZ) active site. Analysis of the Rg values for both complexes of MMP-12 and compounds 69 and 70 revealed an average Rg value of 1.491 nM and 1.484 nM, respectively. Therefore, the lower Rg values indicated the compact characteristics of both these complexes. The statistical values of the RMSD, RMS fluctuation, and Rg for both complexes are listed in **Table 9**. Moreover, the box plot of the RMSD, RMS fluctuation, and Rg for both complexes are provided in **Figure 31**.

Table 9. The statistical values of the RMSD, RMS fluctuation, and Rg for both complexes

Complex	Parameters	Mean	Median	SD
1RMZ-69	RMSD	0.588	0.321	0.355
	Rg	1.491	1.492	0.012
	RMSF	0.189	0.152	0.256
1RMZ-70	RMSD	0.421	0.263	0.287
	Rg	1.484	1.484	0.012
	RMSF	0.157	0.118	0.199

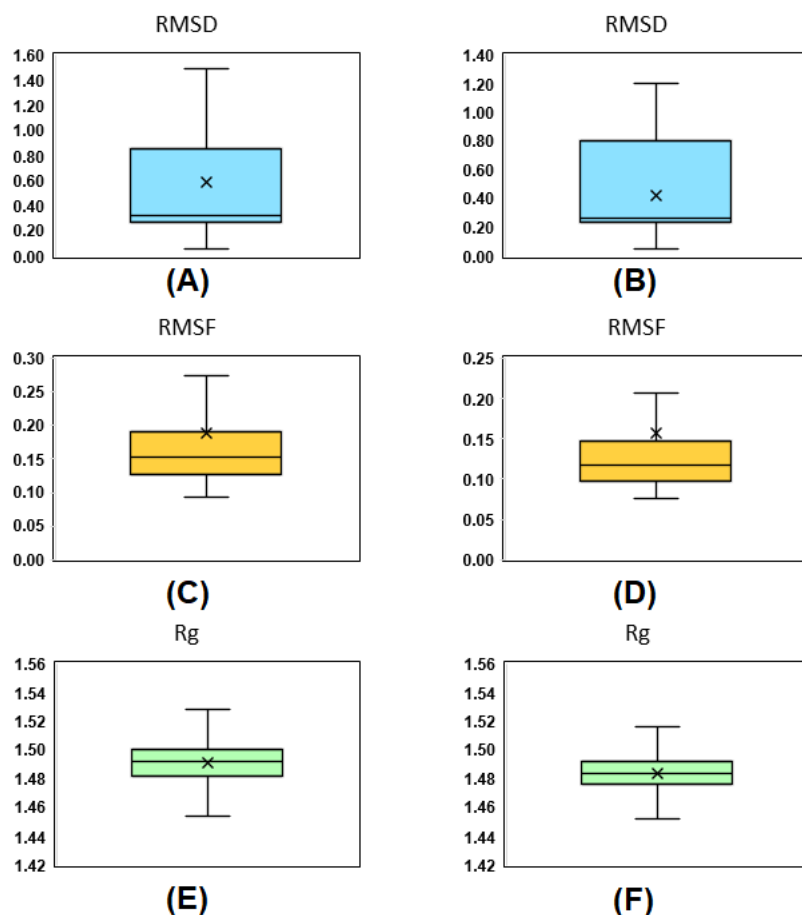


Fig. 31. (A) Boxplot for the RMSD of MMP-12 (PDB ID: 1RMZ) and compound **69** complex; (B) Boxplot for the RMSD of MMP-12 (PDB ID: 1RMZ) and compound **70** complex; (C) Boxplot for the RMS Fluctuation of MMP-12 (PDB ID: 1RMZ) and compound **69** complex; (D) Boxplot for the RMS Fluctuation of MMP-12 (PDB ID: 1RMZ) and compound **70** complex; (E) Boxplot for the Rg of MMP-12 (PDB ID: 1RMZ) and compound **69** complex; (F) Boxplot for the Rg of MMP-12 (PDB ID: 1RMZ) and compound **70** complex.

The hydrogen bond (H-bond) contact analysis of the affected complexes has exhibited mostly one hydrogen bond interactions between compound **69** whereas a greater number and frequency of H-bonds were established (2-3 H-bonds) by the compound **70** at the active site of MMP-12 (**Figures 32A** and **32B**). Interestingly, no H-bond contacts were established for compound **69** noticed around the 48-60 ns timeframe (**Figure. 32A**). Contradictorily, compound **70** showed almost steady H-bond interaction at the active site (**Figure. 32B**).

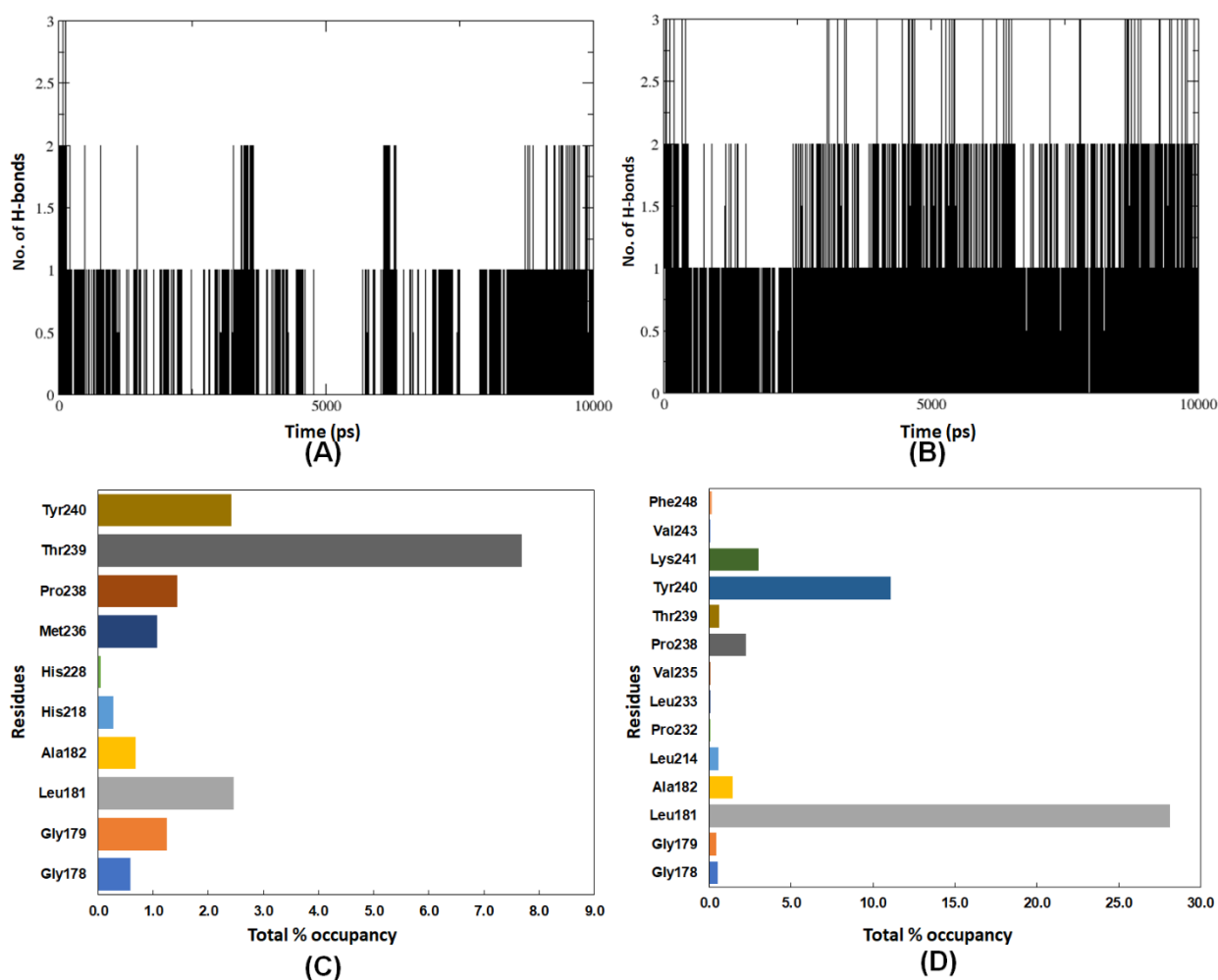


Fig. 32. (A) Number of hydrogen bond formations for the MMP-12-compound **69** complex; (B) Number of hydrogen bond formations for the MMP-12-compound **70** complex; (C) total percentage of hydrogen bond occupancy for the MMP-12-compound **69** complex; (D) total percentage of hydrogen bond occupancy for the MMP-12-compound **70** complex

The total hydrogen bond occupancy of the simulated compounds has shown a greater and more diverse number of hydrogen bond associations made by compound **70** compared to compound **69**. From the hydrogen bond (H-bond) occupancy of these compounds, it was observed that numerous amino acid residues such as Gly178, Gly179, Leu181, Ala182, Leu214, Pro232, Leu233, Val235, Pro238, Thr239, and Tyr240 created H-bond interaction with compound **69** (Figure. 32C) at the active site where the compound **70** was established interaction with Gly178, Gly179, Leu181, Ala182, His218, His228, Met236, Pro238, Thr239, and Tyr240 along with Lys241, Val243, and Phe238 (Figure. 32D).

It is interesting to note that, regardless of the same *in vitro* MMP-12 inhibitory activity and high structural similarity, compound **70** showed a majority of synergy at the MMP-12 active site. On the other hand, compound **69**, though incapable of forming a higher number of H-bonds, was capable of interacting with several Ω -loop amino acid residues near the S1' pocket of the enzyme which are essential not only for MMP-12 inhibitory potency as well as isoform selectivity of the molecules. Thus, despite having different frequencies and diversity of H-bond interactions for the compounds **69** and **70** at the MMP-12 catalytic site, these molecules were able to provide a similar *in vitro* enzyme inhibitory activity for MMP-12. This observation suggests that targeting both the S1' loop and Ω -loop residues at the S1' pocket of MMP-12 possibly delivers highly potent MMP-12 selective inhibitors with stable binding at the active site.

Chapter 6: Conclusion & Future Perspective

The current study revealed that out of all the MMPs, MMP-12 is the only MMP that is involved in inflammatory diseases due to the presence of the macrophage. Due to this MMP-12 is involved in major diseases like asthma, COPD, arthritis, and several types of solid cancers. This unique feature has made MMP-12 as one of the major targets for drug designing. Various studies have been reported about the role of MMP-12 in different pathological conditions and how selective MMP-12 inhibitors can be used to tackle these conditions. Though many MMP12 inhibitors are undergoing various stages of clinical trials, Foresee Pharmaceuticals' FP025 recently carried out phase II clinical trials that assessed its effectiveness in treating subjects with clinically stable, mild allergic asthma and blood eosinophilia for the allergen (HDM)-induced late asthmatic response (LAR) [184]. AZD1236, a dual MMP-9/MMP-12 inhibitor, completed phase II clinical studies examined for the management of COPD but was pulled from the same phase when AstraZeneca already assessed the safety of individuals with cystic fibrosis [184]. However not a single MMP-12 inhibitor has passed the clinical trials due to low solubility and poor pharmacokinetic profiles. To overcome this challenge several methods like QSAR study can be used for designing new molecules in the future. There is also a large amount of crystallographic data available in the protein data bank (PDB), as this will help in determining the curtail structural features and also help to acquire knowledge about the binding pattern and crucial amino acid residue in the active site of the MMP-12 inhibitors. Moreover, the ligand-based, and the structure-based method may also help in designing compounds having MMP-12 inhibitory activity. Ligand and structure-based methods are more advantageous than synthesis methods due to being more cost-effective and less time-consuming. The use of different regression-based and classification-based methods like MLR, HQSAR, 3D-QSAR, LDA, Bayesian recursive and SARpy methods were performed on compounds having MMP-12 inhibitory activity in combination with molecular docking and MD simulation studies. The regression-based studies showed that the hydrophobic P1' substituent is sufficient to occupy the hydrophobic S1' pocket of MMP-12, where the steric and/or hydrogen bond donor feature comprising P1' substituent can boost binding stability by interacting with the amino acid residues at the terminal end of the S1' pocket. Also, The MLR model favors compounds with fewer nitrogen atoms and suggests that this is advantageous for MMP-12 inhibition due to the large influence of these molecules' ionising potential. The HQSAR study also identified the dibenzofuran P1' substituent of these compounds as the better fit for the S1' pocket. Whereas the classification-based QSAR methods like LDA, Bayesian classification, recursive partitioning, and SARpy analysis were important for the extraction of the different features that helped in the characterization of the substructures, depending on

whether it had a positive or negative impact towards the MMP-12 inhibitory activity. From the above methods, it was observed that the substitution at the 8th positions with a five-membered ring structure having an oxygen, nitrogen, or combination of both like 1,2,4-oxadiazole has increased the MMP-12 inhibitory activity. In the case of the substitution at the seventh position either with the amine group or the amine attached to the oxygen decreased the MMP-12 inhibitory activity. The classification-based methods also helped in the comparative study of the two main derivatives, and it was observed that the dibenzofuran moiety had better MMP-12 inhibitory activity compared to the dibenzothiophene. The statistical validation of the classification-based method (i.e., sensitivity, specificity, precision, accuracy, MCC and F1) was important for checking the performance of the model, whereas in some cases the ROC score and graph were also important. The results of this study have therefore clarified the structural characteristics of these dibenzofuran and/or dibenzothiophene derivatives as well as their binding pattern, which will undoubtedly help in the future development of potent and selective inhibitors as therapeutics against MMP-12-related diseases. In addition, the MD simulation analysis revealed that, in addition to the other typical interactions, the interaction of molecules with the Pro238 residue in the Ω -loop plays a critical role in the potency and MMP-12 selectivity of these carboxylic acid derivatives.

References

1. M.A. Aslam, K. Riaz, M.M. Saleem, *Gradient-based impedance synthesis for breast and lung cancer cell screening deploying planar and nano-structured electrodes*, Med. Biol. Eng. Comput. 59 (2021) 1709-1721.
2. R.A. Weinberg, *How cancer arises*, Sci. Am. 275 (1996) 62-70.
3. M.S. Niloy, M.S. Shakil, M.M.H. Alif, R.J. Rosengren, *Using natural compounds to target KRAS mutated non-small cell lung cancer*, Curr. Med. Chem. 28 (2021) 8098-8115.
4. A. Lahiri, A. Maji, P.D. Potdar, *Lung cancer immunotherapy: Progress, pitfalls, and promises*. Mol Cancer. 22 (2023) 40
5. D. Ha, P.J. Mazzone, A.L. Ries, A. Malhotra, M. Fuster, *The utility of exercise testing in patients with lung cancer*. J. Thorac. Oncol. 11 (2016) 1397-1410.
6. T. Djuric, and M. Zivkovic, *Overview of MMP Biology and Gene Associations in Human Diseases", In the Role of Matrix Metalloproteinase in Human Body Pathologies*, IntechOpen. 20 (2017) 1.
7. N. Cui, M. Hu, and R.A. Khalil, *Biochemical and biological attributes of matrix metalloproteinases*. Prog. Mol. Biol. Transl. Sci. 147 (2017), pp. 1-73.
8. S. Banerjee , S.A. Amin, and T. Jha. *A fragment-based structural analysis of MMP-2 inhibitors in search of meaningful structural fragments*. Comput. Biol. Med. 144 (2022) 105360.
9. Z.Y. Guo and L.P. Jiang, *Matrix metalloproteinase 12 (MMP12) as an adverse prognostic biomarker of vascular invasion in hepatic cell carcinoma*. Eur. Rev. Med. Pharmacol. Sci. 26 (2022) 2238-2249.
10. M. Li, L. Zhou, S. Li, L. Fang, L. Yang, X. Wu, C. Yang, Y. Bao, S. Lan, Z. Tong, and S Zheng, *MMP12 is a potential therapeutic target for adamantinomatous craniopharyngioma: Conclusions from bioinformatics analysis and in vitro experiments*. Oncol. Lett. 22 (2021), pp. 1-8.
11. M.K. He, Y. Le, Y.F. Zhang, H.Y. Ouyang, P.E. Jian, Z.S. Yu, L.J. Wang, and M. Shi, *Matrix metalloproteinase 12 expression is associated with tumor FOXP3+ regulatory T cell infiltration and poor prognosis in hepatocellular carcinoma*. Oncol. Lett. 16 (2018) 475-482.
12. A. Noël, Z. Perveen, R. Xiao, H. Hammond, V. Le Donne, K. Legendre, M.R. Gartia, S. Sahu, D.B. Paulsen, A.L. and Penn, *Mmp12 is upregulated by in utero second-hand smoke exposures and is a key factor contributing to aggravated lung responses in adult emphysema, asthma, and lung cancer mouse models*. Frontiers Physiol. 12 (2021) 1-25.

13. E. Ella, Y. Harel, M. Abraham, H. Wald, O. Benny, A. Karsch-Bluman, D. Vincent, D. Laurent, G. Amir, U. Izhar, and O.M. Shapira, *Matrix metalloproteinase 12 promotes tumor propagation in the lung. J. Thorac. Cardiovasc. Surg.* 155 (2018) 2164-2175.
14. H.A. Eide, A.R. Halvorsen, V. Sandhu, A. Fåne, J. Berg, V.D. Haakensen, E.H. Kure, O.T. Brustugun, C.E. Kiserud, J.A. Kyte, Å Helland. *Non-small cell lung cancer is characterised by a distinct inflammatory signature in serum compared with chronic obstructive pulmonary disease. Clin. Translation. Immunol.* 5 (2016) 109.
15. R. Guha, *On the interpretation and interpretability of quantitative structure–activity relationship models. J. Comput. Aided. Mol. Des.* 22 (2008) 857-871.
16. P.P. Roy, S. Paul, I. Mitra, and K. Roy, *On two novel parameters for validation of predictive QSAR models. Molecules Basel, Switzerland,* 14 (2009) 1660-1701.
17. R. Perkins, H. Fang, W. Tong, and W.J. Welsh, *Quantitative structure-activity relationship methods: Perspectives on drug discovery and toxicology. Environ. Toxicol. Chem.* 22 (2003) 1666-1679.
18. C. Le Quement, I. Guenon, J.Y. Gillon, S. Valenca, V. Cayron-Elizondo, V. Lagente, and E. Boichot, *The selective MMP-12 inhibitor, AS111793 reduces airway inflammation in mice exposed to cigarette smoke. Brit. J. Pharmacol.* 154 (2008) 1206-1215.
19. S Mondal, N Adhikari, S Banerjee, SA Amin, T Jha. *Matrix metalloproteinase-9 (MMP-9) and its inhibitors in cancer: A minireview. Eur. J. Med. Chem.* 194 .(2020) 112260.
20. M Fernández-Fanjul, AR Folgueras, S Cabrera, C López-Otín, *Matrix metalloproteinases: Evolution, gene regulation and functional analysis in mouse models. Biochem. Biophys. Acta.* 1803 (2010) 3-19.
21. J. Hu, P.E. Van den Steen, Q.X. Sang, G. Opdenakker, *Matrix metalloproteinase inhibitors as therapy for inflammatory and vascular diseases. Nat Rev Drug Discov.* 6 (2007) 480-498.
22. C.M. Overall, *Molecular determinants of metalloproteinase substrate specificity: Matrix metalloproteinase substrate binding domains, modules, and exosites. Mol. Biotechnol.* 22 (2002) 51-86.
23. Y. Itoh, *Membrane-type matrix metalloproteinases: Their functions and regulations. Matrix. Biol.* 44-46 (2015) 207-23.
24. M.D. Covington, R.C. Burghardt, A.R. Parrish, *Ischemia-induced cleavage of cadherins in NRK cells requires MT1-MMP (MMP-14). Am. J. Physiol. Renal. Physiol.* 290 (2006) 43-51.

25. S. Barrantes -Hernandez, M. Bernardo, M. Toth, R. Fridman, *Regulation of membrane type-matrix metalloproteinases*. Sem. Cancer. Biol. 12 (2002) 131-138.
26. V.J. Craig, L. Zhang, J.S. Hagood, C.A. Owen, *Matrix metalloproteinases as therapeutic targets for idiopathic pulmonary fibrosis*. Am. J. Respir. Cell. Mol. Biol. 53 (2015) 585-600.
27. Y. Liu, Y.V. Li, Z. Liu, L. Zhang, M. Anniko, M. Duan. *Prognostic significance of matrix metalloproteinase-20 overexpression in laryngeal squamous cell carcinoma*. Acta Otolaryngol. 131 (2011) 769-773.
28. G. Velasco, A.M. Pendás, A. Fueyo, V. Knäuper, G. Murphy, C. Otín -López, *Cloning and characterization of human MMP-23, a new matrix metalloproteinase predominantly expressed in reproductive tissues and lacking conserved domains in other family members*. J. Biol. Chem. 274 (1999) 4570-4576.
29. T. Skoog, K. Ahokas, C. Orsmark, L. Jeskanen, K. Isaka, U. Kere -Saarialho. *MMP-21 is expressed by macrophages and fibroblasts in vivo and in culture*. Exp. Derm. 15:(2006) 775-783.
30. K. Maskos, *Crystal structures of MMPs in complex with physiological and pharmacological inhibitors*. Biochimie. 87 (2005) 249-63.
31. G. Murphy, H. Stanton, S. Cowell, G. Butler, V. Knäuper, S. Atkinson, J. Gavrilovic., *Mechanisms for pro matrix metalloproteinase activation*. APMIS : Acta patho microbio, et immune Scandi, 107 (1999) 38-44.
32. C.L. Quément, I. Guénon, J.Y. Gillon, V. Lagente, E. Boichot, *MMP-12 induces IL-8/CXCL8 secretion through EGFR and ERK1/2 activation in epithelial cells*. Ame. J. Phys-Lung. Cellu Mole. Phys. 294 (2008) 1076-1084.
33. B. Lovejoy, A.R. Welch, S. Carr, C. Luong, C. Broka, R. Hendricks, J.A. Campbell, K.A. Walker, R. Martin, H. Wart Van, M.F. Browner. *Crystal structures of MMP-1 and-13 reveal the structural basis for selectivity of collagenase inhibitors*. Nat. Stru. Bio. 6 (1999) 217-221.
34. H. Nar, K. Werle, M.M. Bauer, H. Dollinger, B. Jung, *Crystal structure of human macrophage elastase (MMP-12) in complex with a hydroxamic acid inhibitor*. J. Mol. Bio. 312:(2001) 743-751.
35. G. Murphy, S. Atkinson, R. Ward, J. Gavrilovic, J.J. Reynolds, *The role of plasminogen activators in the regulation of connective tissue metalloproteinases*. Ann. N Y. Acad Sci. 667 (1992). pp. 1-12.

36. H. Nakamura, Y. Fujii, E. Ohuchi, E. Yamamoto, Y. Okada, *Activation of the precursor of human stromelysin 2 and its interactions with other matrix metalloproteinases*. Eur. J. Biochem. 253 (1998) 67-75.
37. S.J. Atkinson, T. Crabbe, S. Cowell, R.V. Ward, M.J. Butler, H. Sato, M. Seiki, J.J. Reynolds, G.G. Murphy, *Intermolecular autolytic cleavage can contribute to the activation of progelatinase A by cell membranes*. J. Biol. Chem. 270 (1995) 30479-85.
38. G. Murphy, V. Knäuper, *Relating matrix metalloproteinase structure to function: Why the "hemopexin" domain?*. Matri. Bio. 15 (1997) 511-518.
39. S.D. Shapiro, D.K. Kobayashi, T.J. Ley, *Cloning and characterization of a unique elastolytic metalloproteinase produced by human alveolar macrophages*. J. Bio. Chem. 268 (1993), pp. 23824-9.
40. I. Bertini, V. Calderone, M. Fragai, C. Luchinat, S. Mangani, B. Terni, *X-ray Structures of binary and ternary enzyme-product-inhibitor complexes of matrix metalloproteinases*. Angewan. Chem. Inter. 42 (2003) 2673-6.
41. R. Lang, A. Kocourek, M. Braun, H. Tschesche, R. Huber, W. Bode, K. Maskos, *Substrate specificity determinants of human macrophage elastase (MMP-12) based on the 1.1 Å crystal structure*. J. Mol. Bio. 312 (2001) 731-42.
42. I. Bertini, V. Calderone, M. Cosenza, M. Fragai, Y.M. Lee, C. Luchinat, S. Mangani, B. Terni, P. Turano, *Conformational variability of matrix metalloproteinases: beyond a single 3D structure*. Proc. Nat. Acad. Sci. 102 (2005) 5334-9.
43. R. Morales, S. Perrier, J.M. Florent, J. Beltra, S. Dufour, I. De. Mendez, P. Manceau, A. Tertre, F. Moreau, D. Compere, A.C. Dublanchet, *Crystal structures of novel non-peptidic, non-zinc chelating inhibitors bound to MMP-12*. J. Mol. Biol. 341:(2004) 1063-76.
44. A.Y. Jeng, M. Chou, D.T. Parker, *Sulfonamide-based hydroxamic acids as potent inhibitors of mouse macrophage metalloelastase*. Bioorg. Med. Chem. Lett. 8 (1998) 897-902.
45. I. Bertini, V. Calderone, M. Fragai, R. Jaiswal, C. Luchinat, M. Melikian, E. Mylonas, D.I. Svergun, *Evidence of reciprocal reorientation of the catalytic and hemopexin-like domains of full-length MMP-12*. J. Amer. Chem. Soc. 130 (2008) 7011-21.
46. I. Bertini, A. Bhaumik, G. De. Paëpe, R.G. Griffin, M. Lelli, J.R. Lewandowski, C. Luchinat, *High-resolution solid-state NMR structure of a 17.6 kDa protein*. J. Amer. Chem. Soc. 132:(2010) 1032-40.

47. S. Balayssac, I. Bertini, A. Bhaumik, M. Lelli, C. Luchinat, *Paramagnetic shifts in solid-state NMR of proteins to elicit structural information*. *Proce. Nat. Acad. Sci.* 105 (2008) 17284-9.
48. M.A. Markus, B. Dwyer, S. Wolfrom, J. Li, W. Li, K. Malakian, J. Wilhelm, D.H. Tsao. *Solution structure of wild-type human matrix metalloproteinase 12 (MMP-12) in complex with a tight-binding inhibitor*. *Jr. of biomol. NMR.* 41 (2008) 55-60.
49. R.K. Koppiseti, Y.G. Fulcher, A. Jurkevich, S.H. Prior, J. Xu, M. Lenoir, M. Overduin, S.R. Van Doren. *Ambidextrous binding of cell and membrane bilayers by soluble matrix metalloproteinase-12*. *Nat. Commu.* 5 (2014) 5552.
50. S.H. Prior, T.S. Byrne, D. Roszyk -Tokmina, G.B. Fields, S.R. Doren Van, *Path to collagenolysis: collagen V triple-helix model bound productively and in encounters by matrix metalloproteinase-12*. *J. Biol. Chem.* 291 (2016) 7888-901.
51. I. Bertini, V. Calderone, M. Fragai, C. Luchinat, M. Maletta, K.J. Yeo, *Snapshots of the reaction mechanism of matrix metalloproteinases*. *Angewand. Chem. Inter. Ed.* 45 (2006) 7952-5.
52. R. Bhaskaran, M.O. Palmier, N.A. Bagegni, X. Liang, S.R. Doren Van, *Solution structure of inhibitor-free human metalloelastase (MMP-12) indicates an internal conformational adjustment*. *J. Mol. Bio.* 374 (2007) 1333-44.
53. I.P. Holmes, S. Gaines, S.P. Watson, O. Lorthioir, A. Walker, S.J. Baddeley, S. Herbert, D. Egan, M.A. Convery, O.M. Singh, J.W. Gross, *The identification of β -hydroxy carboxylic acids as selective MMP-12 inhibitors*. *Bioorg. Med. Chem. Lett.* 19 (2009) 5760-3.
54. J. Isaksson, S. Nyström, D. Derbyshire, H. Wallberg, T. Agback, H. Kovacs, I. Bertini, A. Giachetti, C. Luchinat, *Does a fast nuclear magnetic resonance spectroscopy-and X-ray crystallography hybrid approach provide reliable structural information of ligand-protein complexes? A case study of metalloproteinases*. *J Med Chem.* 52 (2009) 1712-22.
55. E. Dragoni, V. Calderone, M. Fragai, R. Jaiswal, C. Luchinat, C. Nativi. *Biotin-tagged probes for MMP expression and activation: Design, synthesis, and binding properties*. *Biocon. Chem.* 20 (2009) 719-27.
56. I. Bertini, V. Calderone, M. Fragai, A. Giachetti, M. Loconte, C. Luchinat, M. Maletta, C. Nativi, K.J. Yeo, *Exploring the subtleties of drug receptor interactions: the case of matrix metalloproteinases*. *J. Amer. Chem. Soc.* 129 (2007) 2466-75.

57. L. Devel, S. Garcia, B. Czarny, F. Beau, E. Lajeunesse, L. Vera, D. Georgiadis, E. Stura, V. Dive, *Insights from selective non-phosphinic inhibitors of MMP-12 tailored to fit with an S1' loop canonical conformation*. J. Bio. Chem. 285 (2010) 35900-9.
58. V Borsi, V Calderone, M Fragai, C Luchinat, N Sarti. *Entropic contribution to the linking coefficient in fragment based drug design: a case study*. J. Med. Chem. 10 (2010) 4285-9.
59. E Attolino, V Calderone, E Dragoni, M Fragai, B Richichi, C Luchinat, C Nativi. *Structure-based approach to nanomolar, water soluble matrix metalloproteinases inhibitors (MMPiS)*. Eur. J. Med. Chem. 45 (2010) 5919-25.
60. M. Mori, A. Massaro, V. Calderone, M. Fragai, C. Luchinat, A. Mordini. *Discovery of a new class of potent MMP inhibitors by structure-based optimization of the arylsulfonamide scaffold*. ACS. Med. Chem. Lett. 4 (2013) 565-569.
61. L. Devel, F. Beau, M. Amoura, L. Vera, E. Lajeunesse- Cassar, S. Garcia, B Czarny, E.A. Stura, V. Dive. *Simple pseudo-dipeptides with a P2' glutamate: A novel inhibitor family of matrix metalloproteases and other metzincins*. J. Bio. Chem. 287 (2012) 26647-56.
62. B. Czarny, E.A. Stura, L. Devel, L. Vera, E. Cassar-Lajeunesse, F. Beau, V. Calderone, M. Fragai, C. Luchinat, V. Dive, *Molecular determinants of a selective matrix metalloprotease-12 inhibitor: Insights from crystallography and thermodynamic studies*. J. Med. Chem. 56 (2013) 1149-59.
63. C. Antoni, L. Vera, L. Devel, M.P. Catalani, B. Czarny, E. Cassar-Lajeunesse, E. Nuti, A. Rossello, V. Dive, E.A. Stura, *Crystallization of bi-functional ligand protein complexes*. J Str Biol. 182 (2013) 246-54.
64. Y. Udi, M. Fragai, M. Grossman, S. Mitternacht, R. Arad-Yellin, V. Calderone, M. Melikian, M. Toccafondi, I.N. Berezovsky, C. Luchinat, I. Sagi, *Unraveling hidden regulatory sites in structurally homologous metalloproteases*. J. Mol. Bio. 425 (2013) 2330-46.
65. C. Rouanet-Mehouas, B. Czarny, F. Beau, E. Cassar-Lajeunesse, E.A. Stura, V. Dive, L. Deve, *Zinc-metalloproteinase inhibitors: Evaluation of the complex role played by the zinc-binding group on potency and selectivity*. J Med Chem. 60 (2017) 403-14.
66. E. Nuti, D. Cuffaro, F.D. Andrea, L. Rosalia, L. Tepshi, M. Fabbi, G. Carbotti, S. Ferrini, S. Santamaria, C. Camodeca, L. Ciccone, E. Orlandini, S. Nencetti, E.A. Stura , V.Dive, A. Rossello, *Sugar-Based Arylsulfonamide Carboxylates as Selective and Water-Soluble Matrix Metalloproteinase-12 Inhibitors*. Chem. Med. Chem. 11 (2016) 1626-1637.

67. L. Benda, J. Mareš, E. Ravera, G. Parigi, C. Luchinat, M. Kaupp, J. Vaara, *Pseudo-contact NMR shifts over the paramagnetic metalloprotein CoMMP-12 from first principles*. Angewand. Chem. 128 (2016) 14933-7.
68. T. Bordenave, M. Helle, F. Beau, D. Georgiadis, L. Tepshi, M. Bernes, Y. Ye, L. Levenez, E. Poquet, H. Nozach, M. Razavian, *Synthesis and in vitro and in vivo evaluation of MMP-12 selective optical probes*. Biocon. Chem. 27 (2016) 2407-17.
69. M. Fragai, G. Comito, L. Mannelli, D. Cesare, R. Gualdani, V. Calderone, A. Louka, B. Richichi, O. Francesconi, A. Angeli, A. Nocentini, P. Gratteri, *Lipoyl-homotaurine derivative (ADM_12) reverts oxaliplatin-induced neuropathy and reduces cancer cells malignancy by inhibiting carbonic anhydrase IX (CAIX)*. J. Med. Chem. 60 (2017) 9003-11.
70. S. Tsoukalidou, M. Kakou, I. Mavridis, D. Koumantou, V. Calderone, M. Fragai, E. Stratikos, A. Papakyriakou, D. Vourloumis, *Exploration of zinc-binding groups for the design of inhibitors for the oxytocinase subfamily of M1 aminopeptidases*. Bioorg. Med. Chem. 27 (2019) 115177.
71. E. Nuti, D. Cuffaro, E. Bernardini, C. Camodeca, L. Panelli, S. Chaves, L. Ciccone, L. Tepshi, L. Vera, E. Orlandini, S. Nencetti, *Development of thioaryl-based matrix metalloproteinase-12 inhibitors with alternative zinc-binding groups: Synthesis, potentiometric, NMR, and crystallographic studies*. J. Med. Chem. 61 (2018) 4421-35.
72. M. Książek, T. Goulas, D. Mizgalska, A. Rodríguez-Banqueri, U. Eckhard, F. Veillard, I. Waligórska, M. Benedyk-Machaczka, A.M. Sochaj-Gregorczyk, M. Madej, I.B. Thøgersen, *A unique network of attack, defence and competence on the outer membrane of the periodontitis pathogen Tannerella forsythia*. Chem. Sci. 14 (2023) 869-88.
73. W. Yang, S. Arii, M.J. Rivas- Gorriñ, A. Mori, H. Onodera, M. Imamura, *Human macrophage metalloelastase gene expression in colorectal carcinoma and its clinicopathologic significance*. Canc. 91 (2001) 1277-83.
74. F. Han, S. Zhang, L. Zhang, Q. Hao, *The overexpression and predictive significance of MMP-12 in esophageal squamous cell carcinoma*. Patho. Res. Prac. 213 (2017) 1519-1522.
75. E. Kerkelä, R. Ala-aho, P. Klemi, S. Grénman, S.D. Shapiro, V.M. Kähäri, U. Kere – Saarialho, *Metalloelastase (MMP-12) expression by tumour cells in squamous cell carcinoma of the vulva correlates with invasiveness, while that by macrophages predicts better outcome*. J. Patho. 198 (2002) 258-269.

76. Gorrin-Rivas, M. J. Arii, S. Furutani, M. Mizumoto, M. Mori, A. Hanaki, K. Maeda, M. Furuyama, H. Kondo, Y. & M. Imamura, *Mouse macrophage metalloelastase gene transfer into a murine melanoma suppresses primary tumor growth by halting angiogenesis. Clinical cancer research. J Ameri. Associ. Canc. Rese.* 6 (2000) 1647–1654.
77. MJ Rivas, S. Arii, M. Furutani, T. Harada, M. Mizumoto, H. Nishiyama, J. Fujita, M. Imamura, *Expression of human macrophage metalloelastase gene in hepatocellular carcinoma: correlation with angiostatin generation and its clinical significance. Hepato.* 28 (1998) 986-993.
78. K. Man, K.C.Shih, K.T. Ng, J.W. Xiao, D.Y. Guo, C.K. Sun, Z.X. Lim, Q. Cheng, Y. Liu ,S.T. Fan, C.M. Lo, *Molecular signature linked to acute phase injury and tumor invasiveness in small-for-size liver grafts. Annals. Surg.* 251 (2010) 1154-1161.
79. H.S. Hofmann, G. Hansen, G. Richter, C. Taege, A. Simm, R.E. Silber, S. Burdach, *Matrix metalloproteinase-12 expression correlates with local recurrence and metastatic disease in non–small cell lung cancer patients. Clin. Canc. Rese.* 11 (2005) 1086-92.
80. E. Ella, Y. Harel, M Abraham, H. Wald, O. Benny, A. Karsch-Bluman, D. Vincent, D. Laurent, G. Amir, .U Izhar, O.M. Shapira. *Matrix metalloproteinase 12 promotes tumor propagation in the lung. J Thor Card Surg.* 5 (2018) 2164-75
81. Z. Zhang, S. Zhu, Y. Yang, X. Ma, S. Guo, *Matrix metalloproteinase-12 expression is increased in cutaneous melanoma and associated with tumor aggressiveness. Tum. Biol.* 36 (2015) 8593-8600.
82. J. Zheng, D. Chu, D. Wang, Y. Zhu, X. Zhang, G. Ji, H. Zhao, G. Wu, J. Du, Q. Zhao, *Matrix metalloproteinase-12 is associated with overall survival in Chinese patients with gastric cancer. J. surg. oncol.* 107 (2013) 746-51.
83. T. Asano, M. Tada, S. Cheng, N. Takemoto, T. Kuramae, M. Abe, O. Takahashi, M. Miyamoto, J.I. Hamada, T. Moriuchi, S. Kondo. *Prognostic values of matrix metalloproteinase family expression in human colorectal carcinoma. J. Surg. Rese.* 1 (2008) 32-42.
84. B. Ding, M. Yao, W. Fan, W. Lou, *Whole-transcriptome analysis reveals a potential hsa_circ_0001955/hsa_circ_0000977-mediated miRNA-mRNA regulatory sub-network in colorectal cancer. Aging (Albany NY).* 6 (2020) 5259-5279.

85. S. Van Nguyen, M. Skarstedt, S. Löfgren, N. Zar, R.E. Andersson, M. Lindh, A. Matussek, J.A. Dimberg, *Gene polymorphism of matrix metalloproteinase-12 and-13 and association with colorectal cancer in Swedish patients*. Anticanc Res. 8 (2013) 3247-50.
86. V. Lagente, C. Le. Quement, E. Boichot, *Macrophage metalloelastase (MMP-12) as a target for inflammatory respiratory diseases*. Exp. Opi. Thera Targ. 13 (2009) 287-295.
87. I.K. Demedts, A. Morel-Montero, S. Lebecque, Y. Pacheco, D. Cataldo, G.F. Joos, R.A. Pauwels, G.G. Brusselle, *Elevated MMP-12 protein levels in induced sputum from patients with COPD*. Thor. 61 (2006) 196-201.
88. B. Chelluboina, K.R. Nalamolu, J.D. Klopfenstein, D.M. Pinson, D.Z. Wang, R. Vemuganti, K.K. Veeravalli, *MMP-12, a promising therapeutic target for neurological diseases*. Mole Neurobio. 55 (2018) 1405-1409.
89. Y. Song, Y. Xie, F. Liu, C. Zhao, R. Yu, S. Ban, Q. Ye, J. Wen, H. Wan, X. Li, R. Ma, *Expression of matrix metalloproteinase-12 in aortic dissection*. BMC. Card. Diso.13 (2013) 1-9.
90. L. Lind, B. Gigante, Y. Borne, A. Mälarstig, J. Sundström, J. Ärnlöv, E. Ingelsson, D. Baldassarre, E. Tremoli, F. Veglia, A. Hamsten, *The plasma protein profile and cardiovascular risk differ between intima-media thickness of the common carotid artery and the bulb: a meta-analysis and a longitudinal evaluation*. Athero. 295 (2020) 25-30.
91. J.L Johnson, L. Devel, B. Czarny, S.J. George, C.L. Jackson, V. Rogakos, F. Beau, A. Yiotakis, A.C. Newby, V. Dive, *A selective matrix metalloproteinase-12 inhibitor retards atherosclerotic plaque development in apolipoprotein E-knockout mice*. Arter. Throm. Vasc. Bio. 31 (2011) 528-535.
92. J.L. Johnson, S.J. George, A.C. Newby, C.L. Jackson, *Divergent effects of matrix metalloproteinases 3, 7, 9, and 12 on atherosclerotic plaque stability in mouse brachiocephalic arteries*. Proce. Nat. Acad. Sci. 102 (2005) 15575-80.
93. A.M. Houghton, J.L. Grisolano, M.L. Baumann, D.K. Kobayashi, R.D. Hautamaki, L.C. Nehring, L.A. Cornelius, S.D. Shapiro. *Macrophage elastase (matrix metalloproteinase-12) suppresses growth of lung metastases*. Canc. Rese. 12 (2006) 6149-55.
94. L. Devel, S. Garcia, B. Czarny, F. Beau, E. Lajeunesse, L. Vera, D. Georgiadis, E. Stura, V. Dive, *Insights from selective non-phosphinic inhibitors of MMP-12 tailored to fit with an S1' loop canonical conformation*. J Bio Chem. 46 (2010) 35900-9.

95. J. Zheng, D. Chu, D. Wang, Y. Zhu, X. Zhang, G. Ji, H. Zhao, G. Wu, J. Du, Q. Zhao, *Matrix metalloproteinase-12 is associated with overall survival in Chinese patients with gastric cancer*. J. Surg. Oncol. 7 (2013) 746-51.
96. B. Chelluboina, K.R. Nalamolu, J.D. Klopfenstein, D.M. Pinson, D.Z. Wang, R. Vemuganti, K.K. Veeravalli. *MMP-12, a promising therapeutic target for neurological diseases*. Mol. Neuro. Biol. 55 (2018) 1405-1409.
97. P. Norman. *Selective MMP-12 inhibitors: WO-2008057254*. Exp. Opin. Ther. Pat. 19 (2009) 1029-1034.
98. W. Li, J. Li, Y. Wu, J. Wu, R. Hotchandani, K. Cunningham, I. McFadyen, J. Bard, P. Morgan, F. Schlerman, X. Xu, *A selective matrix metalloprotease 12 inhibitor for potential treatment of chronic obstructive pulmonary disease (COPD): discovery of (S)-2-(8-(methoxycarbonylamino) dibenzo [b, d] furan-3-sulfonamido)-3-methylbutanoic acid (MMP408)*. J. Med. Chem. 7 (2009) 1799-802.
99. W Li, Li, Y. Wu, F. Rancati, S. Vallese, L.Raveglia, J.Wu, R. Hotchandani, N. Fuller, K. Cunningham, P.Morgan., *Identification of an orally efficacious matrix metalloprotease 12 inhibitor for potential treatment of asthma*. J. Med Chem. 17 (2009) 5408-19.
100. Y. Wu, J. Li, J. Wu, P. Morgan, X. Xu, F. Rancati, S. Vallese, L. Raveglia, R. Hotchandani, N. Fuller, J. Bard, *Discovery of potent and selective matrix metalloprotease 12 inhibitors for the potential treatment of chronic obstructive pulmonary disease (COPD)*. Bioorg. Med. Chem. Lett. 22 (2012) 138-43.
101. N. Ando, S. Terashima, *Synthesis of novel ageladine A analogs showing more potent matrix metalloproteinase (MMP)-12 inhibitory activity than the natural product*. Bioorg Med. Chem. Lett. 19 (2009) 5461-3.
102. N. Ando, S. Terashima, *Synthesis and matrix metalloproteinase-12 inhibitory activity of ageladine A analogs*. Chem. Pharmaceu. Bullet. 59 (2011) 579-96.
103. C. Mannino, M. Nievo, F. Machetti, A. Papakyriakou, V. Calderone, M. Fragai, A. Guarna, *Synthesis of Bicyclic Molecular Scaffolds (BTAA) for the Development of New Matrix Metalloproteinases Inhibitors*. Bioorg. Med. Chem. 14 (2006) 7392-403.
104. D. Ma, W. Wu, G. Yang, J. Li, J. Li, Q. Ye. *Tetrahydroisoquinoline based sulfonamide hydroxamates as potent matrix metalloproteinase inhibitors*. Bioorg. Med. Chem. Lett. 14 (2004) 47-50.
105. A.C. Dublanchet, P. Ducrot, C. Andrianjara C., M. O. Gara, R. Morales, D. Compère, A. Denis, S. Blais, P. Cluzeau, K. Courté, J. Hamon, *Structure-based design and synthesis of*

- novel non-zinc chelating MMP-12 inhibitors*. *Bioorg. Med. Chem. Lett.* 15 (2005) 3787-90.
106. C. Baggio, J.V. Velazquez, M. Fragai, T.M. Nordgren, M. Pellecchia. *Therapeutic targeting of MMP-12 for the treatment of chronic obstructive pulmonary disease*. *J. Med. Chem.* 63 (2020) 12911-20.
 107. E. Nuti, D. Cuffaro, F. D'Andrea, L. Rosalia, L. Tepshi, M. Fabbi, G. Carbotti, S. Ferrini, S. Santamaria, C. Camodeca, L. Ciccone. *Sugar-based arylsulfonamide carboxylates as selective and water-soluble matrix metalloproteinase-12 Inhibitors*. *Chem. Med. Chem.* 15 (2016) 1626-37.
 108. J. Aerts, R.E. Vandenbroucke, R. Dera, S. Balusu, E. Van Wonterghem, L. Moons, C. Libert, W. Dehaen, L. Arckens. *Synthesis and validation of a hydroxypyrrone-based, potent, and specific matrix metalloproteinase-12 inhibitor with anti-inflammatory activity in vitro and in vivo*. *Medi. Inflam.* (2015).
 109. M. Badland, D. Compère, K. Courté, A.C. Dublanchet, S. Blais, A. Manage, G. Peron, R. Wigglesworth. *Thiophene and bioisostere derivatives as new MMP12 inhibitors*. *Bioorg. Med. Chem. Lett.* (2011) 528-30.
 110. E. Nuti, L. Panelli, F. Casalini, S.I. Avramova, E. Orlandini, S. Santamaria, S. Nencetti, T. Tuccinardi, A. Martinelli, G. Cercignani, N. D'Amelio. *Design, synthesis, biological evaluation, and NMR studies of a new series of arylsulfones as selective and potent matrix metalloproteinase-12 inhibitors*. *J. Med. Chem.* 52 (2009) 6347-61.
 111. K. Gona, J. Toczek, Y. Ye, N. Sanzida, A. Golbazi, P. Boodagh, M. Salarian, J.J. Jung, S. Rajendran, G. Kukreja, T.L. Wu. *Hydroxamate-based selective macrophage elastase (MMP-12) inhibitors and radiotracers for molecular imaging*. *J Med Chem.* 23 (2020) 15037-49.
 112. G.F. Mangiatordi, T. Guzzo, E.C. Rossano, D. Trisciuzzi, D. Alberga, G. Fasciglione, M. Coletta, A. Topai, and O. Nicolotti. *Design, Synthesis, and Biological Evaluation of Tetrahydro- β -carboline Derivatives as Selective Sub-Nanomolar Gelatinase Inhibitors*. *Chem. Med. Chem.* 13 (2018) 1343-1352.
 113. V. Butsch, F. Börgel, F. Galla, K. Schwegmann, S. Hermann, M. Schäfers, B. Riemann, B. Wünsch, S. Wagner. *Design, (radio) synthesis, and in vitro and in vivo evaluation of highly selective and potent matrix metalloproteinase 12 (MMP-12) inhibitors as radiotracers for positron emission tomography*. *J. Med. Chem.* 9 (2018) 4115-4134.

114. J. Shamsara, A. Shahir-Sadr, *A predictive HQSAR model for a series of tricycle core containing MMP-12 inhibitors with dibenzofuran ring*. In. J. Med. Chem. 7 (2014).
115. F. Hadizadeh, J. Shamsara. Receptor-based 3D-QSAR approach to find selectivity features of flexible similar binding sites: case study on MMP-12/MMP-13. In Jr of Bioinf Res and App. 4 (2015) 326-46.
116. U. Singh, R.P. Gangwal, R. Prajapati, G.V. Dhoke, A.T. Sangamwar, *3D QSAR pharmacophore-based virtual screening and molecular docking studies to identify novel matrix metalloproteinase 12 inhibitors*. Mol. Sim. 5 (2013) 385-96.
117. C. Zhang, K. Wu, L. Huang, K., Y. Zou, Z. Xiong, B. Li, *Virtual screening and discovery of matrix metalloproteinase-12 inhibitors by swarm intelligence optimization algorithm-based machine learning*. Chem. Sele. 36 (2020) 11112-9.
118. B. Li, L. Hu, Y. Xue, M. Yang, L. Huang, Z. Zhang, J. Liu, G, Deng. *Prediction of matrix metal proteinases-12 inhibitors by machine learning approaches*. J. Biomol. Str. Dyn. 10 (2019) 2627-40.
119. H. Zhang, Y. Wang, F. Xu. *Impact of the subtle differences in MMP-12 structure on Glide-based molecular docking for pose prediction of inhibitors*. J Mol Struc. 1076 (2014) 153-9.
120. R.P. Verma, C. Hansch, *Matrix metalloproteinases (MMPs): Chemical–biological functions and (Q) SARs*. Bioorg. Med. Chem. 6 (2007) 2223-68.
121. Z. Zhang, S. Zhu, Y. Yang, X. Ma, S. Guo, *Matrix metalloproteinase-12 expression is increased in cutaneous melanoma and associated with tumor aggressiveness*. Tum. Bio. (2015) 8593-600.
122. A. Laurenzana, A. Biagioni, S. D'Alessio, F. Bianchini, A. Chillà, F. Margheri, C. Luciani, B. Mazzanti, N. Pimpinelli, E. Torre, S. Danese. *Melanoma cell therapy: Endothelial progenitor cells as shuttle of the MMP12 uPAR-degrading enzyme*. Oncotar. 11 (2014) 3711.
123. X. Yang, Y. Dong, J. Zhao, H. Sun, Y. Deng, J. Fan, Q. Yan. *Increased expression of human macrophage metalloelastase (MMP-12) is associated with the invasion of endometrial adenocarcinoma*. Patho-Rese. Prac. 7 (2007) 499-505.
124. V. Lagente, C. Le. Quement, E. Boichot, *Macrophage metalloelastase (MMP-12) as a target for inflammatory respiratory diseases*. Exp. Opin. Thera. Tar. 3 (2009) 287-95.

125. K.T. Ng, X. Qi, K.L. Kong, B.Y. Cheung, C.M. Lo, Poon RT, Fan ST, Man K. *Overexpression of matrix metalloproteinase-12 (MMP-12) correlates with poor prognosis of hepatocellular carcinoma*. Eur. J. Can. 15 (2011) 2299-305.
126. J.S.D. Tamang, S. Banerjee, S.K. Baidya, B. Ghosh, N. Adhikari, T. Jha. *Employing comparative QSAR techniques for the recognition of dibenzofuran and dibenzothiophene derivatives toward MMP-12 inhibition*. J. Bio. Stru. Dyn. (2023) 1-7.
127. ChemDraw Ultra 5.0, Cambridge Soft Corporation, USA, 2010; software available at <http://www.cambridgesoft.com>.
128. P.T. Nguyen, T. Van Dat, S. Mizukami, D.L. Nguyen, F. Mosaddeque, S.N. Kim, D.H. Nguyen, O.T. Dinh, T.L. Vo, G.L. Nguyen, and C. Quoc Duong. *2D-quantitative structure–activity relationships model using PLS method for anti-malarial activities of anti-haemozoin compounds*. Malar J. 20 (2021) 1-15.
129. Discovery Studio 3.0 (DS 3.0). Accelrys Inc., CA, USA, 2015; software available at <http://www.accelrys.com>.
130. C.W. Yap, *PaDEL-descriptor: an open source software to calculate molecular descriptors and fingerprints*. J. Comput. Chem. 32 (2011) 1466-1474.
131. TALETE srl. DRAGON, Milano, Italy, 2007; software available at <http://www.taletе.mi.it/>.
132. S. Mondal, S. Banerjee, S. Amin, and T. Jha, *Structural analysis of arylsulfonamide-based carboxylic acid derivatives: A QSAR study to identify the structural contributors toward their MMP-9 inhibition*. Struct. Chem, 32 (2021) 417-430.
133. S. Banerjee, S.K. Baidya, B. Ghosh, N. Adhikari, and T. Jha, *The first report on predictive comparative ligand-based multi-QSAR modeling analysis of 4-pyrimidinone and 2-pyridinone based APJ inhibitors*. New J. Chem. 46 (2022) 11591-11607.
134. P. Liu and W. Long, *Current mathematical methods used in QSAR/QSPR studies*. Int. J. Mol. Sci, 10 (2009) 1978-1998.
135. The simple, user-friendly and reliable online standalone tools, softwares available at <http://dtclab.webs.com/software-tools>.
136. S. Amin, S. Banerjee, S. Singh, I.A. Qureshi, S. Gayen, and T. Jha, *First structure-activity relationship analysis of SARS-CoV-2 virus main protease (Mpro) inhibitors: An endeavor on COVID-19 drug discovery*. Mol. Divers. 25 (2021) 1827-1838.

137. P.K. Ojha and K. Roy, *Comparative QSARs for antimalarial endochins: Importance of descriptor-thinning and noise reduction prior to feature selection*. Chemomet. Intell. Lab. Sys. 109 (2011) 146-161.
138. A. Golbraikh and A. Tropsha, *Beware of q^2 !*. J. Mol. Graph. Model. 20 (2002) 269-276.
139. J. Shamsara and A. Shahr-Sadr, *A predictive HQSAR model for a series of tricycle core containing MMP-12 inhibitors with dibenzofuran ring*. Int. J. Mol. Sci. 2014 (2014) 1-14.
140. H. Kumar, R. Kumar, B.K. Grewal, and M.E. Sobhia, *Insights into the structural requirements of PKC β II inhibitors based on HQSAR and CoMSIA analyses*. Chem. Biol. Drug Des. 78 (2011) 283-288.
141. G.C. Verissimo, E.F. Dutra, A.L. Dias, P. de Oliveira Fernandes, T. Kronenberger, M.A. Gomes, and V.G. Maltarollo, *HQSAR and random forest-based QSAR models for anti-T. vaginalis activities of nitroimidazoles derivatives*. J. Mole. Graph. Model. 90 (2019) 180-191.
142. R.N. Shinde, K. Srikanth, and M.E. Sobhia, *Insights into the permeability of drugs and drug-like molecules from MI-QSAR and HQSAR studies*, J. Mol. Mod. 18 (2012) 947-962.
143. SYBYL-X 2.0 Software (2012) Tripos Inc., St. Louis. MO, USA; software available at <http://www.certara.com>.
144. M. Seel, D.B. Turner, and P. Willett, *Effect of parameter variations on the effectiveness of HQSAR analysis*. Quant. Struct.-Act. Relat. 18 (1999) 245-252.
145. A. Kumar, G. Panda, and M.I. Siddiqi, *CoMFA and CoMSIA 3D-QSAR analysis of diaryloxy-methano-phenanthrene derivatives as anti-tubercular agents*. J. Mol. Mod. 13 (2007) 99-109.
146. V. Yadav, S. Banerjee, S.K. Baidya, N. Adhikari, and T Jha, *Applying comparative molecular modelling techniques on diverse hydroxamate-based HDAC2 inhibitors: An attempt to identify promising structural features for potent HDAC2 inhibition*. SAR QSAR Env. Res. 13 (2022) 1-22.
147. S. Wu, W. Qi, R. Su, T. Li, D. Lu, and Z. He. *CoMFA and CoMSIA analysis of ACE-inhibitory, antimicrobial and bitter-tasting peptides*. J. Med. Chem. 84 (2014) 100-106.
148. A. Xu, Zhang, S. Han, and L. Wang, *Studies of 3D-quantitative structure–activity relationships on a set of nitroaromatic compounds: CoMFA. advanced CoMFA and CoMSIA*. Chemosphere 48 (2002) 707-715.

149. P. Lu, X. Wei, and R. Zhang, *CoMFA and CoMSIA 3D-QSAR studies on quionolone caroxylic acid derivatives inhibitors of HIV-1 integrase*. J. Med. Chem. 48 (2010) 3413-3419.
150. G.H. Trossini, R.V. Guido, G. Oliva, E.I. Ferreira, and A.D. Andricopulo. *Quantitative structure–activity relationships for a series of inhibitors of cruzain from Trypanosoma cruzi: Molecular modeling, CoMFA and CoMSIA studies*. J. Mole. Graph. Model, 28 (2009) 3-11.
151. F. Briens, R. Bureau, S. Rault, and M. Robba, *Applicability of CoMFA in ecotoxicology: A critical study on chlorophenols*. Ecotox. Env. Safety 31 (1995) 37-48.
152. P.K. Ojha and K. Roy, *First report on exploring structural requirements of 1,2,3,4-tetrahydroacridin-9(10H)-one analogs as antimalarials using multiple QSAR approaches: Descriptor-based QSAR, CoMFA-CoMSIA 3DQSAR, HQSAR and G-QSAR approaches*. Comb. Chem. High Throughput Screen. 16 (2013) 7-21
153. H.Q. Wu, J. Yao, Q.Q. He, and F.E. Chen, *Docking-based CoMFA and CoMSIA studies on naphthyl-substituted diarylpyrimidines as NNRTIs*. SAR QSAR Env. Res. 25 (2014) 761-775.
154. P. Lu, X. Wei, R. Zhang, *CoMFA and CoMSIA studies on HIV-1 attachment inhibitors*. J. Med. Chem. 45 (2010) 1792-1798.
155. S. Yu, J. Yuan, J. Shi, X. Ruan, T. Zhang, Y. Wang, and Y. Du, *HQSAR and topomer CoMFA for predicting melanocortin-4 receptor binding affinities of trans-4-(4-chlorophenyl) pyrrolidine-3-carboxamides*. Chemo. Inte. Lab Sys. 146 (2015) 34-41.
156. C. Xu and Y. Ren, *Molecular modeling studies of [6,6,5] Tricyclic fused oxazolidinones as FXa inhibitors using 3D-QSAR, Topomer CoMFA, molecular docking and molecular dynamics simulations*. Bioorg. Med. Chem. Lett. 25 (2015) 4522-4528.
157. S. Amin, N. Adhikari, S. Gayen, and T. Jha, *First report on the structural exploration and prediction of new BPTES analogs as glutaminase inhibitors*. J. Mol Struc, 1143 (2017) 49-64.
158. M.F. Andrada , E.G. Vega-Hissi , M. R. Estrada a, J.C.G. Martinez, *Application of k-means clustering, linear discriminant analysis and multivariate linear regression for the development of a predictive QSAR model on 5-lipoxygenase inhibitors*, Chem. Int. Lab. Sys. 143 (2015) 122–129.
159. J.A. Castillo-Garit, M.C Vega, M Rolon, Y. Marrero-Ponce, V.V. Kouznetsov, D.F. Torres, A Gómez-Barrio, A.A. Bello, A. Montero, F. Torrens, F. Pérez-Giménez. *Computational*

discovery of novel trypanosomicidal drug-like chemicals by using bond-based non-stochastic and stochastic quadratic maps and linear discriminant analysis. Eur J Pharma Sci. 39 (2010) 30-6.

160. STATISTICA Version 7.1, StatSoft, Inc, Tulsa, USA, 2005
161. A. Nandy, S. Kar, & K. Roy, *Linear discriminant analysis for skin sensitisation potential of diverse organic chemicals*, Mol. Simu. 39(2013), pp. 432–441.
162. Discovery Studio 3.0 (DS 3.0). Accelrys Inc., CA, USA, 2015; software available at <http://www.accelrys.com>
163. N. Adhikari, A. K. Halder, S. Mallick, A. Saha, K. D. Saha, & T. Jha, *Robust design of some selective matrix metalloproteinase-2 inhibitors over matrix metalloproteinase-9 through in silico/fragment-based lead identification and de novo lead modification: Syntheses and biological assays*, Bioorg & Med. Chem. 24(2016) 4291–4309.
164. L. Chen, Y. Li, Q. Zhao, H. Peng, & T. Hou, *ADME evaluation in drug discovery. 10. Predictions of P-glycoprotein inhibitors using recursive partitioning and naïve Bayesian classification techniques*, Mol. Pharm. 8 (2011) 889–900.
165. SA Amin, N Adhikari, T Jha. *Exploration of histone deacetylase 8 inhibitors through classification QSAR study: Part II.* J Mol Stru. (2020) 1204.
166. L. Wang, L. Chen, Z. Liu, M. Zheng, Q. Gu , & J.Xu, *Predicting mTOR inhibitors with a classifier using recursive partitioning and Naïve Bayesian approaches.* PLoS One. 9(2014) 95221
167. S. Nandi, P. Kumar, S. A. Amin, T. Jha, & S. Gayen, (2021). *First molecular modelling report on tri-substituted pyrazolines as phosphodiesterase 5 (PDE5) inhibitors through classical and machine learning based multi-QSAR analysis.* SAR QSAR Env Res, 32(2021) 917–939.
168. X. Pang, W. Fu, J. Wang, D. Kang, L. Xu, Y. Zhao, A. L. Liu, & G. H. Du, *Identification of estrogen receptor α antagonists from natural products via in vitro and in silico approaches.* Oxi. Med. Cellu. Long. (2018) 6040149.
169. S. Amin, K. Ghosh, D. Mondal, S. Gayen and T. Jha, *Exploring indole derivatives as myeloid cell leukaemia-1 (Mcl-1) inhibitors with multi-QSAR approach: a novel hope in anti-cancer drug discovery*, New. J. Chem. 44 (2020) 17494
170. S. Banerjee, S.A. Amin, & T. Jha, *A fragment-based structural analysis of MMP-2 inhibitors in search of meaningful structural fragments.* Comp. Bio. Med. 144 (2022) 105360.

171. N. Adhikari, S. Banerjee, S. K. Baidya, B. Ghosh, , & T. Jha, *Robust classification-based molecular modelling of diverse chemical entities as potential SARS-CoV-2 3CL^{pro} inhibitors: Theoretical justification in light of experimental evidences*. SAR. QSAR. Env. Res. 32 (2021) 473–493.
172. S. Gutti, S. K. Baidya, S. Banerjee, N. Adhikari, & T. Jha, *A robust classification-dependent multi-molecular modelling study on some biphenyl sulphonamide based MMP-8 inhibitors*. SAR. QSAR. Env. Res, 32(2021) 835–861.
173. Schrodinger Suite, Schrodinger LLC, New York, USA, 2019; software available at <https://www.schrodinger.com>.
174. RCS protein Data Bank, <https://www.rcsb.org/> as accessed by 30th January 2023.
175. H.J.C. Berendsen, D. van der Spoel, and R. van Drunen, *GROMACS: A message-passing parallel molecular dynamics implementation*. Comput. Phys. Commun. 1-2 (1995), 43-56.
176. Groningen machine for chemical simulations; software available at <https://www.gromacs.org>.
177. R.B. Best, X. Zhu, J. Shim, P.E. Lopes, J. Mittal, M. Feig, and A.D. Jr Mackerell, *Optimization of the additive CHARMM all-atom protein force field targeting improved sampling of the backbone ϕ , ψ and side-chain $\chi(1)$ and $\chi(2)$ dihedral angles*. J. Chem. Theo Comp. 8(2012), pp. 3257-3273.
178. L.I. Gil Pineda, L.N. Milko, and Y. He, *Performance of CHARMM36m with modified water model in simulating intrinsically disordered proteins: A case study*. Biophys. Rep. 6 (2020) 80-87.
179. CGenFF webserver, <https://cgenff.umaryland.edu/> as accessed on 20 January 2023.
180. A.A. Al-Karmalawy, M.A. Dahab, A.M. Metwaly, S.S. Elhady, E.B. Elkaeed, I.H. Eissa, and K.M. Darwish, *Molecular docking and dynamics simulation revealed the potential inhibitory activity of ACEIs against SARS-CoV-2 targeting the hACE2 receptor*. Front. Chem. 9 (2021) 661230.
181. V.L. Golo and K.V. Shaïtan, *Dynamic attractor for the Berendsen thermostat an the slow dynamics of biomacromolecules*. Biofizika 47(2002) 611-617.
182. H.G. Petersen, *Accuracy and efficiency of the particle mesh Ewald method*. J. Chem. Phys. 103 (1995) 3668.

183. B. Hess, C. Kutzner, D. van der Spoel, and E. Lindahl, *GROMACS 4: Algorithms for highly efficient, load-balanced, and scalable molecular simulation*. J. Chem. Theory Comput. 4 (2008) 435-447.
184. <https://clinicaltrials.gov/>

APPENDIX

Appendix Table A1. Common structures, SMILES notation, of MMP-12 inhibitors having dibenzofuran and dibenzothiophene scaffold.

*test set for regression based # classification based

<i>Cpd. No.</i>	<i>SMILES</i>	<i>MMP-12</i>	
		<i>IC₅₀</i> (nM)	<i>pIC₅₀</i>
1	<chem>OC(=O)[C@H](C(C)C)NS(=O)(=O)c1ccc2c(c1)c1c(o2)cccc1</chem>	38	7.42
2*	<chem>OC(=O)[C@H](C(C)C)NS(=O)(=O)c1ccc2c(c1)c1c(o2)cc(cc1)NS(=O)(=O)C</chem>	170	6.77
3	<chem>OC(=O)[C@H](C(C)C)NS(=O)(=O)c1ccc2c(c1)c1c(o2)cccc1</chem>	600	6.222
4#	<chem>OC(=O)[C@H](C(C)C)NS(=O)(=O)c1ccc2c(c1)c1c(o2)cc(cc1)NS(=O)(=O)C</chem>	11	7.959
5	<chem>OC(=O)[C@@H](C(C)C)NS(=O)(=O)c1ccc2c(c1)c1c(o2)cc(cc1)NS(=O)(=O)C(C)C</chem>	50	7.301
6*	<chem>OC(=O)[C@H](C(C)C)NS(=O)(=O)c1ccc2c(c1)c1c(s2)cc(cc1)NS(=O)(=O)C</chem>	2,100	5.678
7	<chem>OC(=O)[C@H](C(C)C)NS(=O)(=O)c1ccc2c(c1)c1c(o2)cc(cc1)NS(=O)(=O)c1c(noc1C)C</chem>	2,500	5.602
8	<chem>OC(=O)[C@H](C(C)C)NS(=O)(=O)c1ccc2c(c1)c1c(o2)cc(cc1)NS(=O)(=O)c1ccccc1</chem>	100	7
9	<chem>OC(=O)[C@H](C(C)C)NS(=O)(=O)c1ccc2c(c1)oc1c2cc(cc1)NS(=O)(=O)C</chem>	10.03	7.999
10	<chem>OC(=O)[C@H](C(C)C)NS(=O)(=O)c1ccc2c(c1)oc1c2cc(cc1)NS(=O)(=O)CC(F)(F)F</chem>	70	7.155
11*	<chem>OC(=O)[C@@H](C(C)C)NS(=O)(=O)c1ccc2c(c1)sc1c2cc(cc1)NC(=O)OC</chem>	1.8	8.745
12	<chem>OC(=O)[C@H](C(C)C)NS(=O)(=O)c1ccc2c(c1)c1c(o2)cc(cc1)NC(=O)OC</chem>	7.2	8.143
13	<chem>OC(=O)[C@H](C(C)C)NS(=O)(=O)c1ccc2c(c1)c1c(o2)cc(cc1)NC(=O)OCCC</chem>	14	7.854
14	<chem>OC(=O)[C@@H](C(C)C)NS(=O)(=O)c1ccc2c(c1)c1c(o2)cc(cc1)NC(=O)OC(C)C</chem>	39	7.409
15	<chem>OC(=O)[C@H](C(C)C)NS(=O)(=O)c1ccc2c(c1)c1c(o2)cc(cc1)NC(=O)Oc1ccccc1</chem>	45	7.347
16	<chem>OC(=O)[C@H](C(C)C)NS(=O)(=O)c1ccc2c(c1)c1c(o2)cc(c(c1)Br)NC(=O)OC</chem>	1,050	5.979
17	<chem>OC(=O)[C@H](C(C)C)NS(=O)(=O)c1ccc2c(c1)c1c(o2)cc(c(c1)Br)NC(=O)OC</chem>	3,900	5.409
18	<chem>OC(=O)[C@H](C(C)C)NS(=O)(=O)c1ccc2c(c1)oc1c2cc(cc1)NC(=O)OC</chem>	2	8.699
19	<chem>OC(=O)[C@H](C(C)C)NS(=O)(=O)c1ccc2c(c1)oc1c2cc(cc1)NC(=O)OCC</chem>	5	8.301
20	<chem>OC(=O)[C@H](C(C)C)NS(=O)(=O)c1ccc2c(c1)oc1c2cc(cc1)NC(=O)OCCC</chem>	5.6	8.252

21*	<chem>OC(=O)[C@@H](C(C)C)NS(=O)(=O)c1ccc2c(c1)sc1c2ccc(c1)NC(=O)OC</chem>	29	7.538
22	<chem>OC(=O)[C@H](C(C)C)NS(=O)(=O)c1ccc2c(c1)oc1c2cc(cc1)NC(=O)OCC(C)C</chem>	4.7	8.328
23	<chem>OC(=O)[C@H](C(C)C)NS(=O)(=O)c1ccc2c(c1)oc1c2cc(cc1)NC(=O)OCCF</chem>	2.1	8.678
24	<chem>OC(=O)[C@H](C(C)C)NS(=O)(=O)c1ccc2c(c1)oc1c2cc(cc1)NC(=O)Oc1ccccc1</chem>	10.2	7.991
25*	<chem>OC(=O)[C@H](C(C)C)NS(=O)(=O)c1ccc2c(c1)sc1c2ccc(c1)NC(=O)OCC</chem>	6.3	8.201
26*	<chem>OC(=O)[C@H](C(C)C)NS(=O)(=O)c1ccc2c(c1)sc1c2ccc(c1)NC(=O)OCC(C)C</chem>	20.2	7.695
27	<chem>OC(=O)[C@H](C(C)C)NS(=O)(=O)c1ccc2c(c1)oc1c2cc(cc1)NC(=O)Oc1ccccc1Cl</chem>	6.6	8.18
28	<chem>OC(=O)[C@H](C(C)C)NS(=O)(=O)c1ccc2c(c1)oc1c2cc(cc1)NC(=O)Oc1ccc(cc1)F</chem>	8.1	8.092
29*	<chem>OC(=O)[C@H](C(C)C)NS(=O)(=O)c1ccc2c(c1)sc1c2ccc(c1)NC(=O)Oc1ccc(cc1)C</chem>	36.3	7.44
30*	<chem>OC(=O)[C@H](C(C)C)NS(=O)(=O)c1ccc2c(c1)sc1c2ccc(c1)NC(=O)NCC</chem>	260	6.585
31#	<chem>OC(=O)[C@H](C(C)C)NS(=O)(=O)c1ccc2c(c1)oc1c2cc(cc1)NC(=O)Oc1ccc(cc1)C</chem>	14	7.854
32	<chem>OC(=O)[C@H](C(C)C)NS(=O)(=O)c1ccc2c(c1)oc1c2ccc(c1)NC(=O)NCCc1cccs1</chem>	18	7.745
33	<chem>OC(=O)[C@H](C(C)C)NS(=O)(=O)c1ccc2c(c1)oc1c2cc(cc1)NC(=O)N</chem>	7.6	8.119
34	<chem>OC(=O)[C@H](C(C)C)NS(=O)(=O)c1ccc2c(c1)oc1c2cc(cc1)NC(=O)NC1CCCC1</chem>	5	8.301
35	<chem>OC(=O)[C@H](C(C)C)NS(=O)(=O)c1ccc2c(c1)oc1c2cc(cc1)NC(=O)c1ccsc1</chem>	0.9	9.046
36*#	<chem>OC(=O)[C@H](C(C)C)NS(=O)(=O)c1ccc2c(c1)oc1c2cc(cc1)n1cncn1</chem>	13	7.886
37	<chem>OC(=O)[C@H](C(C)C)NS(=O)(=O)c1ccc2c(c1)oc1c2ccc(c1)NC(=O)OCCF</chem>	10	8
38#	<chem>OC(=O)[C@H](C(C)C)NS(=O)(=O)c1ccc2c(c1)oc1c2ccc(c1)NC(=O)Oc1ccc(cc1)F</chem>	16	7.796
39*	<chem>OC(=O)[C@H](C(C)C)NS(=O)(=O)c1ccc2c(c1)oc1c2cc(cc1)n1ccc(n1)C(F)(F)F</chem>	0.7	9.155
40	<chem>OC(=O)[C@@H](C(C)C)NS(=O)(=O)c1ccc2c(c1)c1c(s2)cc(cc1)NS(=O)(=O)C</chem>	4,400	5.357
41	<chem>OC(=O)[C@@H](C(C)C)NS(=O)(=O)c1ccc2c(c1)sc1c2cc(cc1)NS(=O)(=O)C</chem>	60	7.222
42	<chem>OC(=O)[C@H](C(C)C)NS(=O)(=O)c1ccc2c(c1)sc1c2cc(cc1)NS(=O)(=O)C</chem>	50	7.301
43*	<chem>OC(=O)[C@H](C(C)C)NS(=O)(=O)c1ccc2c(c1)oc1c2cc(cc1)N1CCNCC1</chem>	23	7.638
44*#	<chem>OC(=O)[C@H](C(C)C)NS(=O)(=O)c1ccc2c(c1)oc1c2cc(cc1)N1CCN(CC1)C</chem>	18	7.745
45	<chem>OC(=O)[C@@H](C(C)C)NS(=O)(=O)c1ccc2c(c1)c1c(s2)cc(cc1)NC(=O)OC</chem>	2,900	5.538

46 [#]	<chem>OC(=O)[C@H](C(C)C)NS(=O)(=O)c1ccc2c(c1)c1c(s2)cc(cc1)NC(=O)OC</chem>	7,300	5.137
47	<chem>OC(=O)[C@H](C(C)C)NS(=O)(=O)c1ccc2c(c1)sc1c2cc(cc1)NC(=O)OC</chem>	0.4	9.398
48	<chem>OC(=O)[C@H](C(C)C)NS(=O)(=O)c1ccc2c(c1)sc1c2ccc(c1)NC(=O)OC</chem>	9	8.046
49 [*]	<chem>OC(=O)[C@H](C(C)C)NS(=O)(=O)c1ccc2c(c1)oc1c2cc(cc1)c1sccc1</chem>	0.2	9.699
50 ^{*#}	<chem>OC(=O)[C@H](C(C)C)NS(=O)(=O)c1ccc2c(c1)oc1c2cc(cc1)c1sc(cc1)C</chem>	0.2	9.699
51	<chem>OC(=O)[C@@H](C(C)C)NS(=O)(=O)c1ccc2c(c1)oc1c2ccc(c1)NC(=O)OC</chem>	11.1	7.955
52	<chem>OC(=O)[C@H](C(C)C)NS(=O)(=O)c1ccc2c(c1)oc1c2ccc(c1)NC(=O)OC</chem>	14	7.854
53	<chem>OC(=O)[C@H](C(C)C)NS(=O)(=O)c1ccc2c(c1)sc1c2ccc(c1)N</chem>	42	7.377
54 [#]	<chem>OC(=O)[C@@H](C(C)C)NS(=O)(=O)c1ccc2c(c1)sc1c2ccc(c1)NC(=O)OCC</chem>	100.1	7
55	<chem>OC(=O)[C@H](C(C)C)NS(=O)(=O)c1ccc2c(c1)sc1c2ccc(c1)NC(=O)OC(C)C</chem>	23.1	7.636
56	<chem>OC(=O)[C@H](C(C)C)NS(=O)(=O)c1ccc2c(c1)sc1c2ccc(c1)NC(=O)OCCS(=O)(=O)C</chem>	7.6	8.119
57	<chem>OC(=O)[C@H](C(C)C)NS(=O)(=O)c1ccc2c(c1)sc1c2ccc(c1)NC(=O)OCCC#C</chem>	6.1	8.215
58	<chem>OC(=O)[C@H](C(C)C)NS(=O)(=O)c1ccc2c(c1)sc1c2ccc(c1)NC(=O)Oc1ccccc1</chem>	25	7.602
59	<chem>OC(=O)[C@H](C(C)C)NS(=O)(=O)c1ccc2c(c1)sc1c2ccc(c1)NC(=O)Oc1ccc(cc1)F</chem>	28	7.553
60 [*]	<chem>OC(=O)[C@H](C(C)C)NS(=O)(=O)c1ccc2c(c1)oc1c2cc(cc1)c1sc(en1)C</chem>	1.2	8.921
61	<chem>OC(=O)[C@H](C(C)C)NS(=O)(=O)c1ccc2c(c1)sc1c2ccc(c1)NC(=O)NCCc1cccs1</chem>	187	6.728
62 [#]	<chem>OC(=O)[C@@H](C(C)C)NS(=O)(=O)c1ccc2c(c1)sc1c2ccc(c1)NC(=O)Nc1ccccc1</chem>	1,470	5.833
63	<chem>OC(=O)[C@H](C(C)C)NS(=O)(=O)c1ccc2c(c1)sc1c2ccc(c1)NC(=O)Nc1ccccc1</chem>	89	7.051
64 [#]	<chem>OC(=O)[C@H](C(C)C)NS(=O)(=O)c1ccc2c(c1)sc1c2ccc(c1)NC(=O)NCc1ccccc1</chem>	34.1	7.467
65 [#]	<chem>C(=O)([C@H](C(C)C)NS(=O)(=O)c1ccc2c(oc3c2cc(cc3)N2C(=O)OCC2)c1)O</chem>	1.4	8.854
66 ^{*#}	<chem>OC(=O)[C@H](C(C)C)NS(=O)(=O)c1ccc2c(c1)oc1c2cc(cc1)c1nc(on1)C</chem>	8.6	8.066
67 [*]	<chem>OC(=O)[C@H](C(C)C)NS(=O)(=O)c1ccc2c(c1)oc1c2cc(cc1)c1nc(on1)CC(C)C</chem>	5.4	8.268
68 [*]	<chem>OC(=O)[C@H](C(C)C)NS(=O)(=O)c1ccc2c(c1)oc1c2cc(cc1)c1nc(on1)COC</chem>	1.9	8.721
69	<chem>OC(=O)[C@H](C(C)C)NS(=O)(=O)c1ccc2c(c1)oc1c2ccc(c1)N1CCOC1=O</chem>	9.2	8.036
70	<chem>OC(=O)[C@H](C(C)C)NS(=O)(=O)c1ccc2c(c1)sc1c2ccc(c1)N1CCOC1=O</chem>	44	7.357

71 ^{*#}	<chem>OC(=O)[C@H](C(C)C)NS(=O)(=O)c1ccc2c(c1)oc1c2cc(cc1)c1nc(on1)C(F)(F)F</chem>	2.2	8.658
72 [#]	<chem>OC(=O)[C@H](C(C)C)NS(=O)(=O)c1ccc2c(c1)oc1c2ccc(c1)N</chem>	17	7.77
73	<chem>OC(=O)[C@H](C(C)C)NS(=O)(=O)c1ccc2c(c1)oc1c2cc(cc1)n1cccn1</chem>	15	7.824
74 [*]	<chem>OC(=O)[C@H](C(C)C)NS(=O)(=O)c1ccc2c(c1)oc1c2cc(cc1)c1nc(on1)C1CC1</chem>	1.6	8.796
75 [#]	<chem>OC(=O)[C@H](C(C)C)NS(=O)(=O)c1ccc2c(c1)oc1c2cc(cc1)N1CCOCC1</chem>	2.2	8.658
76 [#]	<chem>OC(=O)[C@H](C(C)C)NS(=O)(=O)c1ccc2c(c1)oc1c2cc(cc1)c1cocc1</chem>	0.4	9.398
77	<chem>OC(=O)[C@H](C(C)C)NS(=O)(=O)c1ccc2c(c1)oc1c2cc(cc1)c1oc(cc1)C</chem>	0.1	10
78	<chem>OC(=O)[C@H](C(C)C)NS(=O)(=O)c1ccc2c(c1)oc1c2cc(cc1)c1oc(cc1)Cl</chem>	0.1	10
79	<chem>OC(=O)[C@H](C(C)C)NS(=O)(=O)c1ccc2c(c1)oc1c2cc(cc1)c1[nH]ccc1</chem>	0.4	9.398
80 [#]	<chem>OC(=O)[C@H](C(C)C)NS(=O)(=O)c1ccc2c(c1)oc1c2cc(cc1)c1scn1</chem>	1	9
81	<chem>OC(=O)[C@H](C(C)C)NS(=O)(=O)c1ccc2c(c1)oc1c2cc(cc1)c1nc(on1)CC</chem>	2.9	8.538
82 [#]	<chem>OC(=O)[C@H](C(C)C)NS(=O)(=O)c1ccc2c(c1)oc1c2cc(cc1)c1nc(on1)C(C)C</chem>	4.5	8.347
83 [#]	<chem>OC(=O)[C@H](C(C)C)NS(=O)(=O)c1ccc2c(c1)oc1c2cc(cc1)c1nc(on1)C(C)(C)C</chem>	17	7.77
84	<chem>OC(=O)[C@H](C(C)C)NS(=O)(=O)c1ccc2c(c1)oc1c2cc(cc1)c1nc(on1)C1CCC1</chem>	2.3	8.638
85	<chem>OC(=O)[C@H](C(C)C)NS(=O)(=O)c1ccc2c(c1)oc1c2cc(cc1)c1nc(on1)C1CCCCC1</chem>	7.2	8.143
86 ^{*#}	<chem>OC(=O)[C@H](C(C)C)NS(=O)(=O)c1ccc2c(c1)oc1c2cc(cc1)c1nc(on1)c1ccccc1</chem>	4	8.398
87	<chem>OC(=O)[C@H](C(C)C)NS(=O)(=O)c1ccc2c(c1)oc1c2cc(cc1)c1nc(on1)[C@@H]1CCOC1</chem>	0.3	9.523

Appendix Table A2. The MLR model (*equation 1*) with predicted activity

<i>Cpd No</i>	<i>nHBint5</i>	<i>nN</i>	<i>ATSC6s</i>	<i>AATS0m</i>	<i>piPC6</i>	<i>VE3_Dzi</i>	<i>ATSC1e</i>	<i>VE3_Dzp</i>	<i>pIC₅₀</i>	<i>Predicted activity</i>
1	2	1	-34.7084	121.3084	6.705983	-3.27707	0.066234	-2.09094	7.42	7.546
3	2	2	-27.2945	139.9374	6.86856	-6.17708	0.23821	-8.67094	7.959	7.546

4	2	2	-27.2945	139.9374	6.86856	-6.17708	0.23821	-8.67094	6.77	7.271
5	2	2	-29.0571	129.9913	6.877876	-9.97896	0.335531	-13.8639	7.301	7.271
7	2	2	-41.0494	135.3622	6.967085	-12.0937	0.32213	-13.615	7	7.235
8	4	2	-73.6822	139.9374	6.847275	-5.91099	0.23821	-5.21025	7.999	6.984
9	4	2	-77.4414	155.4422	6.861515	-14.4256	-0.06649	-6.1235	7.155	7.123
10	2	2	-34.7505	121.9051	6.852044	-7.04929	-0.24468	-2.7714	8.143	7.878
12	2	2	-22.0109	113.9263	6.858368	-11.0063	-0.14339	-1.35894	7.409	7.193
13	2	2	-40.0934	119.584	6.912618	-9.58296	-0.15891	-1.71325	7.347	7.610
14	2	2	-32.6801	252.1834	6.915785	-5.9771	-0.30566	-3.47651	5.979	7.288
15	2	2	-32.6801	252.1834	6.915785	-5.9771	-0.30566	-3.47651	5.409	7.412
16	4	2	-73.0503	121.9051	6.830402	-6.67461	-0.24468	-4.62083	8.699	7.404
17	4	2	-66.4765	117.6855	6.833638	-10.534	-0.19133	-2.77225	8.301	5.832
18	4	2	-82.4343	113.9263	6.834714	-8.74863	-0.14339	-1.87562	8.252	5.832
19	4	2	-97.47	110.5559	6.835789	-6.92914	-0.10007	-1.60599	8.328	8.687
20	5	2	-78.6231	124.6071	6.834714	-9.77344	-0.3208	-1.34067	8.678	8.335
22	5	2	-79.4075	142.007	6.909067	-12.4548	-0.23247	-2.5989	8.18	8.161
23	4	2	-86.89	126.0112	6.914296	-9.69281	-0.27549	-1.9934	8.092	8.044
24	4	2	-83.78	115.9831	6.914296	-9.05149	-0.11663	-2.36193	7.854	9.046
27	4	2	-66.9527	138.0388	6.892832	-11.7585	-0.10062	-7.54696	9.046	8.258
28	4	2	-62.7307	124.6071	6.837433	-9.71363	-0.3208	-1.24479	8	8.752
31	2	2	-83.5621	155.6899	6.86856	-6.73213	0.358043	-5.10623	5.678	8.332
33	4	2	-60.1384	155.6899	6.847275	-5.87684	0.358043	-5.33265	7.301	8.443
34	2	2	-81.0234	137.6577	6.852044	-7.82856	-0.12369	-3.73369	5.538	8.636
35	2	2	-81.0234	137.6577	6.852044	-7.82856	-0.12369	-3.73369	5.137	7.795
37	4	2	-62.9221	137.6577	6.830402	-6.6008	-0.12369	-3.55964	9.398	8.266
38	3	2	-69.4061	137.6577	6.833133	-7.49377	-0.12369	-3.95329	7.538	8.477
40	3	2	-57.17	121.9051	6.833133	-6.5097	-0.24468	-3.18314	7.955	7.817
41	3	2	-57.17	121.9051	6.833133	-6.5097	-0.24468	-3.18314	7.854	5.458
42	3	2	-50.008	138.203	6.766084	-3.96832	-0.04348	-1.87597	7.377	5.458
45	3	2	-58.8364	127.9604	6.839577	-10.9818	-0.04238	-1.49319	7.636	7.704
46	3	2	-93.4067	123.8641	6.838506	-6.64637	-0.00758	-1.04313	7.695	7.704
47	3	2	-9.29029	147.8896	6.853398	-5.0445	0.151643	-1.31842	8.119	6.226
48	3	2	-54.7002	132.9639	6.847043	-6.26638	-0.07078	-0.9875	8.215	6.226
51	3	2	-82.8025	139.7947	6.916808	-9.4506	-0.15869	-1.458	7.553	8.381
52	3	3	-58.2778	128.9201	6.83636	-11.6132	-0.09521	-3.27158	6.585	8.381
53	3	3	-61.12	140.6617	6.869502	-5.04292	-0.06991	-2.01776	6.728	7.304

54	3	3	-50.35	127.7971	6.869502	-4.84684	-0.15952	-2.70141	7.745	7.304
55	3	3	-68.5837	129.9969	6.894828	-11.6663	-0.07735	-2.67988	5.833	8.052
56	3	3	-68.5837	129.9969	6.894828	-11.6663	-0.07735	-2.67988	7.051	8.052
57	3	3	-66.6604	125.9353	6.887202	-6.86258	-0.04582	-2.31235	7.467	7.481
58	3	2	-62.0413	122.3523	6.886085	-5.3557	-0.15943	-11.8936	8.854	6.695
59	3	2	-52.2631	122.3523	6.883495	-5.27883	-0.15943	-5.65116	8.036	6.695
61	3	2	-56.314	120.2524	6.766084	-3.5743	-0.14372	-3.64714	7.77	7.110
62	3	4	-55.1871	124.5059	7.079053	-3.66243	0.076734	-4.90969	7.886	6.871
63	3	3	-50.5937	120.8512	7.079053	-3.73075	0.173089	-4.70253	7.824	8.119
64	3	3	-54.9583	137.7829	7.164841	-4.77618	-0.12392	-4.64549	9.155	7.629
65	3	3	-44.0101	108.204	6.865174	-6.81588	-0.0048	-9.69608	7.638	7.083
69	3	1	-50.6574	116.7646	7.104324	-4.76892	0.038815	-4.63435	10	7.256
70	3	1	-49.9626	147.1747	7.104324	-4.68858	-0.0697	-4.50114	10	7.114
72	3	1	-53.3434	131.8994	7.104324	-5.32245	0.122619	-2.8024	9.699	6.484
73	3	2	-48.8851	117.3458	7.079053	-4.30733	-0.01406	-3.27971	9.398	6.942
75	3	2	-54.0616	135.5557	7.104324	-5.03856	0.055679	-3.08116	8.921	7.568
76	3	3	-57.8453	123.6087	7.104324	-4.38902	0.268015	-4.73668	8.066	6.483
77	3	3	-54.3975	119.2908	7.124906	-5.18846	0.318221	-5.89969	8.538	6.483
78	3	3	-51.896	115.444	7.145073	-5.84161	0.363531	-7.03301	8.347	6.983
79	3	3	-49.6377	111.9951	7.164841	-6.24613	0.404619	-7.87937	7.77	8.700
80	3	3	-56.7693	111.9951	7.141072	-8.74121	0.404619	-13.5419	8.268	8.533
81	3	3	-58.1944	121.8697	7.133022	-6.28263	0.164524	-8.48279	8.721	8.159
82	3	3	-64.8939	145.6448	7.164841	-5.48071	-0.11052	-6.68132	8.658	7.961
83	3	3	-53.0894	119.762	7.160919	-5.85377	0.32973	-7.05569	8.796	7.758
84	3	3	-52.9828	115.9586	7.167881	-7.27311	0.372716	-9.64774	8.638	8.476
85	3	3	-56.168	109.4561	7.17403	-12.411	0.447814	-12.4782	8.143	8.797
87	3	3	-54.4743	118.4149	7.172497	-8.32598	0.234901	-13.3272	9.523	8.010

Appendix Table A3. Golbraikh and Tropsha model acceptability criteria of the S-MLR model (*equation 1*)

<i>Parameters</i>	<i>Threshold</i>	<i>Equation 1</i>
Q^2	$Q^2 > 0.5$	0.789
r^2	$r^2 > 0.6$	0.626
$ r0^2 - r'0^2 $	$ r0^2 - r'0^2 < 0.3$	0.050
k	$0.85 < k < 1.13$	0.993

$(r^2 - r\theta^2)/r^2$	$(r^2 - r\theta^2)/r^2 < 0.1$	0.035
k'	$0.85 < k' < 1.15$	1.000
$(r^2 - r'\theta^2)/r^2$	$(r^2 - r'\theta^2)/r^2 < 0.1$	0.116

Appendix Table A4. Summary of 50 HQSAR models

Model	Fragment distinction	R^2	R^2_{cv}	R^2	SE	Length	Component
<i>I</i>	A	0.883	0.686	0.883	0.377	151	6
2	B	0.31	0.259	0.31	0.88	97	1
3	C	0.634	0.48	0.634	0.646	353	2
4	H	0.403	0.172	0.403	0.854	97	6
5	Ch	0.403	0.172	0.403	0.854	97	6
6	DA	0/685	0.408	0/685	0.62	257	6
7	A/B	0.903	0.681	0.903	0.344	401	6
8	A/C	0.895	0.671	0.895	0.358	401	6
9	A/H	0.799	0.579	0.799	0.496	257	6
10	A/Ch	0.877	0.676	0.877	0.387	151	6
11	A/DA	0.859	0.567	0.859	0.415	401	6
12	B/C	0.645	0.519	0.645	0.646	257	2
13	B/H	0.31	0.259	0.31	0.88	97	1
14	B/Ch	0.31	0.259	0.31	0.88	97	1
15	B/DA	0.678	0.425	0.678	0.627	59	6
16	C/H	0.634	0.48	0.634	0.646	353	2
17	C/Ch	0.634	0.48	0.634	0.646	353	2
18	C/DA	0.838	0.538	0.838	0.444	307	6
19	H/Ch	0.403	0.172	0.403	0.854	97	6
20	H/DA	0.685	0.408	0.685	0.62	257	6
21	Ch/DA	0.685	0.408	0.685	0.62	257	6
22	A/B/C	0.898	0.656	0.898	0.353	257	6
23	A/B/H	0.778	0.52	0.778	0.521	353	6
24	A/B/Ch	0.9	0.677	0.9	0.35	353	6
25	A/B/DA	0.851	0.599	0.851	0.426	257	6
26	B/C/H	0.645	0.519	0.645	0.636	257	2
27	B/C/Ch	0.645	0.519	0.645	0.636	257	2
28	B/C/DA	0.835	0.556	0.835	0.449	71	6
29	C/H/Ch	0.634	0.48	0.634	0.646	353	2
30	C/Ch/DA	0.838	0.538	0.838	0.444	307	6

31	A/B/C/H	0.755	0.482	0.755	0.542	199	5
32	A/B/C/Ch	0.873	0.629	0.873	0.39	257	5
33	A/B/C/DA	0.858	0.571	0.858	0.416	257	6
34	A/B/H/Ch	0.773	0.508	0.773	0.526	353	6
35	A/B/H/DA	0.762	0.467	0.762	0.539	353	6
36	A/B/Ch/DA	0.868	0.567	0.868	0.401	199	6
37	A/C/H/Ch	0.756	0.468	0.756	0.546	353	6
38	A/C/H/DA	0.756	0.524	0.756	0.543	53	6
39	A/C/Ch/DA	0.882	0.558	0.882	0.379	401	6
40	A/H/Ch/DA	0.764	0.405	0.764	0.537	257	6
41	B/C/H/Ch	0.645	0.519	0.645	0.636	257	2
42	B/C/H/DA	0.835	0.556	0.835	0.449	71	6
43	B/H/Ch/DA	0.678	0.425	0.678	0.627	59	6
44	C/H/Ch/DA	0.838	0.538	0.838	0.444	307	6
45	A/B/C/H/Ch	0.789	0.447	0.789	0.507	199	6
46	A/B/C/Ch/DA	0.873	0.529	0.873	0.394	401	6
47	A/B/C/H/DA	0.782	0.428	0.782	0.516	257	6
48	A/B/H/Ch/DA	0.767	0.402	0.767	0.533	401	6
49	B/C/H/Ch/DA	0.835	0.556	0.835	0.449	71	6
50	A/B/C/H/Ch/DA	0.76	0.398	0.76	0.535	257	6

Appendix Table A5. Descriptors used in LDA model for the training and the test sets.

Cpd No	IC2	Mor28m	H6m	nCt	F05[C-N]	F05[C-C]	Binary
1	4.207	0.35	0.055	1	2	15	0
2	4.207	0.384	0.042	1	2	15	0
3	4.681	0.74	0.145	1	4	17	0
4*	4.681	0.74	0.303	1	4	17	0
5	4.499	0.522	0.528	1	4	21	0
6	4.814	0.803	0.216	1	5	23	0
7	4.395	0.695	0.254	1	5	23	0
8	4.681	0.534	0.131	1	3	17	0
9	4.782	0.187	0.439	1	3	19	0
10	4.721	0.352	0.203	1	4	18	1
11	4.762	0.252	0.209	1	5	19	0
12	4.535	0.233	0.483	1	4	20	0
13	4.587	0.281	0.274	1	6	21	0
14	4.801	0.279	0.53	1	4	18	0
15	4.801	0.303	0.498	1	4	18	0
16	4.721	0.159	0.191	1	3	19	1
17	4.661	-0.013	0.214	1	3	20	1

18	4.762	-0.04	0.269	1	4	20	1
19	4.539	0.085	0.255	2	5	20	1
20	4.873	0.033	0.217	1	3	20	1
21	4.587	0.193	0.28	1	5	22	0
22	4.759	0.241	0.29	1	5	22	1
23	4.723	0.015	0.179	1	5	22	1
24	4.773	0.21	0.317	1	5	22	0
25	4.682	-0.013	0.178	1	5	17	1
26	4.79	-0.046	0.105	1	7	21	1
27	4.832	0.096	0.223	1	3	24	1
28	4.835	0.215	0.267	1	3	19	1
29	4.687	-0.033	0.404	1	5	21	0
30	4.681	0.894	0.476	1	4	17	0
31*	4.681	0.632	0.464	1	4	17	0
32	4.681	0.786	0.179	1	3	17	0
33	4.681	0.787	0.173	1	3	17	0
34	4.721	0.438	0.36	1	4	18	0
35	4.721	0.4	0.349	1	4	18	0
36*	4.721	0.432	0.153	1	3	19	1
37	4.721	0.346	0.136	1	3	19	1
38*	4.681	0.398	0.388	1	3	18	0
39	4.681	0.351	0.323	1	3	18	1
40	4.681	0.154	0.311	1	3	18	0
41	4.681	0.117	0.251	1	3	18	0
42	4.426	0.37	0.113	1	3	15	0
43	4.623	0.477	0.304	1	3	19	0
44*	4.623	0.419	0.308	1	3	19	1
45	4.499	0.498	0.249	1	3	20	0
46*	4.504	0.501	0.288	2	5	19	0
47	4.965	0.492	0.376	1	3	20	1
48	4.921	0.423	0.327	1	4	20	1
49	4.552	0.346	0.317	1	5	21	0
50*	4.739	0.463	0.339	1	5	21	0
51	4.687	0.436	0.354	1	5	21	0
52*	4.671	0.421	0.342	1	5	19	0
53	5.015	0.578	0.408	1	8	20	0
54*	5.015	0.268	0.383	1	8	20	0
55	4.446	0.32	0.324	1	7	21	0
56	4.446	0.426	0.341	1	7	21	0
57	4.702	0.544	0.479	1	8	21	0
58	4.783	-0.141	0.228	1	3	21	1
59	4.743	0.259	0.264	1	3	19	1
60	4.743	0.523	0.318	1	3	19	0
61	4.426	0.099	0.123	1	3	15	0
62*	4.724	0.145	0.248	1	7	19	0
63	4.686	0.075	0.234	1	5	21	0

64*	4.733	-0.037	0.387	1	5	23	1
65*	4.563	0.292	0.32	1	5	23	0
66*	4.62	0.345	0.356	1	5	24	0
67	4.662	0.343	0.255	1	3	23	1
68	4.644	0.068	0.236	1	1	23	1
69	4.648	0.007	0.248	1	1	25	1
70	4.595	-0.054	0.145	1	1	23	1
71*	4.595	0.089	0.167	1	1	23	1
72*	4.648	0.119	0.207	1	1	25	1
73	4.645	-0.027	0.139	1	3	23	1
74	4.724	0.183	0.224	1	3	21	1
75*	4.768	0.244	0.289	1	3	23	1
76*	4.721	-0.153	0.193	1	5	21	1
77	4.661	-0.125	0.316	1	5	22	1
78	4.535	-0.115	0.349	2	5	23	1
79	4.36	-0.227	0.266	1	5	24	0
80*	4.539	-0.095	0.349	2	7	24	1
81*	4.864	-0.206	0.252	1	6	22	1
82*	4.721	-0.252	0.42	1	5	21	1
83*	4.803	0.023	0.319	2	5	23	1
84	4.798	-0.167	0.333	2	6	24	1
85	4.68	-0.162	0.457	2	8	25	1
86*	4.538	-0.018	0.372	1	8	25	1
87	4.973	0.089	0.341	2	6	24	1

Appendix Table A6. Summary of Classification Functions (LDA model)

Variable	G_1:0 p=.50000	G_2:1 p=.50000
Mor28m	-17.577	-23.922
IC2	277.514	290.858
H6m	-160.490	-173.678
nCt	43.631	48.095
F05[C-N]	-5.934	-6.741
F05[C-C]	5.029	5.485
Constant	-671.544	-739.562

Appendix Table A7. Summary of the discriminant function analysis for the LDA model

Discriminant	Function	Analysis	Summary	(LDA_vWSP_final)
Step 6, N	of vars	in model: 6;	Grouping:	Binary (2 grps)
Wilks' Lambda: .39300 approx. F (6,58)=14.931 p< .0000				

N: 65	Wilks' Lambda	Partial Lambda	F-remove (1,58)	p-level	Toler.	1-Toler. (R-Sqr.)
Mor28m	0.473163	0.830573	11.83132	0.001085	0.837157	0.162843
IC2	0.552258	0.711617	23.50456	0.000010	0.732679	0.267322
H6m	0.459008	0.856185	9.74235	0.002806	0.667161	0.332840
nCt	0.435953	0.901465	6.33975	0.014589	0.751396	0.248604
F05[C-N]	0.440844	0.891464	7.06155	0.010158	0.663524	0.336476
F05[C-C]	0.427689	0.918882	5.12017	0.027410	0.722185	0.277815

Appendix Table A8. Summary of the discriminant function analysis for the LDA model

Chi-Square Tests with Successive Roots Removed (LDA_vWSP_final)						
Roots Remove	Eigen-value	Canonicl R	Wilks' Lambda	Chi-Sqr.	df	p-level
0	1.544554	0.779105	0.392996	56.03733	6	0.000000

Appendix Table A9. Raw coefficients for canonical variables of LDA model

Raw Coefficients (LDA_vWSP_final) for Canonical Variables	
Variables	Root 1
Mor28m	-2.5780
IC2	5.4210
H6m	-5.3581
nCt	1.8136
F05[C-N]	-0.3280
F05[C-C]	0.1854
Constant	-27.5015
Eigenval	1.5446
Cum.Prop	1.0000

Appendix Table A10. Posterior probabilities and squared Mahalanobis distances for the LDA model.

<i>Cpd No</i>	<i>Observed Classification.</i>	<i>Posterior probabilities</i>	<i>Squared Mahalanobis distance</i>
		<i>G_1:0 (Inactives)</i>	<i>G_2:1 (Actives)</i>
1	0	0.705341	0.294659
2	0	0.068756	0.931244
3	0	0.002723	0.997277
4	0	0.593644	0.406356
5	0	0.998641	0.001359
6	0	0.002788	0.997212
7	0	0.998763	0.001237
8	0	0.866979	0.133021
9	0	0.944905	0.055095

10	1	0.994137	0.005863
11	0	0.994389	0.005611
12	0	0.615962	0.384038
13	0	0.618875	0.381125
14	0	0.433703	0.566297
15	0	0.993249	0.006751
16	1	0.952757	0.047243
17	1	0.963269	0.036731
18	1	0.952437	0.047563
19	1	0.103214	0.896786
20	1	0.069643	0.930357
21	0	0.065089	0.934911
22	1	0.006040	0.993960
23	1	0.779185	0.220815
24	0	0.959769	0.040231
25	1	0.354884	0.645116
26	1	0.046741	0.953259
27	1	0.348630	0.651370
28	1	0.406906	0.593094
29	0	0.039128	0.960872
30	0	0.089035	0.910965
31	0	0.642069	0.357931
32	0	0.999800	0.000200
33	0	0.957096	0.042904
34	0	0.954006	0.045994
35	0	0.956936	0.043064
36	1	0.937898	0.062102
37	1	0.154364	0.845636
38	0	0.856603	0.143397

39	1	0.999415	0.000585
40	0	0.343658	0.656342
41	0	0.690449	0.309551
42	0	0.980358	0.019642
43	0	0.934242	0.065758
44	1	0.963022	0.036978
45	0	0.210597	0.789403
46	0	0.266806	0.733194
47	1	0.974499	0.025501
48	1	0.947893	0.052107
49	0	0.953304	0.046696
50	0	0.999445	0.000555
51	0	0.999423	0.000577
52	0	0.004879	0.995121
53	0	0.297701	0.702299
54	0	0.821874	0.178126
55	0	0.910725	0.089275
56	0	0.277074	0.722926
57	0	0.233442	0.766558
58	1	0.010362	0.989638
59	1	0.003159	0.996841
60	0	0.007847	0.992153
61	0	0.073956	0.926044
62	0	0.219337	0.780663
63	0	0.997993	0.002007
64	1	0.017809	0.982191
65	0	0.628830	0.371170
66	0	0.000448	0.999552
67	1	0.035249	0.964751

68	1	0.000245	0.999755
69	1	0.994810	0.005190
70	1	0.282749	0.717251
71	1	0.949924	0.050076
72	1	0.912013	0.087987
73	1	0.791450	0.208550
74	1	0.898493	0.101507
75	1	0.977553	0.022447

Appendix Figure A1. (A) 2D molecular docking interactions between MMP-12 (PDB ID: 1RMZ) and compound 69; (B) 2D molecular docking interactions between MMP-12 (PDB ID: 1RMZ) and compound 70.

